RADIATIONLESS ANNIHILATION OF POSITRONS(Dissertation_全文)

AUTHOR(S):

Mukoyama, Takeshi

RADIATIONLESS ANNIHILATION OF POSITRONS

A Thesis Presented

by

TAKESHI MUKOYAMA

to

the Faculty of Engineering
in partial fulfillment of the requirements
for the degree of Doctor of Engineering

KYOTO UNIVERSITY

KYOTO, JAPAN

August 1968

ACKNOWLEDGMENTS

The present thesis has been submitted to the Department of Nuclear Engineering of Kyoto University in partial fulfilment of the requirements for the degree of Doctor of Engineering. The research work presented in this thesis was performed in the Laboratory directed by Professor Sakae Shimizu, Institute for Chemical Research of Kyoto University from August 1964 to April 1968.

The author wishes to express his sincere thanks to Professor Sakae Shimizu of Kyoto University for his suggestion of the problem and continuous encouragement and advices all through the duration of this work. He is also grateful to Mr. Yasuyuki Nakayama for his valuable help in setting up the measuring system and kind cooperation in the whole course of experimental measurements. Further he is indebted to the other members of Professor Shimizu's Laboratory for many interesting and helpful discussions. Thanks are also due to Dr. J. C. Charlton of the Radiochemical Centre, Amersham, England for his cooperation in preparing a ^{22}Na solution of high specific activity used in the present work, and to Dr. W. R. Johnson of University of Notre Dame for making a preprint of his theoretical paper on the angular distribution of single-quantum annihilation radiation available to him. Without the kind cooperation or dedicated participation of

these workers it would not have been possible to complete this investigation. The typewritting of the final manuscript of this thesis by Miss Yoshiko Hagiwara is also gratefully acknowledged.

TABLE OF CONTENTS

LIST OF TABLES

LIST OF FIGURES

SYNOPSIS

A process of positron annihilation without emission of radiation, *radiationless* or *zero-quantum annihilation*, has been investigated experimentally. A theory for this phenomenon by various pairs of shell electrons has also been developed. This mode of annihilation was first predicted by Brunings in 1934 and has so far been treated only theoretically by Massey and Burhop in 1938. In the present work the expressions for the total cross section of this annihilation process have been obtained relativistically using the Darwin-type solutions of the Dirac equation for an electron and positron in the Coulomb field of a nucleus. The cross sections are calculated numerically by an electronic computer. The monoenergetic positron beam of 300 keV was focused on a thin lead target by the use of a Siegbahn-Slätis intermediate-image beta-ray spectrometer mounted with ^{22}Na as a positron source. The thickness of the target was chosen to be about the range of the focused positrons, taking account of their energy and angle of incidence. The shell electrons ejected from the lead foil by the annihilation process were observed with a lithium-drifted silicon junction detector mounted immediately behind the foil. This detector was used as an energy-selective detector for the ejected shell electrons. The pulses from the detector were analyzed with a 400-channel pulse-height analyzer. The total time of measurements was 370 h.

After subtracting contributions due to the strayed gamma rays and natural background from the observed electron spectrum, an evident peak was observed in the expected energy region of the spectrum. Estimating carefully the background which is ascribed to photoelectrons and/or Compton-recoil electrons from the target produced by gamma rays from single-quantum annihilation or two-quantum annihilation in flight, this peak has been attributed to the shell electrons ejected from the lead foil by the annihilation process to be studied. Using the experimental data, an attempt to estimate the total cross section of this annihilation process in lead has been made. Some approximations were used to evaluate the angular distribution of ejected electrons, geometrical efficiency, and the finite thickness effect of the target. The effect of target thickness being the most important factor in the present experiment has been evaluated carefully by combining experimental and theoretical procedures. The experimental result thus obtained is $\sigma_{exp} = 0.8_{-0.3}^{+0.4} \times 10^{-26}$ cm^2 as a sum of those for K-K, K-L, K-M, and L-L pairs of shell electrons in a lead atom for 300-keV positrons. The calculated cross section for these pairs of atomic electrons in lead atom obtained by the present theory is $\sigma_{cal} = 0.727 \times 10^{-26}$ cm^2. The experimental value is in good agreement with the calculated result within the experimental error. No experimental evidence for this annihilation process in tantalum atom suggests that Z dependence of the total cross section for this

mode would be larger than Z^2. The present work has established the experimental evidence for this mode of positron annihilation, and has furthered understanding of the process.

INTRODUCTION

In this thesis an annihilation process which occurs when a positron interacts with an electron in the neighborhood of an atomic nucleus is studied. When a positron annihilates in collision with an electron, there exist two distinct processes, i.e. annihilation by a free electron and by an electron strongly bound in an atom. In the former case, at least two photons are emitted because of the conservation law of momentum, while in the latter only a single-quantum annihilation can take place. Many theoretical and experimental works on these two types of the annihilation processes have so far been published.

Closely connected with the latter process is a type of annihilation where a positron annihilates without emission of radiation. In this case the excess energy liberated is absorbed by another shell electron in the same atom, resulting in its ejection from the atom. This annihilation process, radiationless annihilation, was first predicted by a theorist in 1934, and has been investigated only theoretically. The theoretical results show that this process, though rare, would be observable. The reason why no experimental evidence of this annihilation mode has yet been reported is ascribed to the difficulty in preparing a monoenergetic positron beam of strong intensity and an energy-selective detector with high resolution for the ejected electrons.

In Chap. I the various modes of annihilation are described. After historical remarks for the positron are given, annihilation processes such as multi-photon annihilation, single-quantum annihilation, and radiationless annihilation are discussed in detail.

In Chap. II the fundamental formulae to estimate the cross section for radiationless annihilation are derived and the earlier theoretical works are discussed.

In Chap. III the total cross sections for radiationless annihilation by various pairs of atomic electrons in lead are calculated. Relativistic wave functions in the Coulomb field of a nucleus are used for the incident positron and the ejected electron.

Chap. IV is devoted to describe the experimental procedures. Various properties of the positron source, beta-ray spectrometer, detector, and target are described in detail and the measurements performed are also shown.

Chap. V provides the discussion on the ejected electron spectrum obtained. Some factors necessary to evaluate the experimental cross section are also given in this chapter. Emphasis is given especially to the finite thickness effect of the target, which is considered as the most important factor in this experiment.

In Chap. VI comparison of the theoretical and experimental results is presented, and then the conclusion obtained is given.

CHAPTER I

ANNIHILATION OF POSITRONS

The experimental discovery of the positive electron by Anderson in 1932 was a brilliant success of the Dirac theory which predicts the existence of a particle with the same mass and opposite charge as compared to an electron. This discovery was immediately confirmed by many workers and soon many sources of these positive electrons were found.

According to the Dirac theory, the electron in the positive energy state may make a radiative transition into a "hole", resulting in the disappearance of the positive and negative electrons and the appearance of electromagnetic radiation. The conservation of momentum requires at least two quanta to be emitted in the case where both particles are in free states. The most probable process is annihilation of the positron and electron at rest, with emission of two photons in opposite directions each with an energy of $m_0 c^2$.

In addition to above mode, there are several types of annihilation process: (1) Three-quantum annihilation, (2) two-quantum annihilation in flight, (3) single-quantum annihilation, and (4) radiationless annihilation. The first one is considered as annihilation through positronium. Before annihilation takes place, the positive and negative electrons form a bound system. This quasi-stable system (positronium)

annihilates with emission of even or odd (at least three) number of quanta, depending on the spin directions of the positron and electron.

There is small probability that a positron can also annihilate in flight with emission of two quanta before losing its kinetic energy. In this case the photon energies are different each other and the photon with the larger energy is emitted in the forward direction. When the electron is strongly bound in a nucleus the third process is possible, since the nucleus of the atom in which the electron is bound takes up excess momentum. The fourth case is considered as a competitive process of the third mode of annihilation: The single-quantum process takes place with one of the shell electrons and simultaneously the excess energy liberated, instead of being radiated as a quantum, is used to eject another electron from the atom concerned.

Some historical sketches of these annihilation modes are given in the following sections.

1. Positron

The existence of the positive electron was first predicted by Dirac in 1930.[1] His relativistic quantum mechanical equation of the electron has a set of solutions corresponding to free electrons of negative kinetic energy, i.e. electrons of negative rest mass, and to free electrons of positive kinetic energy. In a classical theory the negative energy states cause no trouble, because the transition between positive and negative energy states is forbidden. Therefore, once an electron has positive energy at any time, it will never occupy a negative state and the solution corresponding to negative energy state can be excluded by initial conditions. In the quantum theory, however, electrons with positive kinetic energy will tend to fall into a state of lower energy as long as such a state is unoccupied and conservation law of angular and linear momentum can be fulfilled. This means that nothing prevents an electron from making a transition from a positive energy state to a negative energy state with release of energy in the form of radiation or kinetic energy of some other particles, and that the electron with negative kinetic energy makes transition continually to unoccupied negative state of lower energy. On the other hand, no electron of negative rest mass has ever been observed. To overcome these difficulties Dirac suggested that all the negative energy state are already occupied by normal electrons of positive rest mass, and that the electrons filling

up the negative energy states are not observable. This means that one difines the vacuum to consist of no occupied positive energy states and all negative energy states completely filled. Only "holes" in the distribution of negative energy states would be observed as real particles. Since the Pauli's principle prevents two electrons from occupying the same quantum state, an electron of positive energy can make no transition from positive to netative energy state so long as no hole exists in negative energy states. Thus, this theory, called *hole theory*, can successfully explain the absence of electrons with negative rest mass and transitions to these states. According to the hole theory a vacant state in a *sea* of negative energy electrons would appear as a particle with positive mass and positive charge. Dirac first suggested that this particle should be identified with a proton, but Oppenheimer[2] has shown that its mass must be the same as that of a normal electron. This particle is called a *positron*.

The positron was first observed experimentally by Anderson[3] in 1932 among the secondary particles produced by cosmic rays, and a short time later the result was confirmed in the cosmic--ray shower and by the pair creation of gamma rays from radioactive sources by Blackett and Occhialini.[4] Immediately after the discovery of this particle, rough measurements of the specific charge e/m_0 was performed by electric and magnetic deflection. It was revealed that the absolute value is the

same for positrons and electrons within an error of 15%.[5] The accuracy of this value was improved within 2%,[6] and recent measurement has established this equality within 0.01%.[7]

Positrons are generally produced in the laboratory by one of the following two distinct methods; (1) pair creation by x rays or gamma rays and (2) beta decay of radioactive sources. Artificial radioactive substances frequently used as positron emitters are ^{22}Na, ^{64}Cu, and ^{56}Co. Beta decay from these radioisotopes is usually the most convenient source of positrons with low energies (below 2 MeV), while pair creation by bremsstrahlung radiations from particle accelerators provides positrons with higher energies. In both cases positrons have continuous energy distribution and this fact makes experiment with positrons difficult.

When an electron collides with a "hole" representing a positron, there may take place a radiative transition to the unoccupied negative energy state. This transition, called *annihilation* of positron, causes disappearance of both particles and appearance of electromagnetic radiation, total energy of which is $E = E_+ + E_-$, where E_+ and E_- are the total energy (including rest mass) of the positron and electron, respectively. From the condition of momentum conservation it follows that at least two quanta must be emitted unless the electron is strongly bound to a nucleus or is very near to another electron. The most probable process is the case in which the positron comes

to rest before annihilation and which results in the emission of two quanta in opposite directions in the laboratory system, each with an energy equal to $m_0 c^2$. When an external field is present and strong enough to absorb the excess momentum, the electromagnetic energy E produced by annihilation of positron can be emitted as only a single photon. This process is called *single-quantum annihilation*. Alternative modes of annihilation in which no radiation is emitted have been considered. In these processes the excess energy is transfered to another electron bound in the same atom or to a nucleus. In the former case to be studied here an electron is ejected from the atom as a result of the annihilation process, while in the latter either excitation or disintegration of the nucleus would take place.

The experimental studies of process of positron annihilation have been done in considerable details for the most probable case of two-quantum annihilation at rest. In the pioneering work of Thibaud[4] positrons produced by gamma rays from a radioactive substance were used. He could identify the gamma rays of about 0.5 MeV with the annihilation radiation. With the discovery of artificial radioisotopes, an experiment similar to that of Thibaud was performed by Joliot[8] using positrons from radioactive source. He proved that the positive particles emitted in beta decay are identified with positrons produced by pair creation of gamma rays. Klemperer[9] and Alichanian *et al.*[10] demonstrated the simultaneity of the two

photons emitted from the annihilation process by coincidence techniques, and Beringer and Montgomery[11] showed that the two quanta emitted in opposite directions within one degree. The energy of the annihilation radiation has been measured precisely by bent-crystal spectrometer[12] and magnetic spectrometer[13] within an accuracy of one part in 10^4.

Thus, all experimental results are in good agreement with the prediction of Dirac's theory which states that positive electrons are represented by holes in the sea of negative electrons in negative energy states.

2. Multi-photon Annihilation

As pointed out in the previous section, the most probable process is annihilation of the positron and electron at rest. In this case, before annihilation takes place positive and negative electrons may form a bound system similar to the hydrogen atom, excepting that its reduced mass is one half of the rest mass of the electron. This can be easily seen from the fact that both particles attract each other because of their opposite charge. The possible existence of such quasi--stable systems was first suggested by Mohorovičić[14] in 1934. The simplest of them, $e^+ + e^-$, calculated to have an ionization potential of 6.77 keV, was named a *positronium* by Ruark.[15] If a positronium is formed in an excited state, it makes a transition to the lower energy state with emission of a line of the characteristic optical spectrum and finally reaches the ground state. The ground state is one of the S states from which the positronium annihilates with emission of gamma rays. In the ground states the spins of the two electrons can be parallel (^3S, triplet positronium or orthopositronium) or antiparallel (^1S, singlet positronium or parapositronium). These two states are distinguished each other by their annihilation properties. Because of the existence of the selection rule, the annihilation of the ^3S state with emission of even number of gamma rays is forbidden. This selection rule can be easily understood from the fact that since each photon

carries one unit of angular momentum in annihilation process from ^1S state, the emission of even number of quanta only arises from a state of even angular momentum as long as charge--conjugation invariance holds for the electromagnetic interaction. Similarly, the triplet state ^3S must result in the emission of odd number of quanta. Since the probability of emission decreases rapidly as the number of quanta is increased, the annihilation of singlet state is usually two-quantum process whilst that of triplet state is three-quantum process.

The bound states of some other polyelectron systems, for instance, the three-particle system $2e^+ + e^-$ or $e^+ + 2e^-$ having small positive binding energy of about 0.2 eV and four-particle system $2e^+ + 2e^-$ having that of about 0.11 eV, were theoretically found to be stable.[16-19] These states, however, have not yet been observed and are considered to occur with very small probability. Therefore, we shall not discuss them.

A. Two-quantum Annihilation

In the lowest approximation the annihilation of a free positron-electron pair is a second order process which may be represented by the Feynman diagram of Fig. 1. If one neglects the Coulomb interaction between the positron and electron, the annihilation process is expressed by the plane wave approximation and the transition probability is proportional to e^4. The cross section of an electron at rest for annihilation with a positron of total energy Em_0c^2, is expressed in the plane

wave approximation by[1]

$$\sigma_{2\gamma} = \frac{\pi r_0^2}{E+1}\left[\frac{E^2+4E+1}{E^2-1}\ln\left(E+\sqrt{E^2-1}\right) - \frac{E+3}{\sqrt{E^2-1}}\right], \qquad (1)$$

were r_0 is the classical electron radius, $r_0 = e^2/m_0c^2$. In the nonrelativistic limit, Eq. (1) becomes

$$\sigma_{2\gamma} \doteq \pi r_0^2 c/v, \qquad (2)$$

where v is the relative velocity of electron and positron and c is the velocity of the light in vacuum. The rate of annihilation process in a medium containing n electrons per cm^3 is given by

$$R = \sigma n v = \pi r_0^2 c n$$
$$= 4.52 \times 10^9 \times \frac{Z}{A}\rho \ \mu c^{-1}, \qquad (3)$$

where ρ, Z and A are the density, atomic number and atomic weight of the medium, respectively.

It is very difficult to evaluate the effects of the nuclear Coulomb field. Positrons of low kinetic energy are repelled by the atomic nuclei and cannot reach electrons in the inner atomic shells. This means that the wave function of positrons overlaps that of atomic electrons only at the periphery of the atom and two-quantum annihilation process will take place with the valence electrons or with the free electrons. On the other hand the polarization effect of atomic shell provides an attraction, and in some cases the bound state may be formed

between the positron and the atomic electron. An attempt has been made to estimate the annihilation rate in metal taking into account of these effects.[20] The calculated result indicates that Eq. (3) should give the fairly correct value for the annihilation rate.

The fate of a positron in metals is very complicated. The conduction electrons in metals interfere with the formation of positronium. The positronium which might be formed would be soon dissociated by subsequent collision with these electrons. It was first considered that positronium is not formed in these materials. However, theoretical estimates of the annihilation properties of free positrons and electrons failed to explain the experimental results for annihilation by the conduction band of a metal. Recent exact calculations suggest that positronium formation in metals is probable.

In condensed materials such as metals, a comparison of the rate of annihilation with that of energy loss by ionization shows that most positrons should survive long enough to release their energy by ionization and to reach thermal equilibrium with the lattice of metals. This fact indicates that only a little number of positrons annihilate before losing most of their kinetic energy. Though the phenomenon of annihilation *in flight* is such a rare occurrence, it becomes very important when we concern with high-energy gamma rays. This annihilation process is discussed later.

B. Three-quantum Annihilation

When the annihilation by two-quantum emission is ruled out by the selection rule mentioned above, three-quantum emission is the most probable mode of annihilation. This is corresponding to the case where a positron-electron pair is in ^3S state. Thus, by annihilation from the triplet state of positronium three photons are usually emitted. In Fig. 2 the lowest order Feynman diagram is shown. Ore and Powell[21] have first calculated the ratio of the three-quantum to two-quantum rate and find

$$\frac{\sigma_{3\gamma}}{\sigma_{2\gamma}} = \frac{4}{9\pi}(\pi^2-9)\alpha \simeq \frac{1}{1115} , \qquad (4)$$

where α is the fine structure constant. This result implies that a ^1S state annihilates about 10^3 times faster than the corresponding ^3S state. Since the statistical weight of the triplet state in free collisions is three times greater than that of the singlet, the ratio of cross sections after averaging over spin directions is about 1/370. Rich[22] was the first worker to report observation of this phenomenon.

From the conservation law of momentum, three photons must be emitted in the same plane and not all in the same half-plane. Their energy spectrum has been calculated by Ore and Powell[21]. Their result shows that it is continuous extending from zero to a maximum energy of $m_0 c^2$.

C. Annihilation in Flight

It has been demonstrated that most positrons annihilate after they lose their energy by ionization and have only thermal energies. There is, however, a small probability that annihilation resulting in two photons will occur before a positron loses its kinetic energy.

Using Dirac's expression for the probability of transition to a negative energy state, Bethe[23] obtained the cross section for two-quantum annihilation of a positron in flight with a free electron at rest:

$$d\sigma = \frac{\pi r_0^2}{E^2-1}\left[\frac{k}{k'} + \frac{k'}{k} + 2\frac{E+1}{kk'} - \left(\frac{E+1}{kk'}\right)^2\right] dk, \qquad (5)$$

where r_0 is the classical electron radius; the energy of positron, including rest energy, is Em_0c^2; and the energies of the two quanta are km_0c^2 and $k'm_0c^2$, where $k + k' = E + 1$. The conservation laws require the photon energies to lie between the extreme values

$$k = \frac{1}{2}(E+1) \pm \frac{1}{2}(E^2-1)^{1/2}, \qquad (6)$$

corresponding to emission in the forward and backward directions.

This process has been observed by many workers as the sudden cease of fast positron tracks in cloud chamber[24] or photographic emulsions[25] and a high energy *tail* on the secondary electron spectra due to annihilation radiation.[26] Their results, however, gave little information, beyond confirming that positrons do annihilate in flight. More

successful results were obtained by the work of Colgate and Gilbert[27] with high-energy positrons, that of Kendall and Deutsch[28] with low-energy positrons, and that of Gerhart *et al.*[29] with continuous beta-spectra from radioactive sources. The cross sections measured by them were in good agreement with the theoretical values calculated from Eq. (5), but for positrons from ^{35}A and for stopping materials of low atomic number the calculated values tend to be lower than the observed ones.

3. Single-quantum Annihilation

Emission of a single photon by annihilation process is forbidden for a free positron-electron pair owing to impossibility of satisfying both momentum and energy conservation simultaneously. However, a positive electron can be annihilated with emission of a single photon if the negative electron is strongly bound to a nucleus. In this case the nucleus of an atom in which the electron is bound is available to take up excess momentum. In Fig. 3 is shown the diagram of this process. The probability for this mode of annihilation is, in general, considerably smaller than that for the two-quantum annihilation. Rough estimation shows that the cross section value of the single-quantum process in lead at maximum evaluation is less than 20% of that of the two-quantum process in flight. Neglecting the recoil energy of the nucleus, the energy of the emitted photon is given by

$$E_{\gamma} = E_{+} + E_{B} \ , \qquad (7)$$

where E_{+} is the total energy of the incident positron, and E_{B} that of the shell electron bound in the atom.

Owing to the symmetry between electrons and positrons in Dirac's hole theory, Solomon[30] has pointed out that it is possible to regard the electron as a hole in the uniform distribution of positrons and the positron is represented by a real particle in the positive energy state. Single-quantum

annihilation of positrons is then considered as the capture of the positive electron by the hole in the atomic shell. Since this electron capture is an inverse process of the photoelectric effect, the cross section for single-quantum annihilation of positrons can be deduced easily from the cross section for the corresponding photoelectric effect.

Theoretical calculations of the cross section for single--quantum annihilation were carried out by many authors[23,31-34] using various approximations. In order that the momentum is transferred to the nucleus in the course of annihilation process, the colliding electron must be bound strongly to the nucleus. This implies that single-quantum annihilation is taken place probably with a K electron of high-Z atom. Theoretical calculation of the cross section for this process was first made by Fermi and Uhlenbeck[31] and the cross section value was found to be rather smaller than that for the two--quantum process for a positron of the same energy. Born approximation[23,32,33] shows that the cross section is proportional to Z^5. This fact indicates that this mode of annihilation is more probable for heavy elements than for light ones. However, since for elements with high-Z values greater than 70 the Born approximation is not reliable, the accurate cross section must be smaller than that expected from the Born approximation. The K-shell annihilation cross section of Jaeger and Hulme[34] for lead calculated with relativistic

Coulomb wave function gives small value by factor of 2.

Theoretical calculations of cross section for this process of longitudinally polarized positrons with K-shell electrons have been done under various assumptions such as plane wave approximation[35] and Sommerfeld-Maue approximation.[36] Their results show that the circular polarization of the radiation emitted has the same helicity as that of the longitudinal polarization of the incident positron when positrons are relativistic. Banerjee[37] have also calculated the angular distribution and the total cross section using the Sommerfeld--Maue approximation being analogous to those of photoelectric effect.

Johnson *et al.*[38] have recently calculated exactly the total cross section for single-quantum annihilation by K-shell electrons in the Coulomb field of a nucleus. Their results agree well for $Z = 82$ but not in detail with previous calculations of Jaeger and Hulme,[34] and show that the Born approximation is too large by a factor of nearly 2. Last year relativistic calculations of accurate angular distributions of radiation accompanying single-quantum annihilation of positrons by K-shell electrons in various elements ranging from $Z = 47$ to 92 was made by Johnson[39]. He showed that these angular distributions differ from the corresponding Born approximation, both in magnitude and shape. The angular distribution peaks sharply in the forward direction and falls off rapidly at backward

angles. This behavior is in conflict with the Born approximation which predicts an angular distribution vanishing at both forward and backward angles.

There have been several attempts to observe this mode of annihilation.[29,40-42] Meric[40] was the first experimental worker who was successful in detection of this phenomenon. Her experiment based on the theoretical prediction that the cross section for single-quantum annihilation varies with about Z^5 while the cross section for two-quantum annihilation varies with Z. Therefore, single-quantum process would be negligible in aluminum as compared with that in lead. If absorption curves using aluminum absorbers are observed for gamma rays produced by annihilation of positrons with these substances as targets, one would expect a difference between the two curves which would be due to the greater number of hard gamma rays produced by the process to be studied in lead. As a positron emitter she used ^{64}Cu. The trochoidal method was employed to separate the positrons from the nuclear gamma rays of this nuclide. She measured coincidence counting rates in two G-M counters between which an aluminum absorber of varying thickness were inserted. The gamma-ray energies were measured in terms of the range of the converted electrons in aluminum. The ratio of the number of real coincidences to the number obtained with no absorber was plotted against the energy of gamma rays, i.e. thickness of the aluminum absorber.

Using so-called absorption technique and from the result that the absorption curve for lead is above that for aluminum, she demonstrated the existence of a high-energy gamma-ray component which was more prevalent in lead than in aluminum.

In the experiment of Farmer and Streib[41] 5.0-mCi ^{11}C produced by the (p, α) reaction using the cyclotron was used as a positron source. This source carried by N_2 gas was introduced into chambers lined with Pb, Ta, or Al. The gamma rays from these chambers was presumed as photons by positron annihilation in the inner-wall materials of the chambers. The spectra of these photons after being filtered by 2.5-cm Pb were observed with a scintillation spectrometer using a 5.0-cm thick NaI(Tl). They reported that results for gamma-ray energies above 1.4 MeV indicate reasonable agreement with theoretical results for single-quantum annihilation and two--quantum annihilation in flight.

Whalen[42] measured a difference of counting rates for lead and aluminum target using coincidence technique between a hard gamma and characteristic x rays. The observed signal, attributed to single-quantum annihilation, gave a cross section approximately twice the theoretical value of Jaeger and Hulme.[34] Owing to the low counting rates measurements with any high-Z target but lead was impossible and consequently no check of Z dependence was made. Experiments were hampered by the rarity of the events and the large background rates.

Recently Sodickson *et al.*[43] attempted to measure the cross section for this annihilation. Monoenergetic positron beam of 100–400 keV was produced from approximately 1 mCi of ^{22}Na using an orange-peel spectrometer. Thick targets of high-Z materials ranging Z = 73 to 90 were used to obtain the Z dependence of the cross section. The foil thickness of each material was chosen as to be slightly greater than the extrapolated ranges of the positrons involved. The event was identified by detecting the high-energy gamma ray and the emission of a K x ray in coincidence. The gamma-ray and x-ray detectors were both NaI(Tl) crystals and pulses from them were fed to a conventional fast-slow coincidence system, time resolution of which is 100 nsec, and then recorded by a scaler. The experimental data were analyzed under the assumption that the direction of the incident positron becomes isotropic after a negligible penetration length. They concluded that they had observed single-quantum annihilation of positrons. The process they observed occurs in lead with a cross section equal, within a factor of 2, to the theoretical value of Jaeger and Hulme[34], and its Z dependence agrees well with a cross section proportional to Z^5.

Immediately after the work of Sodickson *et al.* two similar studies were reported by Göttingen group.[44,45] Flammersfeld *et al.*[44] performed a thin-target experiment and observed monoenergetic gamma rays due to single-quantum annihilation.

They used 10-mCi ^{64}Cu, 1-mCi ^{56}Co, and 10-mCi ^{66}Ga as positron sources and obtained monoenergetic positron beam in the energy range from 260 to 1400 keV with the aid of an orange-type beta-ray spectrometer. Positrons from the spectrometer pass through very thin anthracene crystal and enter the lead target. Immediately behind the target two scintillation detectors were placed; the one was a plastic scintillator to detect positrons which leak through the lead foil without annihilation and the other was a CsI crystal to detect K-x rays following single-quantum annihilation. Behind them a NaI(Tl) crystal was placed to measure annihilation radiation from the target. Anthracene and NaI crystals provided pulses to a fast coincidence circuit with the resolution of 50 nsec. Pulses from CsI crystal and from the fast coincidence circuit were fed to a slow coincidence circuit, while those from the plastic scintillator was fed to an anticoincidence. The output of this circuit was used as a gate signal and the energy spectrum of annihilation gamma rays was recorded by a 256-channel pulse-height analyzer. The experimental data were analyzed under the assumption that the angular distribution of annihilation radiation by this process is similar to that of photoelectric effect by gamma rays if the total energy of the photoelectron is replaced by a negative value. The total cross sections of this mode has been found to be in agreement with calculated values of Jaeger and Hulme[34] in the energy range from 260 to 1400 keV.

The Z dependence of the cross section for single-quantum annihilation has also been studied by Flammersfeld *et al.*[45] with the same experimental apparatus mentioned above. Monoenergetic photons due to single-quantum annihilation in thin foils of elements in the range from Z = 50 to 92 have been observed at two different values of the kinetic energies of incident positrons. According to their measurements with positron kinetic energies of 760 keV and 1100 keV, the exponent of Z in total cross section of this process, $\sigma \approx Z^{\nu}$, is ν = 3.2 ± 0.6 and ν = 3.8 ± 0.8, respectively, which does not agree with the value predicted by the Born approximation ν = 5.

More refined experiment for this annihilation was performed by Mazaki *et al.*[46] in our laboratory. Using a Siegbahn-Slätis type beta-ray spectrometer mounted with a ^{22}Na source, positron beams of kinetic energies between 250 and 400 keV were focused on the disc targets of five different elements ranging from Z = 50 to 92; Sn, Ta, Au, Pb, and U. The thickness of each target was chosen as to be approximately one fifth of the range of the focused positron. Photons emitted as a result of single-quantum annihilation were detected by a NaI(Tl) crystal placed behind the target, while the K-x rays accompanying this annihilation process were measured by a thinner NaI(Tl) detector placed perpendicularly to the target. Between the target and the gamma-ray detector, a surface barrier silicon detector was placed to count the number of positrons passed

through the target without giving rise to the annihilation. Output pulses from the both NaI(Tl) detectors were fed to the coincidence circuit. The positron signals from the silicon detector were matched with those of coincidences in the anticoincidence circuit and the resulting signals were used as the gate pulses for a 400-channel pulse-height analyzer. They applied a skillful technique to estimate the effect of finite target thickness, which seems to be one of the key points of the experiment. The positron flux in the targets used in the experiment was obtained by measuring the energy spectra of positrons passed through the thinner targets of various thicknesses. From the data thus obtained, the number of positrons being able to contribute to single-quantum annihilation was determined. By carefully evaluating the factors affecting the value of the cross section and using the exact angular distribution of emitted gamma rays calculated by Johnson,[39] they concluded that the energy dependence of the total cross sections for lead and uranium is in fairly good agreement with the theoretical calculations by Johnson *et al.*[38] and Jaeger and Hulme,[34] and that the exponent of Z in the total cross section for 300-keV positrons is $\nu = 4.93 \pm 0.31$ being in good agreement with the relativistic calculation of Johnson *et al.*[38]

4. Annihilation without Emission of Radiation

A positron colliding with an atom presents a vacant state into which an atomic electron may fall, releasing energy $\sim 2\, m_0 c^2$. In general, the excess energy is emitted as radiation, but it is possible that this energy may either be given to nucleus or to a second electron which then leave the atom with high kinetic energy. In this way a positron will be annihilated without emitting radiation. Theoretical calculations of the cross section for annihilation by the first process have been carried out by Present and Chen.[47] In this mode of annihilation, called *annihilation-disintegration* or *annihilation-excitation*, a positron with insufficient energy to excite or disintegrate a nucleus by collision, annihilates a K electron of an atom with subsequent excitation or disintegration of its nucleus. This process may be described as a transition of an electron from an orbital state into a vacant negative energy state in the continuum corresponding to the incident positron, accompanied by a nuclear transition from the ground state into an excited continuum state corresponding to disintegration or into an discrete state following to de-excitation.

The annihilation cross sections have been calculated in the Born approximation using the complete retarded interaction corresponding to converging spherical waves of electric dipole radiation. Numerical estimates have been made for the disintegration of ^{9}Be with emission of a neutron and also for the

disintegration of ^{238}U resulting in nuclear fission. The total annihilation-disintegration cross section near the threshold in these two cases are $\sim 10^{-34}$ cm^2 for incident positron total energy of $E_+ = 2.3\ m_0 c^2$ and $\sim 10^{-31}$ cm^2 for $E_+ = 11.5\ m_0 c^2$, respectively. The total cross section for an annihilation-excitation of ^{115}In into the principal activation state, which was considered to be located at 1.04 MeV above the ground state at that time, is found to be $\sim 10^{-26}$ cm^2 for $E_+ = 1.10\ m_0 c^2$. Although this cross section is much larger than those calculated above, the process can only take place if the positron has just the right energy. It is practically impossible to produce such a positron beam to fulfil this condition. Owing to the small values of the cross sections, annihilation-disintegration or -excitation process can be negligible.

The possibility that the energy liberated by annihilation of positrons be transferred to other electrons in the same atom has first been suggested by Perrin.[48] He considered two different cases: (1) The excess energy liberated by annihilation is shared with another shell electron and a photon such as they have equal momentum but in opposite directions. Neglecting the binding energy of the shell electron a photon with energy of about 680 keV and an electron with kinetic energy of about 340 keV are emitted simultaneously for the positron of zero kinetic energy. (2) When a positron annihilates with an

electron in the presence of two other atomic electrons, these shell electrons would be ejected in opposite directions with equal kinetic energy of about 510 keV corresponding to zero kinetic energy of the incident positron. The latter process may also be considered to be a kind of radiationless annihilation. However, we use the term *radiationless annihilation* to denote the following process only, since the cross sections for these two processes mentioned above seem to be negligibly small compared with the process to be studied.

As a competitive process of the single-quantum annihilation, there may exist another process by which a positron annihilates without emission of radiation. This mode of annihilation would occur when the single-quantum annihilation takes place with one of the K- or L-shell electrons and when simultaneously the excess energy liberated, instead of being radiated as a quantum, is used to eject another electron from the atom concerned. The annihilation by this process, therefore, may be called *radiationless annihilation*. The energy relation between the incident positron, the ejected electron and a pair of the shell electrons involved is shown in Fig. 4. Let E_α and E_β be the total energies (including rest mass) of the two bound electrons concerned in the atom before transition, and let E_+ be that of an incident positron, the total energy E_- of the electron ejected as a result of the radiationless annihilation can be given by

$$E_{-} = E_{+} + E_{\alpha} + E_{\beta} \quad . \tag{8}$$

It is noted that the figure and diagram shown in Fig. 4 are concerned with the process where the total energy of a shell electron with which a positron annihilates is denoted by a subscript α and that of another shell electron before ejection is by a subscript β. Similar figure and diagram are obtained by exchanging α for β in the case where α is for the electron to be ejected and β is for the electron with which a positron annihilates. The figure and diagram in the latter case is not shown in Fig. 4. However, Eq. (8) is valid for both of these cases.

In 1934 Brunings[49] first pointed out the possibility of this mode of annihilation of the positron and estimated the cross section in the case where two electrons concerned are both in K-shell of a lead atom. Using nonrelativistic calculations involving a number of approximations, he has shown the cross section for lead to be about 10^{-26} cm^2 for the incident positron with kinetic energy being 100–500 keV. More elaborate calculations of the cross section for this process were performed by Massey and Burhop[50] in 1938 by treating various atomic shells rigorously, taking account of the repulsive influence of the nucleus, retardation effect, spin-spin interaction and electron exchange. Their calculations have shown that the total cross section for pairs of electrons in a lead atom would have a maximum value

of between 1 and 1.5 X 10^{-26} cm^2 for incident positrons with kinetic energy of 300 keV.

To the author's knowledge, excepting our preliminary report[51] in 1965 no experimental study on this phenomenon has so far been published. Owing to such a rather small cross section, to demonstrate by experimental evidence this mode of annihilation an intense monoenergetic positron beam and an energy-selective detector with high resolution for the ejected electrons are necessary.

CHAPTER II

THEORETICAL BACKGROUNDS

The interaction between two charged particles can be treated relativistically by taking account of retardation effects. This method dealing with two-electron transition is applicable to calculation of the cross section for radiationless annihilation of positrons. An estimate of the cross section for this annihilation process, where the two shell electrons concerned are K electrons in a lead atom, has first been made by Brunings in 1934. Based upon a number of approximations his nonrelativistic calculations led to a value of about 5×10^{-26} cm^2 for positrons of 100 keV, and also showed that the cross section reaches the maximum value for positrons with kinetic energy equal to the electron binding energy. In 1938 Massey and Burhop treated relativistically this mode of annihilation involving two K electrons in lead. A plane wave is used in their calculations for the ejected electron and allowance was made for the distortion of the incident positron wave function by the Coulomb field of a nucleus. They have also calculated the cross sections by various pairs of shell electrons in the lead atom using the nonrelativistic approximation. The results thus obtained showed that the total cross section in lead has a maximum value of about 10^{-26} cm^2 for incident positrons of kinetic

energy of 300 keV.

In this chapter we shall discuss briefly the procedures by which the cross section is derived, and the results obtained by these workers.

1. Retarded Interaction

The scattering of two charged particles with Coulomb interaction can be treated exactly with nonrelativistic quantum mechanics. In this case these particles move so slowly that interaction between them is described by the potential energy of interaction which is a function of the distance between the particles. The situation becomes very complicated when account must be taken of the retarded interaction as well as the static interaction mentioned above.

A complete relativistic treatment of such an interaction can be done using a theory of quantum electrodynamics which include allowance for radiative effect as well as for vacuum polarization. In this case solutions are found by expansion according to powers of the fine structure constant $\alpha = e^2/\hbar c$. Since the divergences which arise in the theory can be disposed of by the method of mass and charge renormalization, it is possible to calculate the cross section for the interaction of electrons and positrons with electromagnetic radiation to any order of approximation. However, corrections due to radiative effect and vacuum polarization are, in general, quite small and the procedures in which contribution from such effects is neglected give the satisfactory results even for relativistic cases.

The interaction of charged particles between themselves and electromagnetic field is considered to consist of a static

Coulomb interaction between particles and the interaction of each particle with the transverse light field. If we consider the case where light is not actually emitted during the interaction of two particles, the latter interaction comes from the mutual exchange of light waves between the two charged particles. Then as a first approximation, we can use the retarded effects which involve contributions from virtual emission and absorption of transverse wave to the Coulomb field. This solution corresponds to the first order approximation of α.

When two charged particles such as electrons are coupled to the electromagnetic field, the wave function for each particle satisfies the following equation of motion:

$$\gamma_\mu \left(\frac{\partial}{\partial x_\mu} + \frac{ie}{\hbar c} A_\mu \right) \psi + k \psi = 0 \quad , \qquad (9)$$

where the four-vector potential of the electromagnetic field, A_μ, is evaluated at x_1 in the equation for particle 1 and at x_2 in the equation for particle 2, respectively, and k is the reciprocal Compton wavelength. We shall use common time t for both particles. When particle 1 makes a transition from state $\psi_i^{(1)}$ to $\psi_f^{(1)}$, taking into account of the Lorentz condition for A_ν, the field A_ν at x_2 generated by particle 1 satisfies the well-known wave equation:

$$\frac{\partial^2 A_\nu}{\partial x_\mu \partial x_\mu} = -\frac{4\pi}{c} j_\nu \quad , \qquad (10)$$

where the current four-vector j_μ due to the transition of the

particle 1 is expressed as

$$j_\mu = -ie\,c\,\psi_f^{(1)*}\gamma_{1\mu}\psi_i^{(1)} \quad , \qquad (11)$$

where $\gamma_{1\mu}$ is the Dirac's γ-matrix. In Eq. (11) the subscript 1 refers to particle 1. By the analogy with classical electrodynamics the solution of Eq. (10) can be given by

$$A_\nu(\mathbf{r}_2, t) = \frac{1}{c}\int \frac{j_\nu(\mathbf{r}_1, t')}{R}\, d\mathbf{r}_1 \quad , \qquad (12)$$

where $R = |\mathbf{r}_1 - \mathbf{r}_2|$ and $t' = t - R/c$. Since $j_\nu(\mathbf{r}_1, t)$ has a time dependence given by $\exp[i(W_f - W_i)t/\hbar] = \exp(-i\omega t)$, replacement of t by $t - R/c$ gives a factor

$$e^{-i\omega t} e^{ik_0 R},$$

where

$$k_0 = \omega/c = (W_f - W_i)/\hbar c \quad ,$$

and W_i and W_f are the total energy of particle 1 before and after the transition, respectively. If we consider that particle 2 makes a transition from state $\psi_i^{(2)}$ to $\psi_f^{(2)}$ under the influence of $A_\mu(\mathbf{r}_2, t)$, the matrix element for this transition is written as

$$H_{fi} = ie\int \psi_f^{(2)*}\gamma_{2\mu} A_\mu(\mathbf{r}_2)\psi_i^{(2)}\, d\mathbf{r}_2 \quad , \qquad (13)$$

where $A_\mu(\mathbf{r}_2)$ is the time-independent part of four-vector potential $A_\mu(\mathbf{r}_2, t)$:

$$A_\mu(\mathbf{r}_2, t) = A_\mu(\mathbf{r}_2)\, e^{-i\omega t} \quad .$$

From Eqs. (11) and (12), Eq. (13) can be expressed as

$$H_{fi} = e^2 \int \psi_f^{(2)*}(\mathbf{r}_2)\psi_f^{(1)*}(\mathbf{r}_1)\gamma_{1\mu}\gamma_{2\mu}\frac{e^{ik_0R}}{R}\psi_i^{(2)}(\mathbf{r}_2)\psi_i^{(1)}(\mathbf{r}_1)\,d\mathbf{r}_1 d\mathbf{r}_2 . \quad (14)$$

Using the properties of γ-matrix this equation may be written in the alternative expression

$$H_{fi} = e^2 \int \psi_f^{(2)*}(\mathbf{r}_2)\psi_f^{(1)*}(\mathbf{r}_1)(1-\alpha_1\cdot\alpha_2)\frac{e^{ik_0R}}{R}\psi_i^{(2)}(\mathbf{r}_2)\psi_i^{(1)}(\mathbf{r}_1)\,d\mathbf{r}_1 d\mathbf{r}_2 , \quad (14')$$

where α_1 and α_2 are the Dirac matrices, and the operator α_1 operates only on the function $\psi_i^{(1)}(\mathbf{r}_1)$ while the operator α_2 operates on the function $\psi_i^{(2)}(\mathbf{r}_2)$.

It can be easily seen that the first term in Eq. (14') represents the Coulomb interaction between two charged particles which arises from the virtual emission and absorption of longitudinally polarized photons, and that the second term expresses the relativistic current-current interaction contributed from both transversely and longitudinally polarized photons. In Eq. (14), it is noted that the matrix element given by this expression is correct only to the first order in e^2 or α.[52]

This method was first introduced by Møller[53] in the calculation of the cross section for electron-electron scattering and has been successfully applied to many cases where two charged particles concern such as internal conversion of gamma rays and Auger effect.

According to the law of quantum mechanics, transition probability is given by

$$\text{Trans. prob.}/\text{sec} = \frac{2\pi}{\hbar} |H_{fi}|^2 \rho_E , \qquad (15)$$

where ρ_E is the density of final states and obtained in the following manner:

$$\rho_E = \frac{1}{(2\pi\hbar c)^3} \frac{d|p_2}{dE_2} = \frac{p_2^2 dp_2 d\Omega_{p_2}}{(2\pi\hbar c)^3 dE_2} . \qquad (16)$$

In this expression E_2 and $|p_2$ are the total energy and momentum of particle 2 in the final state, respectively, and $d\Omega_{p_2}$ is element of a solid angle subtended by $|p_2$ in the momentum space. From the relativistic energy-momentum relationship, dp_2/dE_2 is equal to $E_2/(p_2 c^2)$. Using this expression Eq. (16) can be written by

$$\rho_E = \frac{p_2 E_2 d\Omega_{p_2}}{(2\pi\hbar)^3 c^5} . \qquad (16')$$

When we consider the problem that the particle 1 is free state and normalized to one particle per cubic centimeter, the cross section σ is given in terms of the transition probability per second as

$$\text{Trans. prob.}/\text{sec} = \sigma v_1 , \qquad (17)$$

where v_1 is the velocity of incoming particle. From the well-known relativistic relation between p_1 and v_1, v_1 is expressed using the total energy of particle 1, E_1, as

$$v_1 = \frac{p_1 c^2}{E_1} .$$

From Eqs. (15) and (17), we can write the cross section σ for interaction of two charged particles with definite spins in

both initial and final states by the following expression:

$$\sigma = \frac{E_1}{p_1 c^2} \times (\text{Trans. prob./sec})$$

$$= \frac{1}{(2\pi)^2 \hbar^4 c^7} \frac{p_2 E_1 E_2}{p_1} \int |H_{fi}|^2 d\Omega_{p_2} , \quad (18)$$

Radiationless annihilation of positrons is considered that when an electron bound in an atom undergoes a transition from positive-energy state to negative-energy state giving up energy $k_0 \hbar c$, one of other atomic electrons is lifted from the bound state to free state. In this case the wave functions in Eq. (14') are taken as: $\psi_i^{(1)}(\mathbf{r}_1)$ is the bound-state electron in an atom, $\psi_f^{(1)}(\mathbf{r}_1)$ the incident positron, $\psi_i^{(2)}(\mathbf{r}_2)$ the other bound--state electron in the same atom, and $\psi_f^{(2)}(\mathbf{r}_2)$ the electron ejected from the atom as a result of the process considered. The bound-state wave functions of electrons are normalized to unit volume as usual, while continuum-state wave functions of the electron and positron must exhibit the asymptotic forms of plane waves plus the corresponding spherical waves.

The above discussion takes no account of the antisymmetrical property of the electron in the quantum mechanics. Let $|B|^2$ be the transition probability given by the above choise of electron wave functions, and $|C|^2$ be the probability obtained by supposing the bound electron 2 to annihilate with the incident positron and the bound electron 1 to be ejected. The latter case corresponds to the choice of the bound-state wave functions of electrons as follows: $\psi_i^{(1)}(\mathbf{r}_2)$ and $\psi_i^{(2)}(\mathbf{r}_1)$.

It is impossible to distinguish between these two processes experimentally because in both cases the total energy of the ejected electrons is $E_+ + E_\alpha + E_\beta$, where E_+ is the total energy of the incident positron, and E_α and E_β are those of bound electrons in the initial states, respectively. Owing to the Pauli's exclusion principle for the electron, the number of ejected electrons per unit time by both kinds of transitions is given by

$$|A|^2 = |B - C|^2 . \qquad (19)$$

This expression includes the effect of electron exchange, and to obtain the cross section must be averaged over possible initial states and summed up over all final states.

2. Nonrelativistic Calculations

Theoretical calculations of the cross section for the radiationless annihilation of a positron were first made by Brunings[49] in 1934. Introducing many assumptions, he calculated the nonrelativistic cross section for this process in the case where two bound electrons concerned are both in the K shell of a lead atom. The approximations used by him to estimate the cross section are as follows: (1) For both shell electrons, nonrelativistic K eigenfunctions are used. (2) Kinetic energies of the incident positron and the ejected electron are so large comparing with the K-shell binding energy of a lead atom that we can use Born approximation. This means that both particles are expressed as plane waves. (3) Perturbation is only the static Coulomb interaction between the two charged particles, and the retardation effects are ignored.

The last assumption is easily derived from Eq. (14') in the nonrelativistic limit with $c \longrightarrow \infty$, and then the matrix element is written as

$$H_{fi} = \iint \phi_+^*(\mathbf{r}_1)\, \phi_-^*(\mathbf{r}_2)\, \frac{e^2}{R}\, \psi_\alpha(\mathbf{r}_1)\, \psi_\beta(\mathbf{r}_2)\, d\mathbf{r}_1\, d\mathbf{r}_2 , \qquad (20)$$

where $\phi_+(\mathbf{r})$, $\phi_-(\mathbf{r})$, $\psi_\alpha(\mathbf{r})$ and $\psi_\beta(\mathbf{r})$ are the wave functions for the incident positron, the ejected electron and two K-shell electrons, respectively.

The total cross section σ is given by

$$\sigma = \frac{2\pi}{\hbar}\frac{1}{v_+}\sum\int |H_{fi}|^2 \rho_E \, d\Omega_{p_-} , \qquad (21)$$

where $\sum$ means the average over the spin directions of the incident positron and the summation over those of the ejected electron, and ρ_E is the density of the final states of ejected electrons.

Wave functions of the bound electrons used by him are

$$\psi_\alpha = \sqrt{\frac{\alpha^3}{\pi\hbar^3 c^3}}\, e^{-\frac{\gamma}{a_0}r}\left[0,\ 1,\ -i\Delta_0 \sin\theta e^{i\phi},\ -i\Delta_0\cos\theta\right], \qquad (22a)$$

$$\psi_\beta = \sqrt{\frac{\alpha^3}{\pi\hbar^3 c^3}}\, e^{-\frac{\gamma}{a_0}r}\left[-1,\ 0,\ -i\Delta_0\cos\theta,\ i\Delta_0\sin\theta e^{-i\phi}\right], \qquad (22b)$$

where a_0 is the radius of the first Bohr orbit of hydrogen, $\gamma = Z/137$, and

$$\Delta_0 = \frac{1+\gamma}{1+\sqrt{1-\gamma^2}} .$$

Incident positron wave function with the kinetic energy E_+ and momentum $\hbar p_+$ is given by

$$\phi_+ = \frac{1}{(1+\Delta_+^2)^{1/2}}\left\{\begin{array}{l}\left[1,\ 0,\ -\Delta_+\cos\theta,\ -\Delta_+\sin\theta e^{i\varphi}\right] \\ \left[0,\ 1,\ -\Delta_+\sin\theta e^{-i\varphi},\ \Delta_+\cos\theta\right]\end{array}\right\}, \qquad (23)$$

where

$$\Delta_+ = \frac{cp_+}{E_+ + m_0c^2} .$$

The wave function of free electron with kinetic energy

E_- and momentum $\mathbf{p}_-$ is expressed by

$$\phi_- = \frac{1}{(1+\Delta_-^2)^{1/2}} \left\{ \begin{bmatrix} -\Delta_- \cos\theta, & -\Delta_- \sin\theta e^{i\varphi}, & 1, & 0 \end{bmatrix} \right\} \quad (24)$$
$$\left\{ \begin{bmatrix} -\Delta_- \sin\theta e^{-i\varphi}, & \Delta_- \cos\theta, & 0, & 1 \end{bmatrix} \right\},$$

where

$$\Delta_- = \frac{c\,p_-}{E_- + m_0 c^2} .$$

Using these wave functions and neglecting terms with γ calculation is reduced to the integral

$$I = \int e^{-\frac{\alpha}{\hbar c}(r_1+r_2)} e^{\frac{i}{\hbar}(-\mathbf{p}_+\cdot\mathbf{r}_1 + \mathbf{p}_-\cdot\mathbf{r}_2)} \frac{1}{R}\, d\mathbf{r}_1\, d\mathbf{r}_2 .$$

This integral can be evaluated under the assumption that p_+ is small enough in comparison with $m_0 c$. The cross section σ is obtained by the following form:

$$\sigma = \frac{(32)^2 \pi \Delta_-^2}{(1+\Delta_+^2)(1+\Delta_-^2)} \frac{c}{v_+} r_0^2 \frac{\alpha^8}{c^8 p_-^8} \frac{1}{\left\{ \left(\frac{p_+}{m_0 c}\right)^2 + \left(\frac{\alpha}{m_0 c^2}\right)^2 \right\}^2} , \quad (25)$$

where r_0 is the classical electron radius.

His results show that the cross section for a lead atom has the maximum value when the kinetic energy of the positron is equal to the binding energy of the K-shell electron. However, Brunings' formula, Eq. (25), is valid only for nonrelativistic case where v_+ is very small. Numerical values obtained in this way are given in the first row of Table I, where those obtained from other approximations are also listed for comparison.

3. Relativistic Calculations

The relativistic calculations of the cross section for the process of radiationless annihilation of positrons was performed by Massey and Burhop[50] in 1938. Taking account of retardation effects, spin-spin interaction, and electron exchange effect, and using the matrix element given by the same form as Eq. (14'), the total cross sections have been calculated for the following three cases: (1) Nonrelativistic approximation similar to Brunings' method, (2) relativistic calculation using plane wave for the positron wave function, and (3) relativistic calculation allowing for repulsive influence of the nucleus using the distorted wave function for the incident positron. In cases (1) and (2) they assumed that the incident energy of the positron is so large that its wave function is adequately represented by a plane wave. Since the ejected electron has large kinetic energy, the wave function for this electron is always taken as a plane wave. The main difference between (1) and (2) in low energy region of incident positrons consists in retardation effects.

We shall first derive the formula of the cross section for the cases (1) and (2). Choosing the polar axis along the direction of motion of the incident positron, the positron wave function is expressed as

$$\phi_+(r) = (1+\Delta_+^2)^{-1/2} e^{-ip_+ z/\hbar} (1, 0, -\Delta_+, 0) , \qquad (26)$$

Corresponding to the two possible spin orientations, the wave functions of the ejected electrons are written by

$$\left.\begin{aligned}\phi_-^{\uparrow}(\boldsymbol{r}) &= (1+\Delta_-^2)^{-1/2} e^{i p_- \boldsymbol{n}\cdot\boldsymbol{r}/\hbar} \left(-\Delta_- \cos\theta, -\Delta_- \sin\theta e^{i\varphi}, 1, 0\right) \\ \phi_-^{\downarrow}(\boldsymbol{r}) &= (1+\Delta_-^2)^{-1/2} e^{i p_- \boldsymbol{n}\cdot\boldsymbol{r}/\hbar} \left(-\Delta_- \sin\theta e^{-i\varphi}, \Delta_- \cos\theta, 0, 1\right)\end{aligned}\right\}, \tag{27}$$

where $\boldsymbol{n}(\theta,\varphi)$ is a unit vector in the direction of ejection of the electron.

The K-shell wave functions are as usual,[54]

$$\psi_\alpha(\boldsymbol{r}) = N_K\, g(r) \left(-i\Delta_0 \cos\theta, -i\Delta_0 \sin\theta e^{i\phi}, 1, 0\right), \tag{28a}$$

$$\psi_\beta(\boldsymbol{r}) = N_K\, g(r) \left(i\Delta_0 \sin\theta e^{-i\phi}, -i\Delta_0 \cos\theta, 0, -1\right), \tag{28b}$$

with

$$g(r) = e^{-Zr/a_0}\, r^{\sqrt{1-\gamma^2}-1},$$

$$N_K = \left\{\left(\frac{2Z}{a_0}\right)^{1+2\sqrt{1-\gamma^2}} \frac{1+\sqrt{1-\gamma^2}}{8\pi\,\Gamma(1+2\sqrt{1-\gamma^2})}\right\}^{1/2}.$$

In the above expression Δ_-, Δ_+, Δ_0, and γ is same as in the preceding section, and a_0 is the first Bohr radius of hydrogen.

Using these wave functions and expanding $e^{-i p_+ z/\hbar}$, $e^{i p_- \boldsymbol{n}\cdot\boldsymbol{r}/\hbar}$, and retardation factor into spherical harmonics, we can carry out angular integrations and spin summations by the use of the integral and addition formula for spherical harmonics. The total cross section for this annihilation process thus obtained is expressed as

$$\sigma = r_0^2 \frac{256\pi^3 N_K^4 p_- E_- E_+}{(1+\Delta_+^2)(1+\Delta_-^2)\, p_+} \sum_n \frac{1}{2n+1} \left\{ n(n+1)\left|A_{1n}\right|^2 + \left|A_{2n}\right|^2 \right\}, \tag{29}$$

where $\hbar/m_0 c$, c, and m_0 are taken as units of length, velocity, and mass, respectively. A_{1n} and A_{2n} are expressed as

$$\begin{aligned} A_{1n} = {} & 3\Delta_- (\alpha_{n-1}\delta_{n-1}\beta_{n-1} - \alpha_{n+1}\delta_{n+1}\beta_{n+1}) + i\Delta_0 (\alpha_{n+1}\delta_{n+1}\beta_n \\ & - \alpha_{n-1}\delta_{n-1}\beta_n - \alpha_{n-1}\delta_n\beta_n + \alpha_{n+1}\delta_n\beta_n) \\ & - i\Delta_0\Delta_+\Delta_- (\alpha_n\delta_n\beta_{n-1} - \alpha_n\delta_n\beta_{n+1} + \alpha_n\delta_{n-1}\beta_{n-1} \\ & - \alpha_n\delta_{n+1}\beta_{n+1}) + \Delta_0^2\Delta_- (\alpha_{n-1}\delta_n\beta_{n-1} - \alpha_{n+1}\delta_n\beta_{n+1}) \\ & - \Delta_0^2\Delta_+ (\alpha_n\delta_{n+1}\beta_n - \alpha_n\delta_{n-1}\beta_n) . \end{aligned} \tag{30}$$

$$\begin{aligned} A_{2n} = {} & (2n+1)\Delta_+\alpha_n\delta_n\beta_n - 3\Delta_- (n\alpha_{n-1}\delta_{n-1}\beta_{n-1} \\ & + \overline{n+1}\,\alpha_{n+1}\delta_{n+1}\beta_{n+1}) + i\Delta_0 (n\alpha_{n-1}\delta_{n-1}\beta_n + \overline{n+1}\,\alpha_{n+1}\delta_{n+1}\beta_n \\ & + n\alpha_{n-1}\delta_n\beta_n + \overline{n+1}\,\alpha_{n+1}\delta_n\beta_n) + i\Delta_0\Delta_+\Delta_- (n\alpha_n\delta_{n-1}\beta_{n-1} \\ & + \overline{n+1}\,\alpha_n\delta_{n+1}\beta_{n+1} + n\alpha_n\delta_n\beta_{n-1} + \overline{n+1}\,\alpha_n\delta_n\beta_{n+1}) \\ & + 3\Delta_0^2\Delta_+ (\overline{n+1}\,\alpha_n\delta_{n+1}\beta_n + n\alpha_n\delta_{n-1}\beta_n) \\ & - \Delta_0^2\Delta_- (\overline{n+1}\,\alpha_{n+1}\delta_n\beta_{n+1} + n\alpha_{n-1}\delta_n\beta_{n-1}) . \end{aligned} \tag{31}$$

where $\alpha_u\delta_v\beta_w$ means the radial integral

$$\alpha_u\delta_v\beta_w = \iint g(r_1)\alpha_u(r_1)\delta_v(r_1,r_2)\beta_w(r_2)g(r_2)r_1^2r_2^2\,dr_1\,dr_2 ,$$

with

$$\alpha_n(r_1) = i^n j_n(p_+ r_1) ,$$

$$\beta_n(r_2) = (-i)^n j_n(p_- r_2) ,$$

$$\delta_n(r_1,r_2) = \begin{cases} k_0\, j_n(k_0 r_1)\, h_n(k_0 r_2) & r_1 < r_2 \\ k_0\, j_n(k_0 r_2)\, h_n(k_0 r_1) & r_1 \geq r_2 \end{cases} ,$$

$$k_0 = E_- - E_d .$$

In nonrelativistic case, Δ_+, Δ_0, all retardation effects, and all terms in series excepting those involving $\alpha_0\delta_0\beta_0$ were neglected. With these approximations

$$\alpha_0\delta_0\beta_0 = \frac{2\gamma(10\gamma^2+p_+^2+p_-^2)}{(p_+^2+\gamma^2)(p_-^2+\gamma^2)\{4\gamma^2+(p_+-p_-)^2\}\{4\gamma^2+(p_++p_-)^2\}} . \tag{32}$$

Numerical calculations were carried out for positrons of energies 100, 300, and 500 keV using Eq. (29) and also nonrelativistic approximation. In evaluating Eq. (29) the radial integral $\alpha_u\delta_v\beta_w$ was calculated by double numerical integration. Terms involving values of u greater than 3 were neglected, since they were unimportant from the decrease of $j_u(p_-r_1)$ at small r_1. Results of the calculations for lead are given in the second and third rows of Table I.

In the lower energy region the distortion of the incident positron wave function by the atomic nucleus becomes important. To allow for this we replace the expression (26) by the following which represents the wave function of an electron in a state of negative kinetic energy moving in the Coulomb field of a charge Ze.[55]

$$\phi_+(\mathbf{r}) = (1+\Delta_+^2)^{-1/2}\,(1,\,0,\,-\Delta_+,\,0)\,\chi_+(r) , \tag{33}$$

$$\chi_+(r) = i\sum\left[n\zeta_n' + (n+1)\zeta_{n+1}' + n\mathcal{B}_n\zeta_n + (n+1)\mathcal{B}_{-n-1}\zeta_{n+1}\right](-1)^n P_n(\cos\theta) , \tag{33'}$$

where

$$\zeta_n = \frac{\Gamma(k+1-i\eta)}{\Gamma(2k+1)} (2p_+r)^{k-1} e^{-ip_+r} \exp\left(-\tfrac{1}{2}\pi\eta + \tfrac{1}{2}\pi i k\right)$$
$$\times F(k+1-i\eta, 2k+1, 2ip_+r),$$

$$\zeta_n' = \frac{\Gamma(k+1+i\eta)}{\Gamma(2k+1)} (2p_+r)^{k-1} e^{-ip_+r} \exp\left(-\tfrac{1}{2}\pi\eta - \tfrac{1}{2}\pi i k\right)$$
$$\times F(k+1+i\eta, 2k+1, 2ip_+r),$$

$$B_n = -\frac{n+i\eta'}{k+i\eta} \frac{\Gamma(k+1+i\eta)}{\Gamma(k+1-i\eta)} e^{-\pi i k},$$

$$k = (n^2-\gamma^2)^{1/2},$$

$$\eta = \frac{\gamma c}{v_+},$$

$$\eta' = \eta(1-v_+^2/c^2)^{1/2},$$

and $F(a,b;c)$ is the hypergeometric function.[56] Eqs. (30) and (31) then remain unaltered provided that α_n is replaced by the expression

$$\alpha_n = \frac{i}{2n+1}\left\{n\zeta_n' + (n+1)\zeta_{n+1}' + nB_n\zeta_n + (n+1)B_{-n-1}\zeta_{n+1}\right\}. \quad (34)$$

Numerically evaluating the distorted wave function from the series for the hypergeometric functions involved, the calculation of the double integrals proceeded as before. The distortion was only taken into account for the first two terms of the series. Values obtained in this way for lead are given in the fourth row of Table I. Neglection of the

influence of retardation is mainly responsible for the difference between the values in the second and third rows of Table I for low energy region. At higher energies the main defect of the nonrelativistic calculation comes from neglection of the higher terms of the series in Eq. (32).

Exact calculations led to the conclusion that the total cross section for radiationless annihilation in lead has a maximum value of 0.35×10^{-26} cm^2 for incident positrons of energy 300 keV. It is noted, however, that, strictly speaking, the expression for $\phi_+(\mathbf{r})$ in Eq. (33) is not correct when dealing with a Coulomb field. The second and fourth components do not vanish completely nor is the third component exactly Δ_+ times the first, as would be the case for plane waves.

The contribution from radiationless annihilation by other pairs of atomic electrons in lead was calculated by making the same approximations as those employed in deriving the nonrelativistic formula for the K-K pair. The results obtained in this way for positrons of 100 keV kinetic energy are given in Table II.

CHAPTER III

ADVANCED THEORETICAL CALCULATIONS

To compare with our experimental result, theoretical calculations of the radiationless annihilation of positrons have been made relativistically for a lead atom. The expressions for the total cross sections have been developed for various pairs of shell electrons involving retardation effects, electron exchange, and spin-spin interaction. The bound-state wave functions used are solutions to Dirac's relativistic equation. The incident positron and the ejected electron are described by the Darwin series solutions of the Dirac equation for an electron in the Coulomb field of a nucleus. Each of these continuum wave functions is written as a sum over partial waves. The angular integrations and the sumations over possible spin directions of continuum states and over projection quantum numbers are performed analytically and the results are expressed in terms of angular momentum coupling coefficients. The cross sections are evaluated numerically by an electronic computer and the results for the K-K pair in good agreement with the previous work. The numerical results for various pairs of atomic electrons for positrons of incident energy of 300 keV as well as for the K-K pair for various incident energies are presented in this chapter.

1. Calculation of the Cross Section

The total cross section for radiationless annihilation of positrons are calculated relativistically for the case where both the initial and final electrons as well as the incident positron are considered to be moving in a pure Coulomb field. This implies that higher order effects will be neglected, and the interaction of the electron with the radiation will be treated in lowest order perturbation theory. Furthermore, we neglect the effects of finite nuclear size. With these assumptions the total cross section can be written from Eq. (18), using natural units with $\hbar = m_0 = c = 1$, as

$$\sigma = \frac{E_+ E_- p_-}{(2\pi)^2 p_+} \int \delta(E_+ + E_\alpha + E_\beta - E_-) \sum |A|^2 \, d\Omega_{p_-}. \quad (18')$$

The matrix element A is given by

$$A = B - C \,, \quad (35)$$

where

$$B = e^2 \int d\mathbf{r}_1 \, d\mathbf{r}_2 \, \phi_+^*(\mathbf{r}_1) \, \phi_-^*(\mathbf{r}_2) \, (1 - \boldsymbol{\alpha}_1 \cdot \boldsymbol{\alpha}_2) \, \frac{e^{ik_0 R}}{R} \, \psi_\alpha(\mathbf{r}_1) \, \psi_\beta(\mathbf{r}_2), \quad (35'a)$$

$$C = e^2 \int d\mathbf{r}_1 \, d\mathbf{r}_2 \, \phi_+^*(\mathbf{r}_1) \, \phi_-^*(\mathbf{r}_2) \, (1 - \boldsymbol{\alpha}_1 \cdot \boldsymbol{\alpha}_2) \, \frac{e^{ik_0 R}}{R} \, \psi_\beta(\mathbf{r}_1) \, \psi_\alpha(\mathbf{r}_2). \quad (35'b)$$

In these expressions $\sum$ indicates the average over spin directions of the incident positron and the sums over those of the ejected electron and magnetic quantum numbers of the atomic electrons concerned, $\delta(E_\alpha + E_\beta + E_+ - E_-)$ is the usual δ function, k_0 is the energy transfer in the transition,

e is the charge of the electron, R is the distance between $\mathbf{r}_1$ and $\mathbf{r}_2$, and $\boldsymbol{\alpha}_1$ and $\boldsymbol{\alpha}_2$ are the Dirac matrices,

$$\boldsymbol{\alpha} = \begin{pmatrix} 0 & \boldsymbol{\sigma} \\ \boldsymbol{\sigma} & 0 \end{pmatrix}, \qquad (36)$$

where the σ_i being 2 X 2 Pauli matrices. We denote the energy-momentum vectors of the positron and ejected electron by $(\mathbf{p}_+, iE_+)$ and $(\mathbf{p}_-, iE_-)$, respectively. The wave functions in the matrix element are solutions of the Dirac equation in the Coulomb field of a nucleus: $\psi_\alpha(\mathbf{r})$ and $\psi_\beta(\mathbf{r})$ are for the bound states, $\phi_+(\mathbf{r})$ is for the positron, and $\phi_-(\mathbf{r})$ is for the free electron.

The bound-state wave function in the Coulomb field is given by

$$\psi_\mu(\mathbf{r}) = \begin{pmatrix} g_\kappa(\lambda r)\ \chi_\kappa^\mu(\hat{r}) \\ i f_\kappa(\lambda r)\ \chi_{-\kappa}^\mu(\hat{r}) \end{pmatrix}. \qquad (37)$$

The angular part of Eq. (37) is expressed by[57]

$$\chi_\kappa^m(\hat{r}) = \sum_\tau C(l\,\tfrac{1}{2}\,j;\, m-\tau\ \tau)\, Y_l^{m-\tau}(\hat{r})\, \chi^\tau, \qquad (38)$$

where χ^τ are the Pauli spinors, $C(j_1 j_2 j_3;\, m_1 m_2)$ is the Clebsh-Gordan coefficient, $Y_l^m(\hat{r})$ are the spherical harmonics, $\kappa = \mp(j+\tfrac{1}{2})$ for $j = l \pm \tfrac{1}{2}$, and $\hat{r}$ is a unit vector in the direction of $\mathbf{r}$.

In Eq. (38) l is determined from κ in the following way:

$$l = \kappa \quad \text{for} \quad \kappa > 0,$$
$$l = -\kappa - 1 \quad \text{for} \quad \kappa < 0,$$

while $-\kappa$ gives the value of l according to

$$l = \kappa - 1 \quad \text{for } \kappa > 0,$$

$$l = -\kappa \quad \text{for } \kappa < 0.$$

The angular-momentum coupling coefficients and the spherical harmonics used in this section are those as defined in reference 57.

The continuum-state solution of the Dirac equation for a Coulomb field is[58]

$$\phi_\kappa(\mathbf{r}) = 4\pi \sum_{km} P_{\kappa m}(\hat{p}, \hat{\xi})\, i^l e^{-i\delta_\kappa'} \begin{pmatrix} g_\kappa(r)\, \chi_\kappa^m(\hat{r}) \\ i f_\kappa(r)\, \chi_{-\kappa}^m(\hat{r}) \end{pmatrix}, \tag{39}$$

where the κ sum runs over all nonzero integers and $\hat{\xi}$ is a unit vector in the direction of the electron's spin, and

$$P_{\kappa m}(\hat{p}, \hat{\xi}) = \chi_\kappa^{m*}(\hat{p})\, \chi^\xi, \quad \delta_\kappa' = \eta - \frac{\pi}{2}\gamma - \arg(\gamma + i\gamma) + \frac{l+1}{2}\pi.$$

The positron wave function, which is chosen to represent asymptotically a distorted plane wave with an ingoing spherical wave, is given by

$$\phi_\kappa(\mathbf{r}) = 4\pi \sum_{km} P_{\kappa m}(\hat{p}, -\hat{\xi})\, i^l e^{-i\delta_\kappa'} \begin{pmatrix} -i f_\kappa^c(r)\, \chi_{-\kappa}^m(\hat{r}) \\ g_\kappa^c(r)\, \chi_\kappa^m(\hat{r}) \end{pmatrix}, \tag{40}$$

where

$$P_{\kappa m}(\hat{p}, -\hat{\xi}) = \chi_\kappa^{m*}(\hat{p})\, \chi^{-\xi}.$$

$f_\kappa(\lambda r)$, $g_\kappa(\lambda r)$, $f_\kappa(r)$ and $g_\kappa(r)$ are the radial parts of the wave functions representing the initial and final

electron states, respectively, and $f_\kappa^c(r)$ and $g_\kappa^c(r)$ are those of the continuum positron; the normalization of these continuum states is chosen to give the proper asymptotic form.

We now introduce the well-known expression of the retardation factor

$$\frac{e^{ik_0R}}{4\pi R} = ik_0 \sum_{\ell m} h_\ell(k_0 r_>)\, j_\ell(k_0 r_<)\, Y_\ell^{m*}(\hat{r}_1)\, Y_\ell^{m}(\hat{r}_2)\,, \qquad (41)$$

where j_ℓ is the spherical Bessel function of order ℓ, h_ℓ is the spherical Hankel function of the first kind of order ℓ, and $r_>$ is the greater and $r_<$ the lesser of r_1 and r_2. The above expression does not converge uniformly with respect to both variables r_1 and r_2 for unrestricted values of the variables. Consequently, term by term integration of the series has to be introduced with appropriate care.

Using above representations for the electron and positron wave functions and inserting Eq. (41) into Eq. (35a'), the matrix element B becomes

$$B = -(4\pi)^3 e^2 k_0 \sum_{\kappa_1\kappa_2\ell m_1 m_2 m} i^{-(\ell_1+\ell_2)} e^{i(\delta'_{\kappa_1}+\delta'_{\kappa_2})} \mathcal{P}^*_{\kappa_1 m_1}(\hat{p}_+,-\hat{\varsigma}_1)\, \mathcal{P}^*_{\kappa_2 m_2}(\hat{p}_-,\hat{\varsigma}_2)$$

$$\times \Big\{ B_{-\kappa_1\kappa_2\kappa_3\kappa_4} I^{(1)}_{\kappa_1\kappa_2\ell} + B_{-\kappa_1-\kappa_2\kappa_3-\kappa_4} I^{(2)}_{\kappa_1\kappa_2\ell} + B_{\kappa_1\kappa_2-\kappa_3\kappa_4} I^{(3)}_{\kappa_1\kappa_2\ell} + B_{\kappa_1-\kappa_2-\kappa_3-\kappa_4} I^{(4)}_{\kappa_1\kappa_2\ell}$$

$$+ B'_{-\kappa_1\kappa_2-\kappa_3+\kappa_4} I^{(5)}_{\kappa_1\kappa_2\ell} - B'_{-\kappa_1-\kappa_2-\kappa_3\kappa_4} I^{(6)}_{\kappa_1\kappa_2\ell} - B'_{\kappa_1\kappa_2\kappa_3-\kappa_4} I^{(7)}_{\kappa_1\kappa_2\ell} + B'_{\kappa_1-\kappa_2\kappa_3\kappa_4} I^{(8)}_{\kappa_1\kappa_2\ell} \Big\}, \qquad (42)$$

where the subscript 1 refers to the incident positron, 2 to the ejected electron, 3 and 4 to the atomic electrons concerned.

The radial integrals $I^{(1)}_{K_1K_2\ell}$ ——— $I^{(8)}_{K_1K_2\ell}$ appeared in Eq. (42) are given by

$$I^{(1)}_{K_1K_2\ell} = \iint f^{c*}_{K_1}(r_1)\, g_{K_3}(\lambda r_1)\, g^{*}_{K_2}(r_2)\, g_{K_4}(\lambda r_2)\, h_\ell(k_0 r_>)\, j_\ell(k_0 r_<)\, r_1^2 r_2^2 dr_1 dr_2, \quad (43a)$$

$$I^{(2)}_{K_1K_2\ell} = \iint f^{c*}_{K_1}(r_1)\, g_{K_3}(\lambda r_1)\, f^{*}_{K_2}(r_2)\, f_{K_4}(\lambda r_2)\, h_\ell(k_0 r_>)\, j_\ell(k_0 r_<)\, r_1^2 r_2^2 dr_1 dr_2, \quad (43b)$$

$$I^{(3)}_{K_1K_2\ell} = \iint g^{c*}_{K_1}(r_1)\, f_{K_3}(\lambda r_1)\, g^{*}_{K_2}(r_2)\, g_{K_4}(\lambda r_2)\, h_\ell(k_0 r_>)\, j_\ell(k_0 r_<)\, r_1^2 r_2^2 dr_1 dr_2, \quad (43c)$$

$$I^{(4)}_{K_1K_2\ell} = \iint g^{c*}_{K_1}(r_1)\, f_{K_3}(\lambda r_1)\, f^{*}_{K_2}(r_2)\, f_{K_4}(\lambda r_2)\, h_\ell(k_0 r_>)\, j_\ell(k_0 r_<)\, r_1^2 r_2^2 dr_1 dr_2, \quad (43d)$$

$$I^{(5)}_{K_1K_2\ell} = \iint f^{c*}_{K_1}(r_1)\, f_{K_3}(\lambda r_1)\, g^{*}_{K_2}(r_2)\, f_{K_4}(\lambda r_2)\, h_\ell(k_0 r_>)\, j_\ell(k_0 r_<)\, r_1^2 r_2^2 dr_1 dr_2, \quad (43e)$$

$$I^{(6)}_{K_1K_2\ell} = \iint f^{c*}_{K_1}(r_1)\, f_{K_3}(\lambda r_1)\, f^{*}_{K_2}(r_2)\, g_{K_4}(\lambda r_2)\, h_\ell(k_0 r_>)\, j_\ell(k_0 r_<)\, r_1^2 r_2^2 dr_1 dr_2, \quad (43f)$$

$$I^{(7)}_{K_1K_2\ell} = \iint g^{c*}_{K_1}(r_1)\, g_{K_3}(\lambda r_1)\, g^{*}_{K_2}(r_2)\, f_{K_4}(\lambda r_2)\, h_\ell(k_0 r_>)\, j_\ell(k_0 r_<)\, r_1^2 r_2^2 dr_1 dr_2, \quad (43g)$$

$$I^{(8)}_{K_1K_2\ell} = \iint g^{c*}_{K_1}(r_1)\, g_{K_3}(\lambda r_1)\, f^{*}_{K_2}(r_2)\, g_{K_4}(\lambda r_2)\, h_\ell(k_0 r_>)\, j_\ell(k_0 r_<)\, r_1^2 r_2^2 dr_1 dr_2, \quad (43h)$$

and the angular coupling coefficients by

$$\mathcal{B}_{K_1K_2K_3K_4} = \int \chi^{m_1*}_{K_1}(\hat{r}_1)\chi^{m_3}_{K_3}(\hat{r}_1) Y^{m*}_\ell(\hat{r}_1)\, d\Omega_1 \int \chi^{m_2*}_{K_2}(\hat{r}_2)\, \chi^{m_4}_{K_4}(\hat{r}_2) Y^{m}_\ell(\hat{r}_2)\, d\Omega_2, \quad (44a)$$

$$\mathcal{B}'_{K_1K_2K_3K_4} = \int \chi^{m_1*}_{K_1}(\hat{r}_1)\,\sigma\,\chi^{m_3}_{K_3}(\hat{r}_1) Y^{m*}_\ell(\hat{r}_1)\, d\Omega_1 \int \chi^{m_2*}_{K_2}(\hat{r}_2)\,\sigma\,\chi^{m_4}_{K_4}(\hat{r}_2) Y^{m}_\ell(\hat{r}_2)\, d\Omega_2, \quad (44b)$$

where σ is the well-known Pauli matrix, and $d\Omega_1$ and $d\Omega_2$ are the elements of solid angles subtended by $\mathbf{r}_1$ and $\mathbf{r}_2$.

Integrating over the solid angles $d\Omega_1$ and $d\Omega_2$, and using the Wigner-Eckart theorem, Eqs. (44a) and (44b) can be written as (See Appendix I)

$$B_{\kappa_1\kappa_2\kappa_3\kappa_4} = (-)^{m_1+m_2+m+1} \frac{1}{4\pi[l]} \sqrt{[j_1][j_2][j_3][j_4][l_1][l_2][l_3][l_4]}$$

$$\times C(l_1 l_3 l; 00)\, C(l_2 l_4 l; 00)\, C(j_1 j_3 l; -m_1 m_3)\, C(j_2 j_4 l; -m_2 m_4)$$

$$\times W(j_1 j_3 l_1 l_3; l\tfrac{1}{2})\, W(j_2 j_4 l_2 l_4; l\tfrac{1}{2})\, \delta_{m_3-m_1,m}\, \delta_{m_2-m_4,m}\,, \qquad (45a)$$

$$B'_{\kappa_1\kappa_2\kappa_3\kappa_4} = (-)^{m_3-m_1} \frac{6[l]}{4\pi} \sqrt{[j_3][j_4][l_3][l_4]}\, C(l_3 l l_1; 00)\, C(l_4 l l_2; 00)$$

$$\times \sum_{f_1 f_2} \sqrt{[f_1][f_2]}\, W(l l_3 j_1 \tfrac{1}{2}; l_1 f_1)\, W(l l_4 j_2 \tfrac{1}{2}; l_2 f_2)\, W(1\tfrac{1}{2} f_1 l_3; \tfrac{1}{2} j_3)$$

$$\times W(1\tfrac{1}{2} f_2 l_4; \tfrac{1}{2} j_4)\, C(j_3 1 f_1; m_3\, m_1+m-m_3)\, C(j_4 1 f_2; m_4\, m_2-m-m_4)$$

$$\times C(l f_1 j_1; -m\, m_1+m)\, C(l f_2 j_2; m\, m_2-m)\, \delta_{m_1+m_2,\, m_3+m_4}\,, \qquad (45b)$$

where $[j] = 2j + 1$, $j = |\kappa| - \tfrac{1}{2}$, and $W(abcd;ef)$ is the Racah coefficient.

The matrix element C is easily obtained from Eq. (45a) and (45b) by exchanging (j_3, l_3, m_3) for (j_4, l_4, m_4). With the aid of the these representations, we can obtain the matrix element A.

Squaring the matrix element A, summing over positron and electron spins, ζ_1 and ζ_2, and integrating over the solid

angle $\Delta\Omega_{p_-}$, we can carry out the sums over m, m_1, m_2, m_3, and m_4.

For simplicity, by choosing the z axis along the direction of the incident positron beam we can write

$$Y_{l_1}^{m_1-\tau_1}(\hat{p}_+) = \left(\frac{2l_1+1}{4\pi}\right)^{1/2} \delta_{m_1,\tau_1}, \qquad (46)$$

where $\delta_{i,j}$ is the Kronecker symbol. Then since

$$\chi_{\kappa_1}^{m_1}(\hat{p}_+) = \left(\frac{2l_1+1}{4\pi}\right)^{1/2} C(l_1 \tfrac{1}{2} j_1; 0 m_1)\, \chi^{m_1}, \qquad (47)$$

the sum over positron spins becomes

$$\sum_{\xi_1} P^*_{\kappa_1 m_1}(\hat{p}_+, -\hat{\xi}_1) P_{\bar{\kappa}_1 \bar{m}_1}(\hat{p}_+, -\hat{\xi}_1) = \frac{\sqrt{[l_1][\bar{l}_1]}}{4\pi} C(l_1 \tfrac{1}{2} j_1; 0 m_1)\, C(\bar{l}_1 \tfrac{1}{2} \bar{j}_1; 0 m_1). \qquad (48)$$

Similarly the sum over final electron spins gives

$$\begin{aligned}\sum_{\xi_2} P^*_{\kappa_2 m_2}(\hat{p}_-, \hat{\xi}_2) P_{\bar{\kappa}_2 \bar{m}_2}(\hat{p}_-, \hat{\xi}_2) &= \chi^{m_2 *}_{\kappa_2}(\hat{p}_-)\, \chi^{\bar{m}_2}_{\bar{\kappa}_2}(\hat{p}_-) \\ &= \sum_{\tau_2 \bar{\tau}_2} C(l_2 \tfrac{1}{2} j_2; m_2 - \tau_2\, \tau_2)\, C(\bar{l}_2 \tfrac{1}{2} \bar{j}_2; \bar{m}_2 - \bar{\tau}_2\, \bar{\tau}_2)\, (\chi^{\tau_2}, \chi^{\bar{\tau}_2}) \\ &\quad \times Y_{l_2}^{m_2-\tau_2 *}(\hat{p}_-)\, Y_{\bar{l}_2}^{\bar{m}_2-\bar{\tau}_2}(\hat{p}_-). \qquad (49)\end{aligned}$$

Integrating Eq. (49) over the full solid angle $\Delta\Omega_{p_-}$, we obtain

$$\begin{aligned}&\int d\Delta\Omega_{p_-} \sum_{\xi_2} P^*_{\kappa_2 m_2}(\hat{p}_-, \hat{\xi}_2) P_{\bar{\kappa}_2 \bar{m}_2}(\hat{p}_-, \hat{\xi}_2) \\ &= \sum_{\tau_2} C(l_2 \tfrac{1}{2} j_2; m_2 - \tau_2\, \tau_2)\, C(l_2 \tfrac{1}{2} \bar{j}_2; m_2 - \tau_2\, \tau_2)\, \delta_{l_2,\bar{l}_2}\, \delta_{m_2,\bar{m}_2} \\ &= \delta_{\kappa_2,\bar{\kappa}_2}. \qquad (50)\end{aligned}$$

Thus we can neglect sums over $\bar{\kappa}_2$, $\bar{m}_1$, and $\bar{m}_2$. The square of the matrix element A is expressed as

$$\sum_{K_1\bar{K}_1K_2\bar{K}_2 m_1\bar{m}_1 m_2\bar{m}_2 m_3 m_4 l\bar{l} m\bar{m}} A_{K_1K_2K_3K_4l} A_{\bar{K}_1\bar{K}_2\bar{K}_3\bar{K}_4\bar{l}}$$

$$= \sum_{K_1\bar{K}_1K_2 l\bar{l} m_1 m_2 m_3 m_4 m\bar{m}} A_{K_1K_2K_3K_4l} A_{\bar{K}_1K_2\bar{K}_3\bar{K}_4\bar{l}} . \qquad (51)$$

The resulting expression for the total cross section σ can be written as the following form:

$$\sigma = 8\pi e^4 E_+ E_- \frac{p_-}{p_+} \sum_{K_1K_2l\bar{l}} \{k_0^2 B\bar{B} - k_0 k_0' (B\bar{C}+\bar{B}C)$$

$$+ k_0'^2 C\bar{C}\}(1-\tfrac{1}{2}\delta_{k_0,k_0'}) , \qquad (52)$$

where k_0' is the energy transfer in the transition corresponding to the matrix element C, and $B\bar{B}$ is

$$B\bar{B} = \sum_{i=1}^{4}\sum_{j=1}^{4} B_i \bar{B}_j I^{(i)}_{K_1K_2l} I^{(j)*}_{K_1K_2\bar{l}} + \sum_{i=1}^{4}\sum_{j=5}^{8}((\pm)B_i \bar{B}'_j I^{(i)}_{K_1K_2l} I^{(j)*}_{K_1K_2\bar{l}}$$

$$+ (\pm)B'_i \bar{B}_j I^{(j)}_{K_1K_2l} I^{(i)*}_{K_1K_2\bar{l}}) + \sum_{i=5}^{8}\sum_{j=5}^{8}(\pm)B'_i \bar{B}'_j I^{(i)}_{K_1K_2l} I^{(j)*}_{K_1K_2\bar{l}} . \qquad (53)$$

In this expression $(\pm)$ denotes a sign depending on i and j. B_i is $(4\pi)^{3/2}$ times of $P^*_{K_1m_1}(\hat{p}_+,-\hat{\varsigma}_1) P^*_{K_2m_2}(\hat{p}_-,\hat{\varsigma}_2) \mathcal{B}_{K_1K_2K_3K_4}$ given in Eq. (42). B_i and $\bar{B}_i$ are related by the substitution:

$$l \longleftrightarrow \bar{l} , \quad l_3 \longleftrightarrow \bar{l}_3 , \quad l_4 \longleftrightarrow \bar{l}_4 .$$

$B\bar{C}$, $\bar{B}C$, and $C\bar{C}$ can be given by the expression similar to Eq. (53). For K-K and L_I - L_I cases where there are only two electrons in the shell, the summations over m_3 and m_4 give two times of the cross section. To avoid this a factor $(1 - \frac{1}{2}\delta_{k_0,k_0'})$ is multiplied.

In Eq. (53) products of coefficients of $I^{(i)}_{\kappa_1\kappa_2\ell}$'s after summations over magnetic quantum numbers are given by

$$B_i\bar{B}_j = \frac{[j_1][j_2][j_3][j_4][l_1][l_2]}{[\ell]}\sqrt{[l_3][l_4][\bar{l}_3][\bar{l}_4]}\,C(l_1 l_3 \ell;00)$$
$$\times C(l_2 l_4 \ell;00)\,C(l_1 \bar{l}_3 \ell;00)\,C(l_2 \bar{l}_4 \ell;00)\,W(j_1 j_3 l_1 l_3;\ell\tfrac{1}{2})$$
$$\times W(j_2 j_4 l_2 l_4;\ell\tfrac{1}{2})\,W(j_1 j_3 l_1 \bar{l}_3;\ell\tfrac{1}{2})\,W(j_2 j_4 l_2 \bar{l}_4;\ell\tfrac{1}{2})\,\delta_{l,\bar{l}}, \quad (54)$$

$$B_i\bar{B}'_j = (-)^{j_3+j_4+\ell+\bar{\ell}}\,6[j_1][j_2][j_3][j_4][\bar{\ell}]\sqrt{[l_1][l_2][l_3][l_4][\bar{l}_3][\bar{l}_4]}$$
$$\times C(l_1 l_3 \ell;00)\,C(l_2 l_4 \ell;00)\,C(\bar{l}_3 \bar{\ell} l_1;00)\,C(\bar{l}_4 \bar{\ell} l_2;00)$$
$$\times W(j_1 j_3 l_1 l_3;\ell\tfrac{1}{2})\,W(j_2 j_4 l_2 l_4;\ell\tfrac{1}{2})\,X\begin{pmatrix} \bar{\ell} & 1 & \ell \\ \bar{l}_3 & \tfrac{1}{2} & j_3 \\ l_1 & \tfrac{1}{2} & j_1 \end{pmatrix} X\begin{pmatrix} \bar{\ell} & 1 & \ell \\ \bar{l}_4 & \tfrac{1}{2} & j_4 \\ l_2 & \tfrac{1}{2} & j_2 \end{pmatrix}, \quad (55)$$

$$B'_i\bar{B}'_j = (-)^{\ell+\bar{\ell}}\,36[j_1][j_2][j_3][j_4][\ell][\bar{\ell}]\sqrt{[l_3][l_4][\bar{l}_3][\bar{l}_4]}$$
$$\times C(l_3 \ell l_1;00)\,C(l_4 \ell l_2;00)\,C(\bar{l}_3 \bar{\ell} l_1;00)\,C(\bar{l}_4 \bar{\ell} l_2;00)$$
$$\times \sum_L [L]\,X\begin{pmatrix} \ell & 1 & L \\ l_3 & \tfrac{1}{2} & j_3 \\ l_1 & \tfrac{1}{2} & j_1 \end{pmatrix} X\begin{pmatrix} \ell & 1 & L \\ l_4 & \tfrac{1}{2} & j_4 \\ l_2 & \tfrac{1}{2} & j_2 \end{pmatrix} X\begin{pmatrix} \bar{\ell} & 1 & L \\ \bar{l}_3 & \tfrac{1}{2} & j_3 \\ l_1 & \tfrac{1}{2} & j_1 \end{pmatrix} X\begin{pmatrix} \bar{\ell} & 1 & L \\ \bar{l}_4 & \tfrac{1}{2} & j_4 \\ l_2 & \tfrac{1}{2} & j_2 \end{pmatrix}, \quad (56)$$

where $X(abc;def;ghi)$ is the 9-j sympol, and $B'_i\bar{B}'_j$ is the same form as $B_i\bar{B}'_j$. Details of calculations of these coefficients are given in Appendix II.

The angular coupling coefficients in $B\bar{C}$ are expressed as (See Appendix III)

$$B_i \bar{C}_j = (-)^{j_1+j_2+j_3+j_4+l+\bar{l}+1} [j_1][j_2][j_3][j_4][l_1][l_2] \sqrt{[l_3][l_4][\bar{l}_3][\bar{l}_4]}$$
$$\times C(l_1 l_3 l; 00)\, C(l_2 l_4 l; 00)\, C(l_1 \bar{l}_4 \bar{l}; 00)\, C(l_2 \bar{l}_3 \bar{l}; 00)$$
$$\times W(j_1 j_3 l_1 l_3; l\,1/2)\, W(j_2 j_4 l_2 l_4; l\,1/2)\, W(j_1 j_4 l_1 \bar{l}_4; \bar{l}\,1/2)$$
$$\times W(j_2 j_3 l_2 \bar{l}_3; \bar{l}\,1/2)\, W(j_1 j_3 j_4 j_2; l\,\bar{l}) \,, \qquad (57)$$

$$B_i \bar{C}'_j = (-)^{j_1+j_2+l+\bar{l}+1} 6 [j_1][j_2][j_3][j_4][\bar{l}] \sqrt{[l_1][l_2][l_3][l_4][\bar{l}_3][\bar{l}_4]}$$
$$\times C(l_1 l_3 l; 00)\, C(l_2 l_4 l; 00)\, C(\bar{l}_4 \bar{l} l_1; 00)\, C(\bar{l}_3 \bar{l} l_2; 00)$$
$$\times W(j_1 j_3 l_1 l_3; l\,1/2) W(j_2 j_4 l_2 l_4; l\,1/2) \sum_L [L] X \begin{pmatrix} \bar{l} & 1 & L \\ \bar{l}_4 & 1/2 & j_4 \\ l_1 & 1/2 & j_1 \end{pmatrix}$$
$$\times X \begin{pmatrix} \bar{l} & 1 & L \\ \bar{l}_3 & 1/2 & j_3 \\ l_2 & 1/2 & j_2 \end{pmatrix} W(j_1 j_3 j_4 j_2; l\,L) \,, \qquad (58)$$

$$B'_i \bar{C}'_j = (-)^{j_1+j_2+j_3+j_4+l+\bar{l}+1} 36 [j_1][j_2][j_3][j_4][l][\bar{l}] \sqrt{[l_3][l_4][\bar{l}_3][\bar{l}_4]}$$
$$\times C(l_3 l l_1; 00)\, C(l_4 l l_2; 00)\, C(\bar{l}_4 \bar{l} l_1; 00)\, C(\bar{l}_3 \bar{l} l_2; 00)$$
$$\times \sum_{LL'} [L][L'] X \begin{pmatrix} l & 1 & L \\ l_3 & 1/2 & j_3 \\ l_1 & 1/2 & j_1 \end{pmatrix} X \begin{pmatrix} l & 1 & L \\ l_4 & 1/2 & j_4 \\ l_2 & 1/2 & j_2 \end{pmatrix} X \begin{pmatrix} \bar{l} & 1 & L' \\ \bar{l}_4 & 1/2 & j_4 \\ l_1 & 1/2 & j_1 \end{pmatrix}$$
$$\times X \begin{pmatrix} \bar{l} & 1 & L' \\ \bar{l}_3 & 1/2 & j_3 \\ l_2 & 1/2 & j_2 \end{pmatrix} W(j_1 j_3 j_4 j_2; L L') \,. \qquad (59)$$

Coefficients for $\bar{B}C$ are the same forms as expressed by Eqs. (57) - (59).

2. Numerical Evaluation of the Radial Integrals

The radial parts, $I^{(1)}_{K,K,\ell}$ — $I^{(8)}_{K,K,\ell}$, of the matrix elements are written in terms of unspesified radial functions for the bound and continuum states. In this work analytical expressions for the bound and continuum radial wave functions are used, but it is necessary to treat the entire problem numerically because of the expression of retardation factor which contains $r_>$ and $r_<$ as variables. The discussion of this section is separated into three parts covering the bound-state wave function, continuum-state wave function, and radial integral problem.

A. The Bound State

The bound-state radial functions are solutions to Dirac's radial equations in a pure Coulomb potential

$$\frac{d}{dr}\begin{pmatrix} r g_K \\ r f_K \end{pmatrix} = \begin{pmatrix} -K/r & W+1+\frac{\alpha Z}{r} \\ -(W-1+\frac{\alpha Z}{r}) & K/r \end{pmatrix}\begin{pmatrix} r g_K \\ r f_K \end{pmatrix}, \qquad (60)$$

where W is the total energy of the bound electron and α is the fine structure constant. The solutions for K, L, and M shells are well known and of the form[58]

$$f_K = -N(1-W)^{1/2} r^{\gamma-1} e^{-\lambda r}(a_0 + a_1 r + a_2 r^2), \qquad (61a)$$

$$g_K = N(1+W)^{1/2} r^{\gamma-1} e^{-\lambda r}(c_0 + c_1 r + c_2 r^2), \qquad (61b)$$

where the values of the parameters are given in Table III.

Although the parameters for M shell are not listed in Rose's text,[58] they are easily obtained by neglecting higher order terms in series expansion of confluent hypergeometric functions. In Figs. 6 to 9 these bound-state radial functions multiplied by r are given in graphical form for lead.

B. The Continuum State

The continuum radial functions for the electron are also solutions to Eq. (60) and expressed as[59]

$$r f_\kappa = i\left(\frac{W-1}{2W}\right)^{1/2} \frac{(2pr)^\gamma e^{\pi y/2} |\Gamma(\gamma+iy)|}{2p\,\Gamma(2\gamma+1)} \left\{ e^{-ipr+i\eta}(\gamma+iy) \times F(\gamma+1+iy, 2\gamma+1, 2ipr) - c.c. \right\}, \qquad (62a)$$

$$r g_\kappa = \left(\frac{W+1}{2W}\right)^{1/2} \frac{(2pr)^\gamma e^{\pi y/2} |\Gamma(\gamma+iy)|}{2p\,\Gamma(2\gamma+1)} \left\{ e^{-ipr+i\eta}(\gamma+iy) \times F(\gamma+1+iy, 2\gamma+1, 2ipr) + c.c. \right\}, \qquad (62b)$$

with

$$\gamma = (\kappa^2 - \alpha^2 Z^2)^{1/2}, \quad y = \alpha Z W/p, \quad \alpha = e^2,$$

and

$$e^{2i\eta} = -\frac{\kappa - iy/W}{\gamma + iy}.$$

The radial functions for the continuum positron, f_κ^c and g_κ^c, are the same forms with those for the electron but with the sign of Z reversed.

The normalization of these continuum radial functions is done by matching them with free-field solutions at a point chosen so large that the Coulomb potential is negligible. The asymptotic solutions of free-field equations used in this purpose are

$$f_\kappa \xrightarrow[r\to\infty]{} \left[\frac{W-1}{2W}\right]^{1/2} \frac{1}{pr} \sin(pr+\delta_\kappa) , \qquad (63a)$$

$$g_\kappa \xrightarrow[r\to\infty]{} \left[\frac{W+1}{2W}\right]^{1/2} \frac{1}{pr} \cos(pr+\delta_\kappa) , \qquad (63b)$$

where

$$\delta_\kappa = \gamma \log(2pr) - \arg\Gamma(\gamma+i\gamma) + \eta - \tfrac{1}{2}\pi\gamma .$$

The distance of r_0 where this matching is done, is chosen equal to 100.

The confluent hypergeometric series in Eqs. (62a) and (62b) is evaluated by the following formula

$$F(a,b;z) = 1 + \frac{a}{b}z + \frac{a(a+1)}{b(b+1)}\frac{z^2}{2!} + \cdots + \frac{a(a+1)\cdots(a+n-1)}{b(b+1)\cdots(b+n-1)}\frac{z^n}{n!} + \cdots , \qquad (64)$$

and terminated when both the real and the imaginary parts are less than 10^{-6}.

Complex gamma functions are obtained from

$$\ln\Gamma(z) = (z-\tfrac{1}{2})\ln z - z + \tfrac{1}{2}\ln(2\pi) + \frac{1}{12z} - \frac{1}{360z^3} + \frac{1}{1260z^5} - \frac{1}{1680z^7} + \cdots . \qquad (65)$$

The argument, z, is first tested whether $Re(z) > 10$ or not.

When the argument does not satisfy this condition, the recurrence relation

$$\Gamma(z+1) = z\,\Gamma(z),$$

is used until $Re(z) > 10$. This routine is checked to 6 - 7 places against the Abramov's table.[60]

The real gamma functions are computed using the formula for $0 \leq x \leq 1$ from the NBS table[61] as

$$\Gamma(x+1) = 1 + a_1 x + a_2 x^2 + \cdots\cdots + a_5 x^5, \qquad (66)$$

where

$$a_1 = -0.5748464, \quad a_4 = 0.4245549,$$
$$a_2 = 0.9512363, \quad a_5 = -0.1010678.$$
$$a_3 = -0.6998588,$$

The arguments of real gamma functions are reduced by the following recurrence relation:

$$\Gamma(1+x) = x\,\Gamma(x) \quad \text{for } x \geq 1/2.$$

An accuracy of six significant figures is accomplished.

C. The Radial Integrals

The spherical Bessel function and spherical Hankel function are generated using recurrence relations and are checked against the NBS table[61] for selected values of l. The errors are less than one part in 10^5.

The radial integrals $I^{(1)}_{\kappa,\kappa_2 l}$ —— $I^{(8)}_{\kappa,\kappa_2 l}$ are evaluated by the double numerical integration using Simpson's rule with step size h. Contribution beyond r = 40 are neglected since the bound-state wave function has decreased by a factor of

10^{-5} from its maximum value.

Step sizes of h = 0.2 and 0.4 are considered. These two step sizes are used in selected cases and yield results which agree to three significant figures for the case of the K-K pair with the incident energy of positron of 300 keV. The step size adopted here is h = 0.4. Agreement is deteriorated somewhat at higher energies.

3. Numerical Results

Calculations to obtain the theoretical value of the cross section for this process in lead were carried out using the method previously described. Equation (18') was programmed for the Kyoto University's KDC-II Computer[62] for $_{82}$Pb, for an incident positron energy $E_+ = 1.587$ corresponding to the kinetic energy of 300 keV, and for the K, L, and M shells. Another program was written for also $_{82}$Pb and the K-K pair but for various incident positron energies. In both cases the sums over κ_1, κ_2, and l were terminated at $|\kappa_1| = 3$, $|\kappa_2| = 5$, and $l = 5$. All other parameters were determined in terms of $|\kappa_1|$ through the selection rules contained in the angular momentum coupling coefficients.

The total cross sections obtained for the annihilation of a positron by one of the K electrons in lead, the excess energy being used to eject the other K electron, can be compared with previous theoretical results of Brunings[49] and Massey and Burhop.[50] This comparison is given in Table I for positron kinetic energies of 100, 300, and 500 keV. The present results agree well with earlier relativistic calculations allowing for nuclear repulsion given by Massey and Burhop. In Fig. 10 is shown the calculated cross section for the K-K pair of the shell electrons in a lead atom as a function of the kinetic energy of the incident positron together with results of Massey and Burhop which are

represented by circles in the figure.

Table IV gives the calculated results for different pairs of atomic electrons in a lead atom for a positron having an incident kinetic energy of 300 keV. The kinetic energies of ejected shell electrons in this table are calculated from binding energies of various shell electrons in lead using the values of Wapstra *et al.*[63] The values for $K\text{-}M_{II}$, $L_I\text{-}M_I$, $L_{II}\text{-}L_I$, and other pairs of atomic electrons have not been calculated, since these seemed to be considerably small for this positron energy.

Errors in this calculation are ascribed to three sources; the number of partial waves included, radial integrals, and vector-coupling coefficients. As described in the preceding section, we limited the number of partial waves to $|K_1| = 3$ and $|K_2| = 5$. The number of partial waves needed to determine the total cross section to any desired accuracy increases with energy. For the ejected electron the energy of which is considerably high, more number of $|K|$'s seems to be necessary, but the error from this source is estimated to be 1%.

The errors in radial integrals are due to the errors of computer programs and of integration procedures. The errors in integration arises from the choise of the step size, h, and the upper limit of the integration, r_{max}.

The programs for determining Clebsch-Gordan and Racah coefficients, and 9-j sympols were checked against numerical

tables[64-68] and found to be in good agreement. Therefore, the main source of error comes from the first two of the above three.

CHAPTER IV

EXPERIMENTAL PROCEDURES

The experimental arrangement used in the present work is shown in Fig. 11. It consists of a Siegbahn-Slätis type intermediate-image beta-ray spectrometer, a lead target, and a lithium-drifted silicon junction detector. A monoenergetic positron beam was produced by the use of the beta-ray spectrometer mounted with ^{22}Na as a positron emitter, and entered the lead target in which annihilation took place. The solid state detector placed immediately behind the lead foil was used as an energy-selective detector for the electrons ejected from the target by the process to be studied. The output pulses from the detector were analyzed with a TMC 400-channel pulse-height analyzer.

Reflecting a very small probability expected for the radiationless annihilation, there should be several requirements, which are essential for the succesful performance of the experiment with this annihilation process. (1) The positron source should be considerably strong. (2) The beta-ray spectrometer should have high transmission. (3) This spectrometer has also to have high electron-to-positron rejection ratio. (4) The energy resolution of the energy--selective detector for the ejected electrons must be high. (5) The target material must be in the high-Z region.

In this chapter the performance of each of these apparatuses used in this work is discussed in detail and the experimental method used for the detection of electrons ejected by this mode of annihilation of positrons is described.

1. Positron Source

In the actual performance of the experiment, one has to consider some conditions for the radioactive nuclide used as a positron source.

First, the most favorable kinetic energy of incident positrons for this experiment is about 300 keV. The theoretical calculations indicate that the total cross section for the radiationless annihilation involving K-K pair of electrons within a lead atom has the maximum value for positrons of this kinetic energy, as shown in Fig. 10. Therefore, it is desirable that for a positron emitting nuclide to be used ratio of positrons in this energy region to the total number is as large as possible, i.e. the peak position of the positron spectrum from the source is in the vicinity of 300 keV.

Second, the half life of the positron emitter to be used should be considerably long. Owing to the rather low probability of the phenomenon, measurements have to be continued for long period. To avoid an appreciable change in the source intensity in the course of the measurements, the half life longer than a year is desirable.

Third, no gamma rays with energy of greater than 1 MeV do accompany the positron decay, or the internal conversion coefficient of the transition due to the de-exitation is not large, if gamma rays are emitted. The contributions from

gamma rays can be removed by the procedures described later. However, since the number of events which we want to observe is very small, conversion electrons of this energy, if leak through the beta-ray spectrometer, mask the peak due to the process to be studied and make it difficult to detect this process of annihilation experimentally.

Taking accounts of these requirements, it was concluded that ^{22}Na is the most convenient source for this experiment. Decay scheme of this nuclide is shown in Fig. 12.[69] The ground state of ^{22}Na has the half life of 2.60 y and β^+ decay from ^{22}Na feeding into the 1275-keV state in ^{22}Ne has the maximum energy of 543 keV. The relative intensity of this positron decay is considered about 90%. Although the 1275-keV de-excitation gamma ray follows the positron emission, the internal-conversion coefficient of this transition is so small, reported as $(6.77 \pm 0.45) \times 10^{-6}$, [70] that conversion electrons emitted from this transition would not interfere our measurements. Fig. 13 shows the positron spectrum from ^{22}Na which was measured by a Siegbahn-Slätis type beta-ray spectrometer with the solid--state detector used in this experiment. In this figure the low-energy portion of the spectrum is cut off by the discriminator used for output from the detector. It is seen from the figure that the peak position is about 200 keV and at 300 keV the number of positrons is about 75% of its maximum value in the energy spectrum, therefore positrons of energy of 300 keV are

obtained in good efficiency from this source.

The radioactive sodium chloride solution of very high specific activity obtained from the Radiochemical Centre at Amersham was concentrated by the evaporation method. The source was prepared by mounting an evaporation residuum of this solution on a slightly concave hole of 2.5 mm in diameter on a surface of pure aluminum foil of 5.4 mg/cm^2 thickness. On account of hygroscopic property of sodium chloride, it was covered by silver of about 0.1 mg/cm^2 using the vacuum deposition technique. The distortion effect of positron spectrum, which might be caused by the silver deposition, was checked by comparing the positron spectrum of ^{22}Na before and after the silver coating. A weak source of ^{22}Na-chloride of 1 mCi having the same form as the high-intensity source was also prepared by similar procedures. This source was used to check the effect of the silver deposition. These measurements were performed with the beta-ray spectrometer using another ^{22}Na source of lower intensity as a positron emitter and a G-M counter as a detector, and it was acertained that no such effect was observed in the energy region concerned with the present experiment. Total intensity of ^{22}Na in this source was estimated to be about 12 mCi, but the effective intensity of this source as a positron emitter was much smaller than this value owing to the rather large amount of solids (about 2.0 mg) in the evaporation residuum.

As an electron source the circular deposit of ^{32}P-HNO_3 of the same form as the sodium source but without silver coating was formed by evaporating the solution. The source strength was about 1 mCi. Using this ^{32}P and the weak ^{22}Na sources the measurements necessary for correction factors were also done, as described later.

2. Beta-ray Spectrometer

The beta-ray spectrometer used to get a monoenergetic positron beam in the whole course of the measurements was a Siegbahn-Slätis intermediate-image type manufactured by LKB-Produkter Fabriksaktiebolag in Sweden.[71]

The intermediate-image spectrometer is a special type of long-lens beta-ray spectrometer. In this spectrometer the field along the axis is shaped to be minimum between the source and the detector contrary to the ordinary lens type. At a certain field gradient the ring focus image is formed in the middle of the instrument, the so-called intermediate image focusing, whereafter a second, nearly point-shaped image is obtained on the axis in front of the detector, because the electron trajectories are approximately symmetrical with respect to a central plane perpendicular to the spectrometer axis. Then the electron optical geometry is determined by the distance between the source and the detector, and by the diameters and annular widths of the entrance slit near the source as well as the exit slit in the central plane shown by C in Fig. 11. The corresponding field gradient necessary to produce the intermediate image is found by varying the ratio of the currents through the different coils.

This spectrometer has several advantages over other types of instruments, which make it particularly suitable for the

present experiment. It has an excellent spiral electron--positron separation baffle with twelve blades made of brass sputtered by aluminum to reduce scattering effect of electrons and gamma rays, and in spite of introduction of this baffle it gives considerable high transmission at a given, moderate, resolving power. Furthermore, because of the existence of the second point image, a very small detector can be used with a consequent reduction in the background. This is in contrast to the state of affairs in the solenoidal and long-lens spectrometer, in which there is a considerable divergence of the trajectories beyond the ring focus. It is also very unlikely that electrons scattered from baffles or the walls of the vacuum chamber will reach the detector. This is of importance in cases such as this experiment having other strong backgrounds.

In Fig. 11 is shown the geometrical arrangement of the spiral separation baffle, annular slit with an opening of 0.8 mm, central lead gamma-ray stop covered by brass, lead shields limiting the stray electrons and gamma rays, and the detector. The annular slit C is situated perpendicularly to the axis at the mid-point of the spectrometer. Particles of the positive sign charge spiralling down along the axis of the spectrometer will be transmitted by the separation baffle S, while particles of negative sign charge will be stopped by this baffle. By sliding the position of the spiral

separator and adjusting the opening and position of the lead baffles near the detector, the condition for the highest value to the electron-to-positron rejection ratio was found. This ratio is defined as the ratio of the yield of electrons reaching the detector when the direction of the exciting coil current is set so as to forbid electrons through the separation baffle to the yield when the current is switched into the opposite direction.

In the intermediate-image focussing spectrometer with a spiral baffle, a few electrons which would reach the detector through the baffle when the current direction is set unfavourably for these electrons are considered to be all elastically scattered electrons from the blades of the spiral baffle.

The electron-to-positron rejection ratio was measured by the use of the internal K-conversion line of 625-keV from ^{137}Cs source for the same geometrical conditions as this experiment. The value obtained is about 2×10^{-5}. In the experiment of radiationless annihilation, there seems to be some leak of electrons which are ejected by internal conversion process of the 1275-keV state in ^{22}Ne. This leak of inelastically scattered electrons does not, however, interfere with the measurements of the electron spectrum to be studied, since the conversion coefficient of the 1275-keV transition is very small.

The kinetic energy of the positrons we selected using the beta-ray spectrometer, was fixed at 300 keV, near the maximum of the positron spectrum of ^{22}Na, to secure the highest possible beam intensity. The transmission of the spectrometer was reduced approximately to 65% of its original value by introducing the baffle system. The momentum resolution and overall transmission of this spectrometer in the present experimental conditions were found to be about 1.8% and 4.0%, respectively, for the 300-keV positrons.

3. Detector

The G-M tube or scintillation detector is frequently applied as a detector in the magnetic beta-ray spectrometer. However, as already pointed out on Chap. I, an energy-selective detector with high resolution is essential for the measurement of the ejected electrons from the target by the annihilation process. In the present experiment a lithium-drifted silicon junction detector was used for counting electrons because of its high energy-resolution for this particles and insensitivity to the presence of magnetic field.

The resolution of a plastic or anthracene scintillation detector depends on the energy of incident electrons, and, for instance, for the 625-keV K-conversion line of ^{137m}Ba the resolution is about 15%, while that of the solid state detector used in this work is 3.1% at room temperature. Moreover, when the scintillation detector is used in the magnetic beta-ray spectrometer, it is necessary to have the scintillator placed at some distance from the photomultiplier tube, since existing magnetic field may deteriorate the tube. A light guide for transferring the light from the scintillator to the multiplier tube must be used, but this decreases the light collection efficiency remarkably as well as makes the energy resolution poorer. Considering these facts, it seems to be very difficult to use the scintillation detector in order to observe the

electron spectrum as a result of the annihilation process to be studied. Therefore, the solid state detector is only suitable one for the present purpose.

In the past several years nuclear spectrometers have been prepared from semiconductor crystals and applied to many problems in nuclear physics. The major problem in the nuclear application arises from the finite range of the particle to be detected, with the resulting requirement that for optimum energy-spectrum measurement all the ionization produced by the particle should be within the electric field in the detector. At the early stage of the development the most successful solid-state radiation detectors have been the surface barrier and p-n junction silicon detectors. These units, while serving admirably for alpha particles, low-energy protons, deuterons, and fission fragments, are not suitable for measuring electrons, photons, high-energy protons, or minimum ionizing particles. This inherent restriction was imposed because of the shallow depletion region and low atomic number of the silicon. In these detectors it is difficult to achieve thick sensitive layers; depleted regions deeper than 0.5 mm equivalent to a range of about 400-keV electrons require high resistivity and high reverse bias. The poor availability of high resistivity silicon with satisfying properties for detector construction has limited the application of silicon detectors only to the low-energy electron spectroscopy.

A method to obtain deep sensitive layers with the added advantage of starting from an easily available p-type silicon, is the lithium-ion-drift technique developed by Pell.[72] In this method, silicon has been diffused with a lithium impurity, and resistivities as high as 10^5 ohm·cm and sensitive thicknesses up to several mm have been produced. Such detectors have shown very good response to electrons, gamma rays, and other long-range particles, and are especially suitable for spectroscopy of electrons with energies up to some MeV. The development of this type of solid state detector promised us the possibility for observing radiationless annihilation.

In this experiment, as shown in Fig. 11, immediately behind the lead foil, a lithium-drifted silicon junction detector was mounted as an energy-selective detector for the shell electrons ejected from the target by the process to be studied. This p-i-n junction detector with an i-layer of 2-mm thickness and 8 mm in diameter was prepared in our laboratory.[73] The area covered by the focused electron beam was smaller than the sensitive area of the detector. Its response to the incident monoenergetic electrons was examined by mounting it at the focus point of the spectrometer using a ^{32}P source, with and without lead foils of 35.0 and 75.3 mg/cm^2 before the detector. The relationship of pulse height vs electron energy observed was quite linear, even if the lead foil was situated before the detector, in the energy region from 150 to 1700 keV, as shown

in Fig. 14. Typical response of the silicon detector to electrons of 1146 keV, the presumed kinetic energy of the electrons ejected from the lead foil by the radiationless annihilation for the K-K pair in this atom, with and without the lead foil of 75.3 mg/cm^2 is shown in Fig. 15. The energy resolution and peak-to-total ratio for the incident monoenergetic electrons as a function of energy are also shown in Fig. 16 and Fig. 17, respectively.

There is a defect in the application of solid state detectors as radiation counter. This is due to radiation damage. Radiation can produce lattice defects in the single crystals in semiconductor detectors. The number and importance of these defects depend critically on the mass, charge, and energy of the incident particles as well as the nature of the detector structure employed. Lithium-drifted detectors are especially radiation-damage sensitive because of their low internal fields and consequent short trapping lengths. An added problem arises from the tendency of lithium to precipitate out on radiation-produced vacancies. Systematic study of the effect of radiation damage on this type of detectors has not yet been undertaken. But, Mann and Yntema[74] have studied this effect with protons, alpha particles, and fast neutrons, and Coleman and Rodgers[75] with ^{60}Co gamma rays. In general as a result of radiation damage a degradation of resolution and an increase of leakage current are observed.

In the view point of radiation damage, the thicker the lead foil is, the better is it for the present detector since the number of positrons transmitting it decreases. The optimum thickness of the lead target is determined taking into this fact. This is discussed in Sec. 4 in this chapter.

It is important to note that the solid state detector used as an electron spectrometer requires correction for the backscattering of electrons in the detector. This effect causes decrease in the number of electrons obtained from the measurement. This is considered in Sec. 5.

4. Target

The element used as a target must be chosen by considering the theoretical values of the cross section for radiationless annihilation. According to the rough estimation from the nonrelativistic formula, the cross section for radiationless annihilation will increase approximately proportionally to Z^2. This fact indicates that the high-Z material is favourable to observe this phenomenon. Therefore, lead (Z = 82) was considered to be most suitable for this investigation. There are two reasons why this element was chosen as the target:
(1) Pure foils of various thicknesses are easily obtained.
(2) The calculated cross section for the K-K pair in a lead atom has the maximum value in the visinity of incident-positron kinetic energy of 300 keV (See Fig. 10). The latter fact is very important when we use ^{22}Na source as a positron emitter. As shown in Fig. 13, positron spectrum from ^{22}Na has a broad peak about 200 keV, so we can use this positron source effectively.

A thin lead foil was used as a target placed at the focus point of the beta-ray spectrometer. This target was placed 1 mm before the detector and supported by an aluminum frame, as shown in Fig. 11.

It is very difficult to estimate the optimum thickness of the lead target. To secure the number of positrons, the target

must be as thick as possible within the range of incident positrons, while in order to reduce the attenuation effect of ejected electrons it is desired to be thin enough. Taking account of these requirements conflicting with each other, it is impossible to determine theoretically the thickness of the foil. Since no theory dealing with flux distribution of electrons and positrons in the foil has been developed, the target thickness was determined using the experimental data of numbers of electrons above 1 MeV ejected from the lead foils of various thicknesses. This series of measurements was performed in the same conditions as the present experiment. It was found that as the thickness of the foil is increased, the number of electrons reaching the solid state detector rises to a maximum, and then gradually decreases. The maximum is observed with the foil thickness being about the range of incident positrons. The reason for this behavior is a character of radiationless annihilation, i.e. a slow positron makes a collision with a lead atom and an electron of much greater kinetic energy is ejected. The energy loss of an electron traversing the foil is much less than that of a positron and so it is desirable to annihilate all the positrons in it. The value of the range of 300-keV positrons in lead is taken from the tabulation of Nelms[76] to be 166 mg/cm^2. The thickness of the foil used for the experiment was chosen to be 75.3 mg/cm^2 by using this value of the range and taking into account of

the incident angle of the positron beam to the target, which was estimated to be 60° in our beta-ray spectrometer.

The additional advantage of this thickness is that the target stops almost all the incident positrons. This target prevents large number of positrons from impinging upon the solid detector and causing the radiation damage. The main disadvantage of such a thick-target experiment lies in the fact that correction for the finite target thickness must be considered. Correction for this effect is discussed in the next chapter.

5. Detection Efficiency of the Detector

In order to obtain the cross section value, it is necessary to determine the detector response to monoenergetic positrons and electrons. This was done by analyzing the pulse-height spectrum observed by the detector. The response to monoenergetic particles could be reduced to two components; a Gaussian distribution and a low-energy tail. This tail is expected to be due mainly to positrons or electrons which backscatter out of the silicon crystal before losing their total energies. No remarkable difference between electrons and positrons with the same energy has been observed in the response of the solid detector and the backscattering coefficient in silicon, therefore the discussion below is limited to the case of the electron.

We can obtain the total number of electrons impinging upon the detector surface by summing up the number of counts for each channel in the observed pulse-height spectrum. However, in the p-i-n junction detector we must consider the effect of the dead layer due to the surface density of lithium and its diffusion depth. Our detector has a thin dead layer of about 10 μ, but the electron which loses its total energy or backscatters out of detector in this layer, is not counted by the detector. Furthermore, output pulses from a solid state detector distribute continuously as seen in the response curve (See Fig. 15), while those from a G-M counter has

constant height. Owing to this fact, we can easily separate noises from signals in the latter type of detector, but in the former the low-energy parts of signals are masked by disturbing noises. To avoid this effect, pulses from the solid detector are discriminated by electronic circuit. At the same time this discrimination cuts off the low-energy part of the electron spectrum. Therefore, the total number of electrons measured with the solid state detector is less than that of electrons incident on the detector surface.

The detection efficiency of the silicon detector is defined as the ratio of the total number of electrons detected by the solid detector to the number of electrons entering the detector. By mounting the silicon detector at the focus point of beta-ray spectrometer, the detection efficiency of the detector for positrons of 300 keV, ε_p, was estimated by comparing the counts with those measured by a G-M counter with a thin window of 0.625-mg/cm^2 thick rubber hydrochloride. In this case, taking into consideration the resolving time of the G-M counter, another ^{22}Na source of lower intensity was used. By a similar procedure but using a ^{32}P source we could estimated also ε_e, i.e. the detection efficiency for electrons with energies which would be expected for the shell electrons ejected from a lead atom by the annihilation process to be studied. Here, the detection efficiencies of the G-M counter with such a thin window for these positrons and electrons were

supposed to be 100%.

As shown in the next chapter, it is a ratio $\varepsilon_p/\varepsilon_e$ that is necessary for our experiment. The value of $\varepsilon_p/\varepsilon_e$ was thus estimated reasonably to be 1.00 ± 0.05.

6. Measurements

The solid-state electron spectrometer consists of a lithium-drifted silicon junction detector, a low-noise amplifier system, and a TMC 400-channel pulse-height analyzer. The detector was operated with a bias of 40 V at room temperature. The amplifier system is in many respects similar to ORTEC 101-201 low-noise amplifier system. The preamplifier connected to the detector has a low-noise charge-sensitive input circuit and pulse shaping consists of RC networks for two integrations and one differentiation, the time constants of which are all maintained equal to one microsecond. The pulses from the silicon detector were fed to the multichannel pulse-height analyzer through this amplifier system, and recorded with it.

After measurements of characteristics of the detector described in this chapter, such as response to monoenergetic electrons, detection efficiency for 300-keV positrons ε_p, peak--to-total ratio, and energy resolution, several exploratory runs were made to determine the optimum thickness of the target using lead targets of various thicknesses. On the basis of these data the target thickness was chosen to be 75.3 mg/cm^2. Then, electron spectra passing through this target were measured with various energies of incident electrons (See Fig. 15), and the relationship of channel number vs incident-electron energy (See Fig. 14) was obtained. Using these results, the

most probable kinetic energy of the ejected shell electrons from K-K pair in lead after passing through the target was determined and the detection efficiency for electrons of this energy ε_e was measured as mentioned in the previous section.

To estimate the cross section for this annihilation process we must measure the number of 300-keV positrons impinging upon the lead target. Considering the strong intensity of our positron source, direct measurement of positrons with the solid state detector seemed to be very difficult. The effective intensity of ^{22}Na source, however, was much weaker than we expected, owing to the self-absorption in the residuum contained in this source. Therefore, the total number of 300-keV positrons could be measured directly by the silicon detector mounted at the focus point of the beta-ray spectrometer and determined by integrating the area under the observed pulse-height distribution. In order to avoid the radiation damage produced by a large number of positrons from the strong ^{22}Na source, time period of this measurement was limited as short as possible enough to get good statistics of counting.

The spectrum of the shell electrons ejected from the lead target was observed in a similar manner but with the lead target at the focus point. The lead foil was inserted in the focus position and data were taken for 12 h. The ^{22}Na source was then covered with 8-mm thick Lucite plate to stop all the positrons, and backgrounds due to the strayed gamma rays from

the ^{22}Na source and natural radiation were measured with the same experimental conditions. Thus each experimental run for the ejected electrons was followed by a background run. This sequence of data taking was repeated many times until the desired statistics had been obtained. The total time of measurements of the ejected electron spectrum was about 400 h. Since long-term operation of the apparatus was required, good stability of the whole system was essential in the present work. Stability of gain of the detector and electronic system was checked before and after each 12-h experimental run. The data were printed out every 12 h and only the runs without noticeable drift were summed as the final result.

CHAPTER V

EXPERIMENTAL RESULTS AND CORRECTIONS

The ejected electron spectrum, observed by the procedures described in the preceding chapter, has been investigated with great care. After subtraction of the contributions due to gamma rays from the source and natural radiations, there are several mechanisms by which electrons in the energy region of interest may be ejected from the lead target. The possible sources of these backgrounds have been evaluated carefully and the experimental curve was drawn so as to correspond to the line profile obtained by taking into account of the target thickness.

To estimate the experimental value of the total cross section some factors concerned must be calculated: The angular distribution of the ejected electrons, the target-to-detector geometrical efficiency, and the correction factor for finite target thickness. The angular distribution of electrons from radiationless annihilation can be evaluated by combining theoretically that of the single-quantum annihilation and that of the photoelectric effect. Taking account of this distribution the geometrical efficiency is estimated by the Monte Calro method. The effect of the target thickness is the most important factor in this type of experiment.

Owing to the thick-target effect, the ejected electron spectrum which would be a narrow peak is smeared out to give a broad distribution. Since the rigorous treatment of this effect is very difficult, an approximate method has been developed by combining experimental and theoretical procedures.

Details of these estimations are given in this chapter.

1. Experimental Results

The observed spectrum obtained is shown by solid circles in Fig. 18. The relation of channel number vs energy of electrons incident upon the lead target before the silicon detector was calibrated using a ^{32}P source. The energies shown in Fig. 18 are estimated using the calibration line thus obtained (See Fig. 14). An evident peak at about 420 keV can be attributed to the K-shell photoelectrons from the lead target produced by 511-keV gamma rays of the two-quantum annihilation process. A shoulder in the vicinity of 500 keV may be due to the contributions from the L-shell photoelectrons by this process and partially from a sum effect of the K-shell photoelectrons and K x rays from lead. The second shoulder in the vicinity of 600 keV may be explained as to be due to pulses caused by the direct interaction of 511-keV radiation with the silicon detector and by a sum effect of this radiation and K x rays from lead. The observed spectrum in the higher energy region may be understood as the effects of gamma rays resulting from the two-quantum annihilation in flight in lead. In order to evaluate the background contributions from the strayed gamma rays and the natural background a series of measurements were performed under a quite similar experimental arrangement but with a ^{22}Na source covered by a Lucite plates of 8-mm thickness so as to stop positrons. The background thus observed is

shown by open circles in Fig. 18.

With an aim to find a peak due to the radiationless annihilation in lead in the vicinity of an expected kinetic energy (1146 keV) of the K-shell electron ejected by this process for the K-K pair, 12-h measurements were repeated carefully many times in order to get good counting statistics within our scope. The total time of observation was about 400 h. In Fig. 19 is shown the electron spectrum in this energy region obtained after subtracting the strayed gamma-ray and natural backgrounds. As shown in the figure, a small but evident peak is found in the region corresponding to the energies of the ejected electrons. An arrow, noted by 1146 keV, shows the position of a channel number corresponding to that for the peak observed when electrons of this energy are focused on the lead target. Hence, the kinetic energy of these electrons before entering the detector is about 1.02 MeV owing to energy loss in the lead target foil.

In this energy region of the observed spectrum, in addition to a contribution from the annihilation process to be studied there would exist three other possible sources of the contributions as follows: first, internal-conversion electrons from a ^{22}Na source; second, photoelectrons and/or Compton recoil electrons from the lead target by the photons from the two-quantum annihilation in flight in lead; third, similar contribution from the single-quantum annihilation in lead.

Since the conversion coefficient of the 1275-keV transition in ^{22}Ne is very small, $(6.77 \pm 0.45) \times 10^{-6}$, [70] and the electron-to-positron rejection ratio of our spectrometer is also very high as mentioned in Chap. IV, the possible contribution from the first cause can be neglected.

The maximum energy of photons created by the two-quantum annihilation in flight for 300-keV incident positrons is about 980 keV,[23] hence the maximum energy of the K-shell photoelectrons becomes about 900 keV. A few electrons out of those produced by L-shell photoelectric or Compton effect may have higher energy than 900 keV. Reflecting on these facts and the expected spectra to be discussed in Sec. 5 in this chapter (See the solid curve in Fig. 25), the lower end of the peak in Fig. 19 is chosen to be at the channel corresponding to 900-keV electrons detected. Moreover, the experimental and background curves in the figure in the energy range between 900 and 980 keV are drawn so as to minimize contributions from these electrons.

As a predominant source of the background in the vicinity of the observed peak, the photoelectrons and Compton-recoil electrons from the target produced by gamma rays from the single-quantum annihilation should be estimated. The energy of the photon from this process is given by Eq. (7) as

$$E_\gamma = E + m_0 c^2 - B_K , \qquad (7')$$

where E is the kinetic energy of an incident positron and B_K is the binding energy of the shell electron involved. A contribution

from the electrons ejected by the photons was estimated using the calculated cross section for the single-quantum annihilation reported by Johnson *et al.*[38] under an assumption that all the photons are created by this process at the source-side surface of the lead target. A contribution from such a process was found to be only about 10% of the observed counts at the channel number denoted by an arrow in Fig. 19 as the maximum evaluation. The background curve shown by the dashed curve in this figure is drawn by taking into account this estimation as well as the characteristics of the detector.

The experimental curve shown in Fig. 19 is drawn smoothly by combining the above facts and experimental points obtained as well as the expected electron spectrum evaluated in Sec. 5 in this chapter (See Fig. 25). The profile of the observed net peak thus obtained has no shoulder and is somewhat different from the expected one. Owing to the poor statistics of our measurement no shoulder can be distinguished. However, the observed peak shown in Fig. 19 is interpreted as being due to the ejected shell electrons, including those from K, L, and M shells, by the radiationless annihilation of 300-keV positrons in lead.

2. Evaluation of the Cross Section

The measurement of the cross section for radiationless annihilation consists of determining the number of electrons ejected from the target atom by the process to be studied, that of positrons impinging upon the target, that of atoms per unit area of the target, and the target-to-detector geometrical efficiency. The number of electrons ejected in the energy range concerned was estimated from the analysis of the obtained spectrum shown in Fig. 19. It is equal to the area under the peak in the figure, where the dashed base line is drawn by taking into account of background which arises from photoelectrons and/or Compton-recoil electrons in the target produced by gamma rays from single-quantum annihilation of positrons. The number of incident positrons on the target was estimated by measurement without the target using the solid state detector placed at the focusing point of the beta-ray spectrometer, as described in Chap. IV. The number of atoms per unit area of the target was determined from the effective target thickness to be equal to the number of target atoms per cm^2 normal to the direction of the incident positron beam.

The experimental total cross section σ for the radiationless annihilation of positrons incident on the target can be given by the following expression:

$$\sigma = \frac{(N_e/\varepsilon_e)C_e}{n_F G P (N_p/\varepsilon_p) C_p} \quad . \qquad (67)$$

The symbols in the expression are:

N_e = the number of observed ejected shell electrons per unit time,

N_p = the number of 300-keV positrons incident on the lead target per unit time,

n_F = the effective number of lead atoms in the target per unit area,

G = the geometrical efficiency of the silicon detector for electrons ejected from the lead target,

P = the peak-to-total ratio for the incident electrons with the expected energy,

ε_p = the detection efficiency of the silicon detector for incident 300-keV positrons,

ε_e = the same for ejected shell electrons,

C_p = the correction factor for the effect of the finite target thickness for incident positrons,

C_e = the same for ejected shell electrons.

N_e, N_p, and n_F were determined as mentioned above. P and $\varepsilon_p/\varepsilon_e$ were estimated by the procedures described in Chap. IV (See Fig. 17). The methods to estimate the geometrical efficiency G and the correction factor for the effect of the finite thickness of the target C_e/C_p are discussed in the following sections in this chapter.

3. Angular Distribution of Ejected Electrons

The angular distribution of the ejected electrons by radiationless annihilation is necessary to evaluate the cross section for this mode of annihilation. However, theoretical calculation mentioned in Chap. III is only for total cross section. Neither nonrelativistic nor relativistic calculation of the differential cross section for this process has been made. Therefore we must introduce some approximations based on the appreciable assumptions.

To evaluate this angular distribution, it is assumed that the angular distribution of the electrons ejected from any pair of atomic shells by this annihilation process is approximately the same form as that expected for those from the K-K pair. Moreover, radiationless annihilation is assumed to be two-step process; single-quantum annihilation takes place with an incident positron and then another electron is ejected from the same atom as a result of atomic photoeffect by the photon produced in the above annihilation process.

The angular distribution of ejected shell electron was evaluated by considering first the angular distribution of photons from the single-quantum annihilation calculated by Johnson[39] and then that of electrons from the photoelectric effect obtained by Pratt *et al.*[77] Using Lagrange interpolation formula for the atomic number and the incident positron energy, the angular distribution of photons by single-quantum

annihilation for lead at incident positron energy 300 keV was obtained from the calculated values of Johnson and is shown in Fig. 20. The energy of photons emitted by this annihilation process is easily evaluated from Eq. (7) to be 1234 keV. By a similar procedure to the case of single-quantum process, the angular distribution of K-shell photoelectrons for photons of this energy was obtained from the theoretical values calculated by Pratt *et al.*[77] In Fig. 21 is shown the K-shell angular distribution for lead at gamma-ray energy of 1234 keV.

When we note the direction of a photon emission from the single-quantum annihilation with respect to that of an incident positron be (θ_s, φ_s) and the direction of a photoelectron with respect to that of the above photon be (θ_p, φ_p), then the direction of a photoelectron with respect to that of an incident positron (θ, φ) can be given by the following relation:

$$\left.\begin{aligned} \cos\theta &= \cos\theta_s \cos\theta_p + \sin\theta_s \sin\theta_p \cos\varphi_p , \\ \cos(\varphi-\varphi_s) &= (\cos\theta_p - \cos\theta_s \cos\theta)/(\sin\theta_s \sin\theta) , \\ \sin(\varphi-\varphi_s) &= \sin\theta_p \sin\varphi_p / \sin\theta . \end{aligned}\right\} \quad (68)$$

Using the differential cross section for the single-quantum annihilation, $d\sigma_s/d\Omega_s$, and that for the photoelectric effect, $d\sigma_p/d\Omega_p$, satisfying the trigonometric relationships (68), the probability that the bound electron be emitted into a unit solid angle in the direction (θ, φ) can be expressed as

$$P(\theta,\varphi) = \int \frac{d\sigma_s}{d\Omega_s} \frac{d\sigma_p}{d\Omega_p} d\Omega_s \Big/ \iint \frac{d\sigma_s}{d\Omega_s} \frac{d\sigma_p}{d\Omega_p} d\Omega_s d\Omega . \quad (69)$$

This calculation is very difficult, because $d\sigma_s/d\Omega_s$ and $d\sigma_p/d\Omega_p$ can not be expressed simply as analytical forms. Instead of the use of Eq. (69), known numerical values of these differential cross sections[39,77] for discrete values of θ_s and θ_p were used as distribution functions and then values of θ_s and θ_p were determined by generating uniform pseudorandom numbers r_1 and r_2. The selection of a random azimuthal angle φ_p from a uniform distribution on the interval $[0,2\pi]$ was performed using two random numbers r_3 and r_4 satisfying the condition $r_3^2 + r_4^2 \leq 1$, and a relation $\cos\varphi_p = (r_3^2 - r_4^2)/(r_3^2 + r_4^2)$. Using the numerical values of θ_s, θ_p, and φ_p obtained by this procedure the value of $\cos\theta$ given by Eq. (68) could be evaluated. Since the detection geometry of the present experiment is axially symmetric, $P(\theta,\varphi)$ is independent of φ. By applying the sampling technique to this $\cos\theta$ the distribution function $P(\theta)$ was estimated. The angular distribution of ejected electrons thus obtained is shown in Fig. 22.

It is noted, however, that such a procedure to evaluate the angular distribution of the ejected electrons incident on the detector is only approximate, because radiationless annihilation is a direct process involving an incident positron and two shell electrons, one of which is ejected with the excess energy liberated, and a photon is emitted only virtually.

4. Geometrical Efficiency

The geometrical efficiency G refers to the fraction of shell electrons emitted from the target foil that is detected by the solid detector. G must be calculated by taking account of the solid angle presented by the circular lead target (effective diameter is 6 mm) to the circular surface of the silicon detector (8 mm in diameter) as well as the angular distribution of the ejected shell electrons. An analytical calculation of the solid angle subtended by a radioactive source to a circular-disc detector is difficult except for the case of a point isotropic source. In the case of a disc source coaxial with the disc detector and lying in a plane separated from it by a distance, evaluations of the solid angle have been done by a series expansion or by a double numerical integration. If the emitted particles from the source have an complicated angular distribution, an analytical calculation of the geometrical efficiency becomes extremely difficult. There exist, however, a method to obtain the source-to-detector geometry to any desired degree of accuracy in any condition. Monte Calro technique, the essence of which is that a computer is used to perform a "Gedanken Experiment" to simulate the angular distribution of emitted particles from a point uniformly situated on a hypothetical disc, was applied to estimate geometrical efficiency in the present work.

The computer program uses random numbers to give the

point of origin of the emission and the direction cosines. The program then ascertains whether or not a line with the randomly selected direction from the distribution function $P(\theta)$ obtained in the preceding section, originating at the randomly chosen point on the disc target intersects a circular disc representing the detector.

Each history is selected as following: A point on the disc target is randomly selected, and the direction of emission of an electron is chosen randomly using $P(\theta)$, and then the position on the detector which the electron impacts is obtained. If the electron does not strike the detector surface, the number of hits is unchanged. Otherwise, we add one to this number. A method for choosing the direction of emission from a given probability distribution $P(\theta)$ using a sequence of random numbers equidistributed in the interval [0, 1] is as following: we denote a number selected from a uniform distribution in the interval [0, 1] by r, and consider a discrete distribution the i-th of which has a probability $P_i = P(\theta_i)$. If the event k is associated with a random number r as

$$\sum_{i=1}^{k-1} P_i < r \leq \sum_{i=1}^{k} P_i \quad , \qquad (70)$$

then we may determine the direction of emission θ from the linear interpolation formula

$$\theta = \theta_k - \frac{P_k - r}{P_k - P_{k-1}} (\theta_k - \theta_{k-1}) \, . \qquad (71)$$

The ratio of the number of hits to tries thus obtained gives the geometrical efficiency. The program permits a choice of the number of interactions (emissions) to satisfy the condition contained in the input data. This condition is given as the minimum desired coefficient of variation, defined as δ_G/G, where δ_G is the standard deviation of G. A reasonable value of the coefficient and the number of histories were taken to be 0.01 and 20 000, respectively. The computer code is written for KDC-II computer[62] in HARP-5020 and the flow diagram of this code is shown in Fig. 23. The numerical value of G thus obtained and used in the present work is 0.538 ± 0.005.

5. Evaluation of Effect of Target Thickness

As discussed in Chap. II, the thickness of the target was determined so that the number of ejected electrons reaching the detector is as much as possible. The thickness of 75.3 mg/cm^2 thus chosen is nearly corresponding to the range of 300-keV positrons in the present experimental geometry. The ejected electron spectrum observed using this target would be distorted by the finite thickness effect of the target. In this section ~~is~~ are described the procedures to estimate the profile of the electron spectrum and obtain an analytical expression for the finite thickness correction factor C_e/C_p in Eq. (67).

In the observed spectrum of the electrons ejected from the lead target there can be expected a peak due to the radiationless annihilation process. However, this peak would be smeared out owing to the effect of the target thickness (75.3 mg/cm^2), including degradation of kinetic energies of incident positrons and ejected electrons in the lead foil. For estimation of the number of electrons ejected from the observed curve, consideration for its resonable profile should be necessary, taking account of the effect of the target thickness, energy resolution of the solid detector, and the geometrical arrangement of the target and detector. Since the rigorous treatment of the problem is very difficult, an approximate solution has been developed using theoretical and experimental procedures based upon some appropriate assumptions.

Assumption adopted to simplify the problem are as follows: (1) The 300-keV positrons impinge upon the central focus area (6 mm in diameter) of the lead foil at an angle of incidence equal to 60°. (2) The target foil is so thin that any appreciable angular deflection can be neglected for the incident positrons in the target before the annihilation and for the ejected electrons before escaping from the target. (3) The angular distribution of the electron ejected from any pair of shell electrons by this annihilation process is given by the distribution function $P(\theta)$ obtained in the preceding section (See Fig. 22).

The geometry for detecting the ejected shell electrons and mathematical terms used in the present calculations are shown schematically in Fig. 24. The incident positrons with kinetic energy of E_0 = 300 keV enter into the target foil at an angle of incidence of α = 60°. As these positrons penetrate into the foil their energy and number decrease because of various interactions with the target atoms, such as annihilation in flight and inelastic scattering. The number of positrons at a distance x from the surface of the target can be expressed by a function $N(E,x)$, where E is the kinetic energy of the positron at x. Then the number of the electrons, which escape from the target and are detected by the detector of $2b$ = 8.0 mm in diameter placed at a distance a = 1.0 mm from the target, can be given by (See Appendix IV)

$$R(E'')dE'' = n \sum_{\substack{\text{all electron} \\ \text{pairs}}} \int_0^T \int_0^{E_0} \int_{\alpha-\delta}^{\alpha+\delta} N(E,x)\sigma(E)K(E,E'';x,\theta)P(\theta)\sin\theta\, d\theta\, dE\, dx\, dE'', \quad (72)$$

where the summation is over all the pairs of shell electrons involved, $P(\theta)$ is the angular distribution of the ejected electrons, θ is the angle between the direction of the momentum of the incident positron and that of the ejected electron, $\sigma(E)$ is the total cross section per atom for the radiationless annihilation of positrons with kinetic energy E, T is a thickness of the target, n is the number of atoms per unit volume of the target, and

$$\tan\delta = \frac{b}{a} \quad .$$

The electron detection probability, $K(E,E'';x,\theta)$, is defined as the probability that the electron ejected at x as a result of radiationless annihilation of the positron of energy E escapes from the target and is detected by the detector with energy between E'' and $E'' + dE''$. $R(E'')dE''$ given by this expression represents the energy distribution of the ejected shell electrons detected by the solid detector.

The energy spectrum of positrons $N(E,x)$ in Eq. (72) can be obtained by solving a space-dependent transport equation for positrons. Generally, it is a linear integro-differential equation of the form

$$\frac{1}{v}\frac{\partial N}{\partial t} + \Omega \cdot \nabla N + \mu N = \int_E^\infty dE' \int_{4\pi} d\Omega' N(E', \Omega', \mathbf{r}, t) \psi(E', \Omega'; E, \Omega) , \quad (73)$$

where t is time, v is the velocity of the positron, $N(E, \Omega, \mathbf{r}, t)$ is flux of positron at time t and position $\mathbf{r}$ with energies in the interval $(E, E + dE)$, $\mu(E)$ is probability, per unit pathlength, of an interaction of any type between the positron and the target, and $\psi(E', \Omega'; E, \Omega)$ is probability, per unit pathlength, that a positron with energy E' and direction Ω' will, as a result of a collision, acquire an energy in the interval $(E, E + dE)$ and a direction in the interval $(\Omega, \Omega + d\Omega)$. It is, however, very difficult to solve this equation even numerically because of mathematical complexities, which arise from the large number of variables (up to six) from the boundary conditions imposed by the experimental configurations and from a variety of interactions to be taken into account jointly; elastic scattering by atomic nucleus, inelastic scattering by atomic electrons, annihilation, and bremsstrahlung. For this reason, we have attempted to find $N(E,x)$ experimentally by observing the energy spectrum of positrons passed through targets of various thicknesses.

Using lead foils of thicknesses being 13.1, 26.7, 35.0, 51.6, 65.7, and 75.3 mg/cm^2, energy spectra of positrons passed through these foils were measured for positrons of incident energy of 300 keV by attaching them immediately before the

silicon detector mounted at the focus of the beta-ray spectrometer. Each positron spectrum thus obtained was considered to give an approximation to the energy spectrum of positrons inside the lead target used at the corresponding thickness, neglecting the difference in the boundary condition. By this procedure we could evaluate $N(E,x)$.

To estimate the electron detection probability, $K(E,E'';x,\theta)$, similar measurements with incident electrons with different energies were performed by replacing the ^{22}Na source by a ^{32}P source and using the lead foils of the thicknesses above mentioned. The minimum energy of ejected electrons from this annihilation process is easily obtained from Eq. (8) as to be 846 keV, corresponding to the case where the positron of zero kinetic energy annihilates with the K-K pair, while the maximum energy is 1290 keV which corresponds to the 300-keV positron and the L-L pair. Taking account of these values, in the energy interval from 846 to 1290 keV eleven incident energies of electrons were chosen; 846, 896, 946, 996, 1046, 1096, 1146, 1180, 1218, 1250, and 1290 keV. From experimental data thus obtained, the electron detection probability for $\theta = 0$, $K(E,E'';\ T - x,0)$, could be evaluated as a ratio of the number of electrons detected in the channel corresponding to the kinetic energy of E'' to the total number of incident electrons corresponding to annihilation of positron with kinetic energy E. Since $K(E,E'';x,\theta)$ is a function of $(T - x)/\cos(\theta - \alpha)$,

$K(E,E'':x,\theta)$ could be easily evaluated from the experimental values of $K(E,E'';\ T - x,0)$ using the Lagrange interpolation formula for x and θ.

As the total cross section $\sigma(E)$ in Eq. (72), for K-K pair we used the values calculated by the method mentioned in Chap. III (See Fig. 10). For other pairs of shell electrons it was assumed that energy dependence of the cross section is the same form as that for the K-K pair. The normalization for the total cross section for any of the other pairs was made at the positron kinetic energy of 300 keV using the theoretical values for σ_{other}(300 keV) and σ_{K-K}(300 keV) calculated in Chap. III (See Table IV). Then $\sigma_{other}(E)$ for arbitrary energy E is written as

$$\sigma_{other}(E) = \frac{\sigma_{other}(300\,keV)}{\sigma_{K-K}(300\,keV)} \cdot \sigma_{K-K}(E) . \qquad (74)$$

By the use of these experimental data of $N(E,x)$ and $K(E,E'';x,\theta)$, and of the calculated values of $P(\theta)$ and $\sigma(E)$, Eq. (72) for $R(E'')$ could be integrated numerically using KDC-II.[62] By these complicated procedures the expected spectrum of the ejected shell electrons detected was obtained, as shown by the solid curve in Fig. 25. It is conceived that this spectrum may give the reasonable profile expected from our observation of the spectrum, which is due to the annihilation process with 300-keV incident positrons. This result was taken into consideration when the experimental curve in Fig. 19

was drawn.

If the effect of the target thickness is assumed to be negligible, we get the following equation (See Appendix IV):

$$R_0(E'')dE'' = n N_0 T \sec\alpha \sum_{\substack{\text{all electron} \\ \text{pairs}}} \sigma(E_0) \int_{\alpha-\delta}^{\alpha+\delta} K(E_0, E''; T, \theta) P(\theta) \sin\theta \, d\theta \, dE'', \quad (75)$$

where N_0 is the total number of positrons incident on the target. This expression gives the energy spectrum of the ejected electrons when the effect of the target thickness is neglected. The spectrum obtained by integrating Eq. (75) numerically is shown by the dashed curve in Fig. 25.

The correction factor for the effect of target thickness, C_e/C_p, can be defined as a ratio of the number of detected electrons estimated from Eq. (75) to that estimated from Eq. (72). Using these equations, the analytical expression of C_e/C_p can be obtained as (See Appendix IV)

$$C_e/C_p = \frac{N_0 T \sec\alpha \sum_{\substack{\text{all electron} \\ \text{pairs}}} \sigma(E_0) \int_{E_{min}}^{E_{max}} \int_{\alpha-\delta}^{\alpha+\delta} K(E_0, E''; T, \theta) P(\theta) \sin\theta \, d\theta \, dE''}{\sum_{\substack{\text{all electron} \\ \text{pairs}}} \int_{E_{min}}^{E_{max}} \int_0^T \int_0^{E_0} \int_{\alpha-\delta}^{\alpha+\delta} N(E, \chi) \sigma(E) K(E, E''; \chi, \theta) P(\theta) \sin\theta \, d\theta \, dE \, d\chi \, dE''}, \quad (76)$$

In the present work, since the lower limit of the observed peak portion is chosen at 900 keV for the reason mentioned before, this energy should be taken as E_{min}. As E_{max} we can adopt a value for the higher energy end of the expected spectrum given by Eq. (75), i.e. 1400 keV shown by the dashed

curve in Fig. 25. The value of C_e/C_p can be estimated by measuring a ratio of areas under the curves of electron spectra shown in Fig. 25, but limited within an energy range from 900 to 1400 keV. Moreover, it is noted that the integration of E'' in the numerator in Eq. (76) must be carried out only for the peak portion of the electron spectrum in this energy region. The lower energy side of the peak (dashed curve) is presumed as shown by the dotted curve in Fig. 25. This peak is considered to be the total absorption peak due to the ejected shell electrons in the case where no effect of the target thickness is taken into account. The numerical value of C_e/C_p thus estimated and used in the present work is 1.4 ± 0.1. The error given is evaluated only from the counting statistics involved.

CHAPTER VI

DISCUSSION AND CONCLUSIONS

In this chapter we first discuss the theoretical and experimental total cross sections for radiationless annihilation of positrons obtained by the procedures described in Chaps. III - V, and compare them each other for positrons with incident energy of 300 keV in lead. The sources of the large experimental error for our final experimental value are also discussed.

The Z dependence of the cross section is of great interest to assist comprehension of this mode of positron annihilation. With an aim to obtain some information on the Z dependence we have attempted to observed this process using a thin tantalum foil as a target under quite similar experimental conditions, but no experimental evidence has been found. An account of our experimental work with tantalum is given in Sec. 2. A conclusion on the Z dependence deduced from this work is also given in this section.

Finally, the conclusions obtained are given in Sec. 3, where we add also some reflection on the present work and point out a few necessary improvements to further the development of the experimental study on this particular type of positron annihilation.

1. Comparison between Theory and Experiment

In the present experiments, the electrons ejected from radiationless annihilation by the K-K pair cannot be resolved out from those by other pairs. Consequently, before the theoretical calculation can be compared with experiment, the calculated cross section for various atomic shells must be summed up to give the total cross section. The total cross section for radiationless annihilation calculated for positrons of the kinetic energy of 300 keV is

$$\sigma_{cal} = 0.727 \times 10^{-26} \text{ cm}^2.$$

On the other hand, by inserting numerical values of the factors concerned into the right-hand side of Eq. (67) we have obtained the experimental total cross section for this annihilation process of 300-keV positrons in lead as

$$\sigma_{exp} = 0.8_{-0.3}^{+0.4} \times 10^{-26} \text{ cm}^2,$$

as a sum of those for K-K, K-L, K-M, and L-L pairs of shell electrons. In the last column of Table IV is given this experimental result for comparison.

The error shown is mainly ascribed to an uncertainty in the determination of N_e, caused by the poor statistics of our measurements. As the numerical value of the denominator of Eq. (76) for C_e/C_p, we adopted the area under the solid curve between 900 and 1400 keV in Fig. 25. However, examining our observed spectrum of the ejected electrons shown in Fig. 19,

a value somewhat smaller than that we adopted may be more reasonable for the present purpose. This means that a slightly larger value of C_e/C_p may give a more close approximation for this correction factor. The asymmetry of the error, larger "plus" error, in our experimental cross section reflects this fact. This value of the total cross section is about one third of our preliminary result[51] reported in 1965. This is caused by more careful re-examining of the experimental data as well as by introducing improved evaluations of the geometrical efficiency of the detector G and of the correction factor C_e/C_p. The latter has been estimated by necessary measurements of the positron and electron energy distribution in lead foils based upon reasonable assumptions, as described in the preceding chapter.

Both experimental and calculated results obtained by the present work agree with each other within the experimental error.

2. Radiationless Annihilation in Tantalum

We have also attempted to observe radiationless annihilation in tantalum atom ($Z = 73$) for 300-keV incident positrons. A series of experiments were performed by similar procedures. The lead target was replaced by a tantalum foil, while all other experimental conditions remained same. The thickness of the target was determined similar to the case for lead so that the effective thickness is nearly equal to the range of 300-keV positrons. From the table prepared by Nelms,[76] the value of range in tantalum for this energy of positrons is taken to be 159 mg/cm^2 by interpolation technique for Z. Using this value and taking into account of the incident angle of positrons, the thickness of the tantalum foil was chosen to be 89.5 mg/cm^2.

The 12-h measurement was repeated 20 times to give the total time of measurements being 240 h. Carefully examining the electron spectrum thus observed, we can say with fair certainty that it looks like there exists no peak in the ejected electron spectrum at the place where we expect.

There are two reasons why the peak in the electron spectrum was not observed: (1) The positron spectrum and/or the electron detection probability in the tantalum foil differ considerably from those in the lead foil. (2) The Z dependence of the total cross section for this annihilation process is large. However, the first one seems very unlikely, since in this region of

nuclear charge Z neither positron spectra nor various interactions of ejected electrons with atoms differ so much from those for lead.

According to the rough estimation using nonrelativistic formula, the total cross section for radiationless annihilation is approximately proportional to Z^2. This fact indicates that the cross section for tantalum atom is 1.26 times smaller than that for lead. No experimental evidence for this phenomenon in tantalum, however, may suggest that Z dependence of the cross section would be larger than Z^2.

3. Conclusions

When an annihilation process of a positron occurs on collision of an atomic electron the energy liberated, instead of appearing as radiation, may be absorbed by another atomic electron, resulting in its ejection from the atom. The cross section for this radiationless annihilation process involving the K electrons of a lead atom for various energies of the incident positron has been calculated relativistically with accuracy, taking into account of the repulsive influence of the nucleus, retardation effect, spin-spin interaction and electron exchange. Calculations have also been made for the contributions from other pairs of electrons in the lead atom for positrons with kinetic energy 300 keV. It is concluded that the total cross section for radiationless annihilation by bound electrons in the lead atom is 0.727×10^{-26} cm^2 for this energy of positrons. The numerical results for the K-K pair in lead agree well with the earier results of Massey and Burhop.

An attempt to detect this annihilation has also been performed using a beta-ray spectrometer and a solid state detector. The 300-keV positrons were focused on a thin lead target by the use of a beta-ray spectrometer mounted with a ^{22}Na source. The shell electrons ejected from the target were observed with a lithium-drifted silicon junction detector placed immediately behind the foil. It is one of the key

point of this experiment how to evaluate the effect of the finite target thickness. We have developed a method to estimate this effect by combining experimental and theoretical results. The conclusion is reached that we have observed radiationless annihilation of positrons and that it occurs in lead with a cross section, $0.8_{-0.3}^{+0.4} \times 10^{-26}$ cm^2, equal to the theoretical value within experimental error. No experimental evidence for this annihilation process in tantalum atom suggests that Z dependence of the cross section would be larger than Z^2.

The error inherent in the experimental result is rather large and our calculations are based in part on some untested assumptions. Nevertheless, the present work has provided the experimental evidence of this particular mode of positron annihilation and assisted comprehension of the process.

Reflecting on the present work, it is hoped that a further experimental study using more elaborate methods with a stronger positron beam and thinner targets should be made to provide additional information on this process. Experimental and theoretical studies on the angular distribution of the ejected shell electrons and Z dependence of the process would also be of great interest.

APPENDIX I

CALCULATIONS OF ANGULAR INTEGRATIONS IN THE MATRIX ELEMENT $\mathcal{B}$

A. Calculation of $\mathcal{B}_{K_1K_2K_3K_4}$

$\mathcal{B}_{K_1K_2K_3K_4}$ is written from Eq. (44a) as the product of two matrix elements as

$$\mathcal{B}_{K_1K_2K_3K_4} = (\chi^{m_1}_{K_1}|Y^{m^*}_{\ell}|\chi^{m_3}_{K_3})\cdot(\chi^{m_2}_{K_2}|Y^{m}_{\ell}|\chi^{m_4}_{K_4}) \quad . \qquad (A1-1)$$

The first matrix element concerning $\hat{r}_1$ is

$$(\chi^{m_1}_{K_1}|Y^{m^*}_{\ell}|\chi^{m_3}_{K_3}) = \sum_{\tau_1\tau_3} C(\ell_1 \tfrac{1}{2} j_1; m_1-\tau_1\ \tau_1)\, C(\ell_3 \tfrac{1}{2} j_3; m_3-\tau_3\ \tau_3)$$

$$\times (\chi^{\tau_1}, \chi^{\tau_3}) \int Y^{m_1-\tau_1 *}_{\ell_1}(\hat{r}_1)\, Y^{m_3-\tau_3}_{\ell_3}(\hat{r}_1)\, Y^{m^*}_{\ell}(\hat{r}_1)\, d\Omega_1 \quad , \qquad (A1-2)$$

where the scaler product $(\chi^{\tau_1}, \chi^{\tau_3})$ means that $\chi^{\tau_1 *}$ is multiplied into χ^{τ_3}. Using the orthonormal property of χ^{τ},

$$(\chi^{\tau_1}, \chi^{\tau_3}) = \delta_{\tau_1,\tau_3} \quad ,$$

and the symmetry rule of the spherical harmonics,

$$Y^{m_1 *}_{\ell_1}(\hat{r}_1) = (-)^{m_1} Y^{-m_1}_{\ell_1}(\hat{r}_1) \quad ,$$

the spin angular matrix element is then

$$(\chi^{m_1}_{K_1}|Y^{m^*}_{\ell}|\chi^{m_3}_{K_3}) = \sum_{\tau_1} C(\ell_1 \tfrac{1}{2} j_1; m_1-\tau_1\ \tau_1)\, C(\ell_3 \tfrac{1}{2} j_3; m_3-\tau_1\ \tau_1)$$

$$\times (-)^{m_1-\tau_1} \int Y^{m^*}_{\ell}(\hat{r}_1)\, Y^{\tau_1-m_1}_{\ell_1}(\hat{r}_1)\, Y^{m_3-\tau_3}_{\ell_3}(\hat{r}_1)\, d\Omega_1 \quad . \qquad (A1-3)$$

We use the coupling rule for the spherical harmonics

$$Y_{l_1}^{\tau_1-m_1} Y_{l_3}^{m_3-\tau_1} = \sum_L \sqrt{\frac{(2l_1+1)(2l_3+1)}{4\pi(2L+1)}}\, C(l_1 l_3 L; 00)$$

$$\times C(l_1 l_3 L; \tau_1-m_1\ m_3-\tau_1)\, Y_L^{m_3-m_1}, \qquad (A1-4)$$

where the arguments of the spherical harmonics are the same, and multiplication of Eq. (A1-4) by $Y_l^{m*}(\hat{r}_1)$ and integration over the full solid angle Ω_1 gives

$$\int Y_l^{m*} Y_{l_1}^{\tau_1-m_1} Y_{l_3}^{m_3-\tau_1} d\Omega_1 = \sqrt{\frac{[l_1][l_3]}{4\pi[l]}}\, C(l_1 l_3 l; 00) C(l_1 l_3 l; \tau_1-m_1\ m_3-\tau_1), \qquad (A1-5)$$

where $[l] = 2l + 1$. Substituting Eq. (A1-4) in Eq. (A1-2) we obtain the matrix element

$$(\chi_{k_1}^{m_1} | Y_l^{m*} | \chi_{k_3}^{m_3}) = \sqrt{\frac{[l_1][l_3]}{4\pi[l]}}\, C(l_1 l_3 l; 00)\, S\, \delta_{m_3-m_1, m}, \qquad (A1-6)$$

where

$$S = \sum_{\tau_1} (-)^{m_1-\tau_1} C(l_1 \tfrac{1}{2} j_1; m_1-\tau_1\ \tau_1) C(l_3 \tfrac{1}{2} j_3; m_3-\tau_1\ \tau_1) C(l_1 l_3 l; \tau_1-m_1\ m_3-\tau_1).$$

This sum is evaluated using techniques developed by Racah.[78] The result is expressed in term of Racah coefficient as

$$S = (-)^{l+l_1+l_3+m_1+\frac{1}{2}} \sqrt{[j_1][j_3]}\, C(j_1 j_3 l; -m_1 m_3) W(j_1 l_1 j_3 l_3; \tfrac{1}{2} l).$$

From the symmetry property of the parity C-coefficient $C(l_1 l_3 l; 00)$, $l_1 + l_3 + l$ must be even integer for the coefficient to be non-vanishing. The resultant expression for the spin angular matrix element is

$$(\chi_{k_1}^{m_1} | Y_l^{m*} | \chi_{k_3}^{m_3}) = (-)^{m_1+\frac{1}{2}} \sqrt{\frac{[j_1][j_3][l_1][l_3]}{4\pi[l]}}\, C(l_1 l_3 l; 00)$$

$$\times C(j_1 j_3 l; -m_1 m_3) W(j_1 l_1 j_3 l_3; l\ \tfrac{1}{2})\, \delta_{m_3-m_1, m}. \qquad (A1-7)$$

The second matrix element is easily obtained by the similar procedures to the first one, and the result is

$$(\chi^{m_2}_{\kappa_2}|Y^{m}_{\ell}|\chi^{m_4}_{\kappa_4}) = (-)^{m}(\chi^{m_2}_{\kappa_2}|Y^{-m*}_{\ell}|\chi^{m_4}_{\kappa_4})$$

$$= (-)^{m+m_2+1/2}\sqrt{\frac{[\ell_2][\ell_4][j_2][j_4]}{4\pi[\ell]}}\,C(\ell_2\ell_4\ell;00)C(j_2j_4\ell;-m_2\,m_4)$$

$$\times W(j_2\ell_2j_4\ell_4;\tfrac{1}{2}\ell)\,\delta_{m_2-m_4,m}\,. \qquad (A1-8)$$

Inserting Eqs. (A1-7) and (A1-8) into Eq. (A1-1), the angular coupling coefficient $B_{\kappa_1\kappa_2\kappa_3\kappa_4}$ is given by

$$B_{\kappa_1\kappa_2\kappa_3\kappa_4} = (-)^{m+m_1+m_2+1}\,\frac{\sqrt{[\ell_1][\ell_2][\ell_3][\ell_4][j_1][j_2][j_3][j_4]}}{4\pi[\ell]}\,C(\ell_1\ell_3\ell;00)$$

$$\times C(\ell_2\ell_4\ell;00)\,C(\ell_1\ell_3\ell;-m_1\,m_3)\,C(\ell_2\ell_4\ell;-m_2\,m_4)$$

$$\times W(j_1\ell_1j_3\ell_3;\tfrac{1}{2}\ell)\,W(j_2\ell_2j_4\ell_4;\tfrac{1}{2}\ell)\,\delta_{m_3-m_1,m}\,\delta_{m_2-m_4,m}\,. \qquad (45a)$$

B. Calculation of $B'_{\kappa_1\kappa_2\kappa_3\kappa_4}$

From Eq. (44b) $B'_{\kappa_1\kappa_2\kappa_3\kappa_4}$ is expressed as

$$B'_{\kappa_1\kappa_2\kappa_3\kappa_4} = (\chi^{m_1}_{\kappa_1}|Y^{m*}_{\ell}\sigma|\chi^{m_3}_{\kappa_3})\cdot(\chi^{m_2}_{\kappa_2}|Y^{m}_{\ell}\sigma|\chi^{m_4}_{\kappa_4})\,. \qquad (A1-9)$$

Writing σ in a spherical basis, the first matrix element in Eq. (A1-9) is

$$(\chi^{m_1}_{\kappa_1}|Y^{m*}_{\ell}\sigma|\chi^{m_3}_{\kappa_3}) = \sum_{\tau_1\tau_3} C(\ell_1\tfrac{1}{2}j_1;m_1-\tau_1\,\tau_1)\,C(\ell_3\tfrac{1}{2}j_3;m_3-\tau_3\,\tau_3)$$

$$\times(\chi^{\tau_1}\sigma\chi^{\tau_3})\int Y^{m_1-\tau_1*}_{\ell_1}(\hat{r}_1)\,Y^{m_3-\tau_3}_{\ell_3}(\hat{r}_1)\,Y^{m*}_{\ell}(\hat{r}_1)\,d\Omega_1\,, \qquad (A1-10)$$

where the components of σ are

$$\sigma_1 = -\frac{1}{\sqrt{2}}(\sigma_x+i\sigma_y)\,,\quad \sigma_0=\sigma_z\,,\quad \sigma_{-1}=\frac{1}{\sqrt{2}}(\sigma_x-i\sigma_y)\,.$$

The vector $(\chi^{\tau_1}, \sigma\chi^{\tau_3})$ is written in the spherical basis as[79]

$$(\chi^{\tau_1}, \sigma\chi^{\tau_3}) = 2\cdot\sqrt{\frac{1}{2}\cdot\frac{3}{2}}\sum_{\lambda} C(\tfrac{1}{2}\,1\,\tfrac{1}{2};\tau_3\lambda)\,\delta_{\tau_1,\tau_3+\lambda}\,\xi_\lambda, \quad (A1\text{-}11)$$

where the spherical basis vectors, ξ_λ, are expressed using the unit vectors e_1, e_2, and e_3 along the Cartesian axes as

$$\xi_1 = -\frac{1}{\sqrt{2}}(e_1 + i e_2),$$

$$\xi_0 = e_3,$$

$$\xi_{-1} = \frac{1}{\sqrt{2}}(e_1 - i e_2).$$

Substituting Eq. (A1-11) in Eq. (A1-10) the matrix element is

$$(\chi^{m_1}_{K_1}|Y^{m^*}_{\ell}\sigma|\chi^{m_3}_{K_3}) = \sqrt{3}\sum_{\tau_1\tau_3\lambda} C(\ell_1\tfrac{1}{2}j_1;\, m_1-\tau_1\,\tau_1)\,C(\ell_3\tfrac{1}{2}j_3;\, m_3-\tau_3\,\tau_3)$$
$$\times C(\tfrac{1}{2}\,1\,\tfrac{1}{2};\,\tau_3\lambda)\,\delta_{\tau_1,\tau_3+\lambda}\,\xi_\lambda \int Y^{m_1-\tau_1^*}_{\ell_1}(\hat{r}_1)\,Y^{m_3-\tau_3}_{\ell_3}(\hat{r}_1)\,Y^{m^*}_{\ell}(\hat{r}_1)\,d\Omega_1.$$

Angular integration of product of three spherical harmonics is done in the similar manner to Eq. (A1-5), and then

$$(\chi^{m_1}_{K_1}|Y^{m^*}_{\ell}\sigma|\chi^{m_3}_{K_3}) = (-)^m\sqrt{\frac{3[\ell][\ell_3]}{4\pi[\ell_1]}}\,C(\ell_3\ell\ell_1;00)\cdot S', \quad (A1\text{-}12)$$

where

$$S' = \sum_{\tau_3\lambda} C(\ell_1\tfrac{1}{2}j_1;\, m_1-\tau_3-\lambda\;\;\tau_3+\lambda)\,C(\ell_3\tfrac{1}{2}j_3;\, m_3-\tau_3\;\tau_3)$$
$$\times C(\tfrac{1}{2}\,1\,\tfrac{1}{2};\,\tau_3\lambda)\,C(\ell_3\ell\ell_1;\, m_3-\tau_3\;-m)\,\delta_{m_3-m,\,m_1-\lambda}\,\xi_\lambda.$$

Using $\lambda = m_1 - m_3 + m$ and the contraction of Clebsch-Gordan coefficients

$$C(\ell_3\ell\ell_1;\, m_3-\tau_3\;-m)\,C(\ell_1\tfrac{1}{2}j_1;\, m_3-m-\tau_3\;\;m_1-m_3+m+\tau_3)$$
$$= \sum_{f_1}([\ell_1][f_1])^{1/2}\,W(\ell\ell_3 j_1\tfrac{1}{2};\,\ell_1 f_1)\,C(\ell_3\tfrac{1}{2}f_1;\, m_3-\tau_3\;\;m_1-m_3+m+\tau_3)$$
$$\times C(\ell f_1 j_1;\, -m\;\;m_1+m),$$

we can sum over τ_3 and then

$$S' = \sum_{f_1} ([l_1][f_1])^{1/2} C(l f_1 j_1; -m\, m_1+m)\, W(l l_3 j_1 1/2; l_1 f_1)\, \delta_{m_1-m_3+m}$$
$$\times \sum_{\tau_3} C(1/2\, 1/2; \tau_3\, m_1+m-m_3)\, C(l_3 1/2\, j_3; m_3-\tau_3\, \tau_3)$$
$$\times C(l_3 1/2\, f_1; m_3-\tau_3\, m_1+m-m_3+\tau_3)$$
$$= \sum_{f_1} (-)^{2l_3-j_1-f_1} ([l_1][f_1])^{1/2} C(l f_1 j_1; -m\, m_1+m)\, W(l l_3 j_1 1/2; l_1 f_1)$$
$$\times \delta_{m_1+m-m_3} ([1/2][j_3])^{1/2}\, W(1\,1/2\, f_1 l_3; 1/2\, j_3)\, C(1 j_3 f_1; m_1+m-m_3\, m_3)$$
$$= \sum_{f_1} (-)^{2l_3+1-2f_1} ([1/2][l_1][j_3][f_1])^{1/2}\, W(l l_3 j_1 1/2; l_1 f_1)\, W(1\,1/2\, f_1 l_3; 1/2\, j_3)$$
$$\times C(l f_1 j_1; -m\, m_1+m)\, C(j_3 1 f_1; m_3\, m_1+m-m_3)\, \delta_{m_1+m-m_3}. \quad \text{(A1-13)}$$

From the selection rules contained in angular momentum coupling coefficients, $2l_3 + 1 - 2f_1$ must be even. The matrix element (A1-10) is obtained in the following form

$$(\chi^{m_1}_{\kappa_1} | Y^{m*}_{l} \sigma | \chi^{m_3}_{\kappa_3}) = (-)^m \sqrt{\frac{6[l][j_3][l_3]}{4\pi}}\, C(l_3 l l_1; 00) \sum_{f_1} \sqrt{[f_1]}\, W(l l_3 j_1 1/2; l_1 f_1)$$
$$\times W(1\,1/2\, f_1 l_3; 1/2\, j_3)\, C(l f_1 j_1; -m\, m_1+m)\, C(j_3 1 f_1; m_3\, m_1+m-m_3)\, \delta_{m_1+m-m_3}. \quad \text{(A1-14)}$$

The second matrix element is obtained in the similar manner as

$$(\chi^{m_2}_{\kappa_2} | Y^{m}_{l} \sigma | \chi^{m_4}_{\kappa_4}) = \sqrt{\frac{6[l][j_4][l_4]}{4\pi}}\, C(l_4 l l_2; 00) \sum_{f_2} \sqrt{[f_2]}\, W(l l_4 j_2 1/2; l_2 f_2)$$
$$\times W(1\,1/2\, f_2 l_4; 1/2\, j_4)\, C(l f_2 j_2; m\, m_2-m)\, C(j_4 1 f_2; m_4\, m_2-m-m_4)\, \delta_{m_2-m-m_4}. \quad \text{(A1-15)}$$

Inserting Eqs. (A1-14) and (A1-15) into Eq. (A1-9) we obtain

$$B'_{\kappa_1\kappa_2\kappa_3\kappa_4} = (-)^m \frac{6[l]}{4\pi} \sqrt{[l_3][l_4][j_3][j_4]}\, C(l_3 l l_1; 00)\, C(l_4 l l_2; 00)$$

$$\times \sum_{f_1 f_2} \sqrt{[f_1][f_2]}\, W(l l_3 j_1 \tfrac{1}{2}; l_1 f_1)\, W(l l_4 j_2 \tfrac{1}{2}; l_2 f_2)\, W(1\tfrac{1}{2} f_1 l_3; \tfrac{1}{2} j_3)$$

$$\times W(1\tfrac{1}{2} f_2 l_4; \tfrac{1}{2} j_4)\, C(l f_1 j_1; -m\, m_1+m)\, C(l f_2 j_2; m\, m_2-m)$$

$$\times C(j_3 1 f_1; m_3\, m_1+m-m_3)\, C(j_4 1 f_2; m_4\, m_2-m-m_4)\, \mathfrak{Y}_{m_1+m-m_3} \cdot \mathfrak{Y}_{m_2-m-m_4} .$$

Since the spherical basis vectors are orthonormal according to

$$\mathfrak{Y}^*_{\mu'} \cdot \mathfrak{Y}_{\mu} = (-)^{-\mu'} \mathfrak{Y}_{-\mu'} \cdot \mathfrak{Y}_{\mu} = \delta_{\mu',\mu} ,$$

it follows that

$$\mathfrak{Y}_{m_1+m-m_3} \cdot \mathfrak{Y}_{m_2-m-m_4} = (-)^{m_3-m-m_1}\, \delta_{m_1+m_2,\, m_3+m_4} .$$

Using this relation we can obtain the matrix element $B'_{K_1K_2K_3K_4}$ as

$$B'_{K_1K_2K_3K_4} = (-)^{m_3-m_1} \frac{6[l]}{4\pi} \sqrt{[l_3][l_4][j_3][j_4]}\, C(l_3 l l_1; 00)\, C(l_4 l l_2; 00)$$

$$\times \sum_{f_1 f_2} \sqrt{[f_1][f_2]}\, W(l l_3 j_1 \tfrac{1}{2}; l_1 f_1)\, W(l l_4 j_2 \tfrac{1}{2}; l_2 f_2)\, W(1\tfrac{1}{2} f_1 l_3; \tfrac{1}{2} j_3)$$

$$\times W(1\tfrac{1}{2} f_2 l_4; \tfrac{1}{2} j_4)\, C(j_3 1 f_1; m_3\, m_1+m-m_3)\, C(j_4 1 f_2; m_4\, m_2-m-m_4)$$

$$\times C(l f_1 j_1; -m\, m_1+m)\, C(l f_2 j_2; m\, m_2-m)\, \delta_{m_1+m_2,\, m_3+m_4} . \qquad (45b)$$

APPENDIX II

CALCULATIONS OF ANGULAR COUPLING COEFFICIENTS IN $B\bar{B}$

From Eqs. (45a) and (45b), $\mathcal{B}_{K_1K_2K_3K_4}$ and $\mathcal{B}'_{K_1K_2K_3K_4}$ are given by

$$\mathcal{B}_{K_1K_2K_3K_4} = (-)^{m_1+m_2+m+1} \frac{\sqrt{[l_1][l_2][l_3][l_4][j_1][j_2][j_3][j_4]}}{4\pi[l]} C(l_1 l_3 l; 00)$$
$$\times C(l_2 l_4 l; 00) C(j_1 j_3 l; -m_1 m_3) C(j_2 j_4 l; -m_2 m_4)$$
$$\times W(j_1 l_1 j_3 l_3; \tfrac{1}{2} l) W(j_2 l_2 j_4 l_4; \tfrac{1}{2} l) \delta_{m_3-m_1,m} \delta_{m_2-m_4,m}, \quad (45'a)$$

$$\mathcal{B}'_{K_1K_2K_3K_4} = (-)^{m_3-m_1} \frac{6[l]}{4\pi} \sqrt{[l_3][l_4][j_3][j_4]}\, C(l_3 l l_1; 00) C(l_4 l l_2; 00)$$
$$\times \sum_{f_1 f_2} \sqrt{[f_1][f_2]}\, W(l l_3 j_1 \tfrac{1}{2}; l_1 f_1) W(l l_4 j_2 \tfrac{1}{2}; l_2 f_2) W(1\tfrac{1}{2} f_1 l_3; \tfrac{1}{2} j_3)$$
$$\times W(1\tfrac{1}{2} f_2 l_4; \tfrac{1}{2} j_4) C(j_3 1 f_1; m_3 m_1+m-m_3) C(j_4 1 f_2; m_4 m_2-m-m_4)$$
$$\times C(l f_1 j_1; -m m_1+m) C(l f_2 j_2; m m_2-m) \delta_{m_1+m_2,m_3+m_4}, \quad (45'b)$$

A. Calculation of $\mathcal{B}_i \bar{\mathcal{B}}_j$

Inserting Eq. (45'a) into Eq. (53), $\mathcal{B}_i \bar{\mathcal{B}}_j$ is written as

$$\mathcal{B}_i \bar{\mathcal{B}}_j = (4\pi)^2 \sum_{m_1 m_2 m_3 m_4 m \bar{m}} \sqrt{[l_1][\bar{l}_1]}\, C(l_1 \tfrac{1}{2} j_1; 0 m_1)$$
$$\times C(\bar{l}_1 \tfrac{1}{2} \bar{j}_1; 0 m_1)\, \mathcal{B}_{K_1K_2K_3K_4}\, \mathcal{B}_{\bar{K}_1\bar{K}_2\bar{K}_3\bar{K}_4}$$
$$= \frac{[l_1][\bar{l}_1][l_2][j_2][j_3][j_4]}{[l][\bar{l}]} \sqrt{[j_1][\bar{j}_1][l_3][\bar{l}_3][l_4][\bar{l}_4]}\, C(l_1 l_3 l; 00) C(\bar{l}_1 \bar{l}_3 \bar{l}; 00)$$
$$\times C(l_2 l_4 l; 00) C(l_2 \bar{l}_4 \bar{l}; 00) W(j_1 j_3 l_1 l_3; l \tfrac{1}{2}) W(\bar{j}_1 j_3 \bar{l}_1 \bar{l}_3; \bar{l} \tfrac{1}{2})$$

$$\times W(j_2 j_4 l_2 l_4; l \tfrac{1}{2}) W(j_2 j_4 l_2 \bar{l}_4; \bar{l} \tfrac{1}{2}) \sum_{m_1 m_2 m_3 m_4 m \bar{m}} (-)^{m+\bar{m}}$$

$$\times C(l, \tfrac{1}{2} j_1; 0 m_1) C(\bar{l}, \tfrac{1}{2} \bar{j}_1; 0 m_1) C(j_1 j_3 l; -m_1 m_3) C(\bar{j}_1 j_3 \bar{l}; -m_1 m_3)$$

$$\times C(j_2 j_4 l; -m_2 m_4) C(j_2 j_4 \bar{l}; -m_2 m_4) \delta_{m_3 - m_1, m} \delta_{m_2 - m_4, m} \delta_{m, \bar{m}} . \quad (A2-1)$$

This expression contains six Clebsch-Gordan coefficients (referred to hereafter as C coefficient) depending on projection quantum numbers m_1, m_2, m_3, m_4, m, and $\bar{m}$. The sums over these quantum numbers are carried out using various properties of C coefficients and Racah coefficients.

The relations between C and Racah coefficients allow us to write

$$C(j_1 j_3 l; -m_1 m_3) C(j_2 j_4 l; -m_2 m_4)$$

$$= (-)^{j_4 + m_4} \left(\frac{[l]}{[j_2]}\right)^{1/2} \sum_L ([l][L])^{1/2} W(j_1 j_3 j_2 j_4; l L) C(j_3 j_4 L; m_3 m_4)$$

$$\times C(j_1 L j_2; -m_1, m_3 + m_4) . \quad (A2-2)$$

Using this expression, the product of six C coefficients can be written as

$$\sum_{m_1 m_2 m_3 m_4 m \bar{m}} (-)^{m+\bar{m}} C(l, \tfrac{1}{2} j_1; 0 m_1) C(\bar{l}, \tfrac{1}{2} \bar{j}_1; 0 m_1) C(j_1 j_3 l; -m_1 m_3)$$

$$\times C(\bar{j}_1 j_3 \bar{l}; -m_1 m_3) C(j_2 j_4 l; -m_2 m_4) C(j_2 j_4 \bar{l}; -m_2 m_4) \delta_{m_3 - m_1, m} \delta_{m_2 - m_4, m} \delta_{m, \bar{m}}$$

$$= \sum_{m_1} C(l, \tfrac{1}{2} j_1; 0 m_1) C(\bar{l}, \tfrac{1}{2} \bar{j}_1; 0 m_1) \sum_{m_3 m_4} (-)^{j_4 + m_4} \left(\frac{[l]}{[j_2]}\right)^{1/2} \sum_L ([l][L])^{1/2}$$

$$\times W(j_1 j_3 j_2 j_4; l L) C(j_3 j_4 L; m_3 m_4) C(j_1 L j_2; -m_1, m_3 + m_4)$$

$$\times C(\bar{j}_1 j_3 \bar{l}; -m_1 m_3) C(j_2 j_4 \bar{l}; -m_2 m_4) \delta_{m_3 - m_1, m} \delta_{m_2 - m_4, m} \delta_{m, \bar{m}} . \quad (A2-3)$$

The summations over m_3 and m_4, keeping m_2 fixed and minding the relation $m_1 = m_3 + m_4 - m_2$, give

$$\sum_{m_3 m_4} (-)^{j_4+m_4} C(j_3 j_4 L; m_3 m_4) C(j_1 L j_2; -m_1, m_3+m_4) C(\bar{j}_1 j_3 \bar{l}; -m_1, m_3)$$
$$\times C(j_2 j_4 \bar{l}; -m_2 m_4) = \left(\frac{[j_2][\bar{l}]}{[j_1][\bar{j}_1]}\right)^{1/2} ([L][l])^{1/2} W(j_3 j_4 j_1 j_2; L \bar{l}) \delta_{j_1, \bar{j}_1}. \quad (A2\text{-}4)$$

From the orthogonality relation of C coefficients, the sum over m_1 yields the result

$$\sum_{m_1} C(l_1 1/2 j_1; 0 m_1) C(\bar{l}_1 1/2 \bar{j}_1; 0 m_1) \delta_{j_1, \bar{j}_1} = \frac{[j_1]}{[l_1]} \delta_{l_1, \bar{l}_1} . \quad (A2\text{-}5)$$

Using Eqs. (A2-4) and (A2-5), and the orthogonal relation of Racah coefficients, Eq. (A2-3) is expressed as

$$\sum_{m_1 m_2 m_3 m_4} C(l_1 1/2 j_1; 0 m_1) C(\bar{l}_1 1/2 \bar{j}_1; 0 m_1) C(j_1 j_3 l; -m_1 m_3) C(\bar{j}_1 j_3 \bar{l}; -m_1 m_3)$$
$$\times C(j_2 j_4 l; -m_2 m_4) C(j_2 j_4 \bar{l}; -m_2 m_4)$$
$$= \frac{[l]}{[l_1]} \sum_L [L][\bar{l}] W(j_1 j_3 j_2 j_4; l L) W(j_3 j_4 j_1 j_2; L \bar{l}) \delta_{\kappa_1, \bar{\kappa}_1}$$
$$= \frac{[l]}{[l_1]} \delta_{\kappa_1, \bar{\kappa}_1} \delta_{l, \bar{l}} . \quad (A2\text{-}6)$$

The resultant expression for $B_i \bar{B}_j$ is given by

$$B_i \bar{B}_j = \frac{[l_1][l_2][j_1][\bar{j}_2][j_3][j_4]}{[l]} \sqrt{[l_3][l_4][\bar{l}_3][\bar{l}_4]}\, C(l_1 l_3 l; 00) C(l_1 \bar{l}_3 l; 00)$$
$$\times C(l_2 l_4 l; 00) C(l_2 \bar{l}_4 l; 00) W(j_1 j_3 l_1 l_3; l 1/2) W(j_1 j_3 l_1 \bar{l}_3; l 1/2)$$
$$\times W(j_2 j_4 l_2 l_4; l 1/2) W(j_2 j_4 l_2 \bar{l}_4; l 1/2) \delta_{l, \bar{l}}. \quad (54)$$

B. Calculation of $B_i \overline{B}'_j$

Using Eqs. (45'a) and (45'b), $B_i \overline{B}'_j$ has the form

$$B_i \overline{B}'_j = (4\pi)^2 \sum_{m_1 m_2 m_3 m_4 m \bar{m}} \sqrt{[l_1][\bar{l}_1]}\, C(l_1 \tfrac{1}{2} j_1; 0\, m_1)\, C(\bar{l}_1 \tfrac{1}{2} \bar{j}_1; 0\, m_1)$$

$$\times B_{\kappa_1 \kappa_2 \kappa_3 \kappa_4} B'_{\bar{\kappa}_1 \bar{\kappa}_2 \bar{\kappa}_3 \bar{\kappa}_4}$$

$$= \frac{6\,[l_1][j_3][j_4][\bar{l}]}{[l]} \sqrt{[\bar{l}_1][l_2][j_1][j_2][l_3][l_4][\bar{l}_3][\bar{l}_4]}\, C(l_1 l_3 l; 00)$$

$$\times C(l_2 l_4 l; 00)\, C(\bar{l}_3 \bar{l} \bar{l}_1; 00)\, C(\bar{l}_4 \bar{l} l_2; 00)\, W(j_1 j_3 l_1 l_3; l \tfrac{1}{2})$$

$$\times W(j_2 j_4 l_2 l_4; l \tfrac{1}{2}) \sum_{f_1 f_2} \sqrt{[f_1][f_2]}\, W(\bar{l} \bar{l}_3 \bar{j}_1 \tfrac{1}{2}; \bar{l}_1 f_1)$$

$$\times W(\bar{l} \bar{l}_4 \bar{j}_2 \tfrac{1}{2}; l_2 f_2)\, W(1 \tfrac{1}{2} f_1 \bar{l}_3; \tfrac{1}{2} j_3)\, W(1 \tfrac{1}{2} f_2 \bar{l}_4; \tfrac{1}{2} j_4)$$

$$\times \sum_{m_1 m_2 m_3 m_4 m \bar{m}} (-)^{m_2 + m_3 + m + 1}\, C(l_1 \tfrac{1}{2} j_1; 0\, m_1)\, C(\bar{l}_1 \tfrac{1}{2} \bar{j}_1; 0\, m_1)$$

$$\times C(j_1 j_3 l; -m_1\, m_3)\, C(j_2 j_4 l; -m_2\, m_4)\, C(j_3 1 f_1; m_3\, m_1 + \bar{m} - m_3)$$

$$\times C(j_4 1 f_2; m_4\, m_2 - \bar{m} - m_4)\, C(\bar{l} f_1 \bar{j}_1; -\bar{m}\, m_1 + \bar{m})\, C(\bar{l} f_2 j_2; \bar{m}\, m_2 - \bar{m})$$

$$\times \delta_{m_3 - m_1, m}\, \delta_{m_2 - m_4, m}\,, \qquad (A2\text{-}7)$$

From the relations between Racah and C coefficients, we can write

$$C(j_3 1 f_1; m_3\, m_1 + \bar{m} - m_3)\, C(\bar{l} f_1 \bar{j}_1; -\bar{m}\, m_1 + \bar{m})$$

$$= (-)^{\bar{l} + \bar{m} - m_3 - f_1} \left(\frac{[\bar{j}_1][f_1]}{[1]}\right)^{1/2} \sum_L [L]^{1/2}\, W(\bar{l} \bar{j}_1 1 j_3; f_1 L)$$

$$\times C(\bar{j}_1 j_3 L; -m_1\, m_3)\, C(\bar{l} L 1; -\bar{m}\, -m_1 + m_3)\,, \qquad (A2\text{-}8)$$

and

$$C(j_4\,1\,f_2;\, m_4\; m_2-\bar{m}-m_4)\, C(\bar{\ell}\, f_2\, j_2;\, \bar{m}\; m_2-\bar{m})$$

$$= (-)^{\bar{\ell}-\bar{m}-m_4-f_2}\left(\frac{[j_2][f_2]}{[1]}\right)^{1/2}\sum_{L'}[L']^{1/2}\, W(\bar{\ell}\, j_2\, 1\, j_4;\, f_2\, L')$$

$$\times C(j_2\, j_4\, L';\, -m_2\; m_4)\, C(\bar{\ell}\, L'\, 1;\, \bar{m}\; -m_2+m_4). \qquad (A2-9)$$

Using the orthogonality relation of C coefficient, the sum over $\bar{m}$, keeping other quantum numbers fixed, gives

$$\sum_{\bar{m}} C(\bar{\ell}\, L\, 1;\, -\bar{m}\; -m_1+m_3)\, C(\bar{\ell}\, L'\, 1;\, \bar{m}\; -m_2+m_4) = (-)^{\bar{\ell}+L-1}\frac{[1]}{[L]}\,\delta_{L,L'}.$$

The term depending on projection quantum numbers in Eq. (A2-7) is written as

$$\sum_{m_1 m_2 m_3 m_4 m \bar{m}} (-)^{m_2+m_3+m+1}\, C(\ell_1\, 1/2\, j_1;\, 0\; m_1)\, C(\bar{\ell}_1\, 1/2\, j_2;\, 0\; m_1)$$

$$\times C(j_1\, j_3\, \ell;\, -m_1\; m_3)\, C(j_2\, j_4\, \ell;\, -m_2\; m_4)\, C(j_3\, 1\, f_1;\, m_3\; m_1+\bar{m}-m_3)$$

$$\times C(j_4\, 1\, f_2;\, m_4\; m_2-\bar{m}-m_4)\, C(\bar{\ell}\, f_1\, j_1;\, -\bar{m}\; m_1+\bar{m})\, C(\bar{\ell}\, f_2\, j_2;\, \bar{m}\; m_2-\bar{m})$$

$$\times \delta_{m_3-m_1,m}\,\delta_{m_2-m_4,m}$$

$$= \sum_{m_1 m_2 m_3 m_4 m} (-)^{m_2-m_4+m-f_1-f_2+\bar{\ell}+L}\, C(\ell_1\, 1/2\, j_1;\, 0\; m_1)\, C(\bar{\ell}_1\, 1/2\, j_1;\, 0\; m_1)$$

$$\times C(j_1\, j_3\, \ell;\, -m_1\; m_3)\, C(j_2\, j_4\, \ell;\, -m_2\; m_4)\sum_{L}\sqrt{[j_1][j_2][f_1][f_2]}$$

$$\times W(\bar{\ell}\, j_1\, 1\, j_3;\, f_1\, L)\, W(\bar{\ell}\, j_2\, 1\, j_4;\, f_2\, L)\, C(j_1\, j_3\, L;\, -m_1\; m_3)$$

$$\times C(j_2\, j_4\, L;\, -m_2\; m_4)\,\delta_{m_1+m_2,\,m_3+m_4}\,\delta_{m_2-m_4,m},$$

$$= \sum_{L} (-)^{\bar{\ell}+L+f_1+f_2} \sqrt{[\bar{j}_1][j_2][f_1][f_2]}\, W(\bar{l}\,\bar{j}_1\, l\, j_3; f_1 L)\, W(\bar{l}\, j_2\, l\, j_4; f_2 L)$$

$$\times \sum_{m_1 m_2 m_3 m_4} C(l, \tfrac{1}{2}\, j_1; 0\, m_1)\, C(\bar{l}, \tfrac{1}{2}\, \bar{j}_1; 0\, m_1)\, C(j_1\, j_3\, l; -m_1\, m_3)$$

$$\times C(j_2\, j_4\, l; -m_2\, m_4)\, C(\bar{j}_1\, j_3\, L; -m_1\, m_3)\, C(j_2\, j_4\, L; -m_2\, m_4). \qquad (A2\text{-}10)$$

From Eq. (A2-6), the summations over m_1, m_2, m_3, and m_4 give the result

$$\sum_{m_1 m_2 m_3 m_4} C(l, \tfrac{1}{2}\, j_1; 0\, m_1)\, C(\bar{l}, \tfrac{1}{2}\, \bar{j}_1; 0\, m_1)\, C(j_1\, j_3\, l; -m_1\, m_3)\, C(j_2\, j_4\, l; -m_2\, m_4)$$

$$\times C(\bar{j}_1\, j_3\, L; -m_1\, m_3)\, C(j_2\, j_4\, L; -m_2\, m_4)$$

$$= \frac{[l]}{[l_1]}\, \delta_{L,l}\, \delta_{\kappa_1, \bar{\kappa}_1}. \qquad (A2\text{-}11)$$

Substituting Eqs. (A2-10) and (A2-11) into Eq. (A2-7), we obtain

$$B_i \bar{B}'_j = (-)^{l+\bar{l}}\, 6\, [j_1][j_2][j_3][j_4][\bar{l}] \sqrt{[l_1][l_2][l_3][l_4][\bar{l}_3][\bar{l}_4]}$$

$$\times C(l_1\, l_3\, l; 00)\, C(\bar{l}_3\, \bar{l}\, l_1; 00)\, C(l_2\, l_4\, l; 00)\, C(\bar{l}_4\, \bar{l}\, l_2; 00)$$

$$\times W(j_1 j_3\, l_1 l_3; l\, \tfrac{1}{2})\, W(j_2 j_4\, l_2 l_4; l\, \tfrac{1}{2}) \sum_{f_1 f_2} (-)^{f_1+f_2} [f_1][f_2]$$

$$\times W(\bar{l}\,\bar{l}_3\, j_1\, \tfrac{1}{2}; l_1 f_1)\, W(\bar{l}\,\bar{l}_4\, j_2\, \tfrac{1}{2}; l_2 f_2)\, W(1\, \tfrac{1}{2}\, f_1\, \bar{l}_3; \tfrac{1}{2}\, j_3)$$

$$\times W(1\, \tfrac{1}{2}\, f_2\, \bar{l}_4; \tfrac{1}{2}\, j_4)\, W(\bar{l}\, j_2\, 1\, j_4; f_2\, l)\, W(\bar{l}\, j_1\, 1\, j_3; f_1\, l). \qquad (A2\text{-}12)$$

Introducing the 9-j symbol of Wigner and using the symmetric properties of the Racah coefficients, we can perform contraction of Racah coefficients in the following way:

$$\sum_{f_1}(-)^{f_1}[f_1]\,W(\bar{l}\,\bar{l}_3\,j_1\tfrac{1}{2};\,l_1 f_1)\,W(1\tfrac{1}{2}\,f_1\,\bar{l}_3;\tfrac{1}{2}\,j_3)\,W(\bar{l}\,j_1\,1\,j_3;\,f_1 l)$$

$$=\sum_{f_1}(-)^{j_3}[f_1]\,W(l\,j_1\,\bar{l}_3\tfrac{1}{2};\,f_1 l_1)\,W(1\,j_3\tfrac{1}{2}\,\bar{l}_3;\,f_1\tfrac{1}{2})\,W(\bar{l}\,j_1\,1\,j_3;\,f_1 l)$$

$$=(-)^{j_3}\,X\begin{pmatrix}\bar{l} & 1 & l\\ \bar{l}_3 & \tfrac{1}{2} & j_3\\ l_1 & \tfrac{1}{2} & j_1\end{pmatrix}. \qquad (A2\text{-}13a)$$

Similarly

$$\sum_{f_2}(-)^{f_2}[f_2]\,W(\bar{l}\,\bar{l}_4\,j_2\tfrac{1}{2};\,l_2 f_2)\,W(1\tfrac{1}{2}\,f_2\,\bar{l}_4;\tfrac{1}{2}\,j_4)\,W(\bar{l}\,j_2\,1\,j_4;\,f_2 l)$$

$$=(-)^{j_4}\,X\begin{pmatrix}\bar{l} & 1 & l\\ \bar{l}_4 & \tfrac{1}{2} & j_4\\ l_2 & \tfrac{1}{2} & j_2\end{pmatrix}. \qquad (A2\text{-}13b)$$

Using the expressions of Eqs. (A2-13a) and (A2-13b), Eq. (A2-12) is rewritten as

$$B_i\overline{B'_j}=(-)^{l+\bar{l}+j_1+j_2}\,6\,[j_1][j_2][j_3][j_4][\bar{l}]\sqrt{[l_1][l_2][l_3][l_4][\bar{l}_3][\bar{l}_4]}$$

$$\times C(l_1 l_3 l;00)\,C(l_2 l_4 l;00)\,C(\bar{l}_3\,\bar{l}\,l_1;00)\,C(\bar{l}_4\,\bar{l}\,l_2;00)$$

$$\times W(j_1 j_3 l_1 l_3;\,l\tfrac{1}{2})\,W(j_2 j_4 l_2 l_4;\,l\tfrac{1}{2})$$

$$\times X\begin{pmatrix}\bar{l} & 1 & l\\ \bar{l}_3 & \tfrac{1}{2} & j_3\\ l_1 & \tfrac{1}{2} & j_1\end{pmatrix}X\begin{pmatrix}\bar{l} & 1 & l\\ \bar{l}_4 & \tfrac{1}{2} & j_4\\ l_2 & \tfrac{1}{2} & j_2\end{pmatrix}. \qquad (55)$$

C. Calculation of $B'_i\overline{B'_j}$

$B'_i\overline{B'_j}$ is given by

$$B'_i\overline{B'_j}=(4\pi)^2\sum_{m_1 m_2 m_3 m_4 m\bar{m}}\sqrt{[l_1][\bar{l}_1]}\;C(l_1\tfrac{1}{2}\,j_1;0\,m_1)\,C(\bar{l}_1\tfrac{1}{2}\,\bar{j}_1;0\,m_1)$$

$$\times B'_{\kappa_1\kappa_2\kappa_3\kappa_4} B'_{\bar{\kappa}_1\kappa_2\bar{\kappa}_3\bar{\kappa}_4},$$

$$= 36[l][\bar{l}][j_3][j_4]\sqrt{[l_1][\bar{l}_1][l_3][l_4][\bar{l}_3][\bar{l}_4]}\, C(l_3 l l_1;00) C(\bar{l}_3 \bar{l} \bar{l}_1;00)$$

$$\times C(l_4 l l_2;00) C(\bar{l}_4 l l_2;00) \sum_{f_1 f_2 \bar{f}_1 \bar{f}_2} \sqrt{[f_1][f_2][\bar{f}_1][\bar{f}_2]}$$

$$\times W(l l_3 j_1 1/2; l_1 f_1) W(l l_4 j_2 1/2; l_2 f_2) W(1 1/2 f_1 l_3; 1/2 j_3)$$

$$\times W(1 1/2 f_2 l_4; 1/2 j_4) W(\bar{l} \bar{l}_3 \bar{j}_1 1/2; \bar{l}_1 \bar{f}_1) W(\bar{l} \bar{l}_4 j_2 1/2; l_2 \bar{f}_2)$$

$$\times W(1 1/2 \bar{f}_1 \bar{l}_3; 1/2 j_3) W(1 1/2 \bar{f}_2 \bar{l}_4; 1/2 j_4) \sum_{m_1 m_2 m_3 m_4 m \bar{m}}$$

$$\times C(l_1 1/2 j_1; 0 m_1) C(\bar{l}_1 1/2 \bar{j}_1; 0 m_1) C(j_3 1 f_1; m_3 m_1+m-m_3)$$

$$\times C(j_4 1 f_2; m_4 m_2-m-m_4) C(l f_1 j_1; -m m_1+m) C(l f_2 j_2; m m_2-m)$$

$$\times C(j_3 1 \bar{f}_1; m_3 m_1+\bar{m}-m_3) C(j_4 1 \bar{f}_2; m_4 m_2-\bar{m}-m_4)$$

$$\times C(\bar{l} \bar{f}_1 \bar{j}_1; -\bar{m} m_1+\bar{m}) C(\bar{l} \bar{f}_2 j_2; \bar{m} m_2-\bar{m}) \delta_{m_1+m_2, m_3+m_4}. \quad (A2-14)$$

In the similar manner to Eqs. (A2-8) and (A2-9), products of C coefficients are expressed as

$$C(j_3 1 f_1; m_3 m_1+m-m_3) C(l f_1 j_1; -m m_1+m)$$

$$= (-)^{l+m-m_3-f_1} \left(\frac{[j_3][f_1]}{[1]}\right)^{1/2} \sum_L [L]^{1/2} W(l j_1 1 j_3; f_1 L)$$

$$\times C(j_1 j_3 L; -m_1 m_3) C(l L 1; -m -m_1+m_3), \quad (A2-15a)$$

$$C(j_4 1 f_2; m_4 m_2-m-m_4) C(l f_2 j_2; m m_2-m)$$

$$= (-)^{\ell - m - m_4 - j_2} \left(\frac{[j_2][f_2]}{[1]}\right)^{1/2} \sum_{L_1} [L_1]^{1/2} W(\ell j_2 1 j_4; f_2 L_1)$$

$$\times C(j_2 j_4 L_1; -m_2 m_4) C(\ell L_1 1; m - m_2 + m_4), \qquad (A2-15b)$$

$$C(j_3 1 \bar{f}_1; m_3 m_3 + \bar{m} - m_3) C(\bar{\ell} \bar{f}_1 \bar{j}_1; -\bar{m} m_1 + \bar{m})$$

$$= (-)^{\bar{\ell} + \bar{m} - m_1 - \bar{f}_1} \left(\frac{[\bar{j}_1][\bar{f}_1]}{[1]}\right)^{1/2} \sum_{L'} [L']^{1/2} W(\bar{\ell} \bar{j}_1 1 j_3; \bar{f}_1 L')$$

$$\times C(\bar{f}_1 j_3 L'; -m_1 m_3) C(\bar{\ell} L' 1; -\bar{m} - m_1 + m_3), \qquad (A2-16a)$$

and

$$C(j_4 1 \bar{f}_2; m_4 m_2 - \bar{m} - m_4) C(\bar{\ell} \bar{f}_2 \bar{j}_2; \bar{m} m_2 - \bar{m})$$

$$= (-)^{\bar{\ell} - \bar{m} - m_4 - \bar{f}_2} \left(\frac{[j_2][\bar{f}_2]}{[1]}\right)^{1/2} \sum_{L_1'} [L_1']^{1/2} W(\bar{\ell} j_2 1 j_4; \bar{f}_2 L_1')$$

$$\times C(j_2 j_4 L_1'; -m_2 m_4) C(\bar{\ell} L_1' 1; \bar{m} - m_2 + m_4). \qquad (A2-16b)$$

From Eqs. (A2-15) and (A2-16), the summations over m and $\bar{m}$ give

$$\sum_m C(\ell L 1; -m\ m_3 - m_1) C(\ell L_1 1; m\ m_4 - m_2) = (-)^{\ell + L - 1} \frac{[1]}{[L]} \delta_{L, L_1},$$

and

$$\sum_{\bar{m}} C(\bar{\ell} L' 1; -\bar{m}\ m_3 - m_1) C(\bar{\ell} L_1' 1; \bar{m}\ m_4 - m_2) = (-)^{\bar{\ell} + L' - 1} \frac{[1]}{[L']} \delta_{L', L_1'}.$$

After the summations over m and $\bar{m}$, the term which depends on projection quantum numbers can be written by

$$\sum_{m_1 m_2 m_3 m_4 m \bar{m}} C(\ell_1 \tfrac{1}{2} j_1; 0\, m_1) C(\bar{\ell}_1 \tfrac{1}{2} \bar{j}_1; 0\, m_1) C(j_3 1 f_1; m_3\ m_1 + m - m_3)$$

$$\times C(j_4 1 f_2; m_4\ m_2 - m - m_4) C(\ell f_1 j_1; -m\ m_1 + m) C(\ell f_2 j_2; m\ m_2 - m)$$

$$\times C(j_3\,1\,\bar{f}_1;\, m_3\; m_1+\bar{m}-m_3)\, C(j_4\,1\,\bar{f}_2;\, m_4\; m_2-\bar{m}-m_4)\, C(\bar{l}\,\bar{f}_1\,\bar{j}_1;\, -\bar{m}\; m_1+\bar{m})$$

$$\times C(\bar{l}\,\bar{f}_2\,\bar{j}_2;\, \bar{m}\; m_2-\bar{m})\,\delta_{m_1+m_2,\, m_3+m_4}$$

$$= (-)^{j_1+j_2+\bar{f}_1+\bar{f}_2+l+\bar{l}}\,[j_2]\sqrt{[j_1][\bar{j}_1][f_1][f_2][\bar{f}_1][\bar{f}_2]}\sum_{LL'}(-)^{L+L'}$$

$$\times W(l\,j_1\,1\,j_3;\, f_1 L)\, W(l\,j_2\,1\,j_4;\, f_2 L)\, W(\bar{l}\,\bar{f}_1\,1\,j_3;\, \bar{f}_1 L')$$

$$\times W(\bar{l}\,j_2\,1\,j_4;\, \bar{f}_2 L')\sum_{m_1 m_2 m_3 m_4} C(l_1\tfrac{1}{2}\, j_1;\, 0\, m_1)\, C(\bar{l}_1\tfrac{1}{2}\,\bar{f}_1;\, 0\, m_1)$$

$$\times C(j_1 j_3 L;\, -m_1 m_3)\, C(j_2 j_4 L;\, -m_2 m_4)\, C(\bar{f}_1 j_3 L';\, -m_1 m_3)$$

$$\times C(j_2 j_4 L';\, -m_2 m_4). \qquad (A2-17)$$

The sums over m_1, m_2, m_3, and m_4 can be performed in the similar manner to Eq. (A2-6) and give

$$\sum_{m_1 m_2 m_3 m_4} C(l_1\tfrac{1}{2}\, j_1;\, 0\, m_1)\, C(\bar{l}_1\tfrac{1}{2}\,\bar{f}_1;\, 0\, m_1)\, C(j_1 j_3 L;\, -m_1 m_3)$$

$$\times C(j_2 j_4 L;\, -m_2 m_4)\, C(\bar{f}_1 j_3 L';\, -m_1 m_3)\, C(j_2 j_4 L';\, -m_2 m_4)$$

$$= \frac{[L]}{[l_1]}\,\delta_{L,L'}\,\delta_{\kappa_1,\bar{\kappa}_1}. \qquad (A2-18)$$

Substituting Eqs. (A2-17) and (A2-18) into Eq. (A2-14), the resultant expression for $B_i' \bar{B}_j'$ is

$$B_i'\bar{B}_j' = (-)^{l+\bar{l}}\,36\,[j_1][j_2][j_3][j_4][l][\bar{l}]\sqrt{[l_3][l_4][\bar{l}_3][\bar{l}_4]}$$

$$\times C(l_3\, l\, l_1;\, 00)\, C(l_4\, l\, l_2;\, 00)\, C(\bar{l}_3\,\bar{l}\, l_1;\, 00)\, C(\bar{l}_4\,\bar{l}\, l_2;\, 00)$$

$$\times \sum_{f_1 f_2 \bar{f}_1 \bar{f}_2} (-)^{f_1+f_2+\bar{f}_1+\bar{f}_2}\,[f_1][f_2][\bar{f}_1][\bar{f}_2]\, W(l\, l_3\, j_1\tfrac{1}{2};\, l_1 f_1)$$

$$\times W(l l_4 j_2 \tfrac{1}{2}; l_2 f_2)\, W(1\tfrac{1}{2} f_1 l_3; \tfrac{1}{2} j_3)\, W(1\tfrac{1}{2} f_2 l_4; \tfrac{1}{2} j_4)$$

$$\times W(\bar{l} \bar{l}_3 j_1 \tfrac{1}{2}; l_1 \bar{f}_1)\, W(\bar{l} \bar{l}_4 j_2 \tfrac{1}{2}; l_2 \bar{f}_2)\, W(1\tfrac{1}{2} \bar{f}_1 \bar{l}_3; \tfrac{1}{2} j_3)$$

$$\times W(1\tfrac{1}{2} \bar{f}_2 \bar{l}_4; \tfrac{1}{2} j_4) \sum_L [L]\, W(l j_1 1 j_3; f_1 L)$$

$$\times W(l j_2 1 j_4; f_2 L)\, W(\bar{l} j_1 1 j_3; \bar{f}_1 L)\, W(\bar{l} j_2 1 j_4; \bar{f}_2 L). \quad (A2\text{-}19)$$

By symmetric properties of Racah coefficients, we can contract the sum over f_1, leading to the form of 9-j symbol.

$$\sum_{f_1} (-)^{f_1} [f_1]\, W(l l_3 j_1 \tfrac{1}{2}; l_1 f_1)\, W(1\tfrac{1}{2} f_1 l_3; \tfrac{1}{2} j_3)\, W(l j_1 1 j_3; f_1 L)$$

$$= (-)^{j_3} \sum_{f_1} [f_1]\, W(l j_1 l_3 \tfrac{1}{2}; f_1 l_1)\, W(1 j_3 \tfrac{1}{2} l_3; f_1 \tfrac{1}{2})\, W(l j_1 1 j_3; f_1 L)$$

$$= (-)^{j_3} X \begin{pmatrix} l & 1 & L \\ l_3 & \tfrac{1}{2} & j_3 \\ l_1 & \tfrac{1}{2} & j_1 \end{pmatrix}. \quad (A2\text{-}20)$$

Similarly the sums over f_2, $\bar{f}_1$, and $\bar{f}_2$ can be performed. The final expression for $B_i' \bar{B}_j'$ is

$$B_i' \bar{B}_j' = (-)^{l+\bar{l}} 36\, [j_1][j_2][j_3][j_4][l][\bar{l}] \sqrt{[l_3][\bar{l}_3][l_4][\bar{l}_4]}$$

$$\times C(l_3 l l_1; 00)\, C(l_4 l l_2; 00)\, C(\bar{l}_3 \bar{l} l_1; 00)\, C(\bar{l}_4 \bar{l} l_2; 00)$$

$$\times \sum_L [L] X \begin{pmatrix} l & 1 & L \\ l_3 & \tfrac{1}{2} & j_3 \\ l_1 & \tfrac{1}{2} & j_1 \end{pmatrix} X \begin{pmatrix} l & 1 & L \\ l_4 & \tfrac{1}{2} & j_4 \\ l_2 & \tfrac{1}{2} & j_2 \end{pmatrix} X \begin{pmatrix} \bar{l} & 1 & L \\ \bar{l}_3 & \tfrac{1}{2} & j_3 \\ l_1 & \tfrac{1}{2} & j_1 \end{pmatrix}$$

$$\times X \begin{pmatrix} \bar{l} & 1 & L \\ \bar{l}_4 & \tfrac{1}{2} & j_4 \\ l_2 & \tfrac{1}{2} & j_2 \end{pmatrix}. \quad (56)$$

APPENDIX III

CALCULATIONS OF ANGULAR COUPLING COEFFICIENTS IN $B\bar{C}$

From Eqs. (45a) and (45b), $B_{\kappa_1\kappa_2\kappa_3\kappa_4}$, $B'_{\kappa_1\kappa_2\kappa_3\kappa_4}$, $C_{\kappa_1\kappa_2\kappa_3\kappa_4}$, and $C'_{\kappa_1\kappa_2\kappa_3\kappa_4}$ are written by

$$B_{\kappa_1\kappa_2\kappa_3\kappa_4} = (-)^{m_1+m_2+m+1} \frac{\sqrt{[l_1][l_2][l_3][l_4][j_1][j_2][j_3][j_4]}}{4\pi[l]} C(l_1 l_3 l; 00)$$
$$\times C(l_2 l_4 l; 00)\, C(j_1 j_3 l; -m_1 m_3)\, C(j_2 j_4 l; -m_2 m_4)$$
$$\times W(j_1 l_1 j_3 l_3; \tfrac{1}{2} l)\, W(j_2 l_2 j_4 l_4; \tfrac{1}{2} l)\, \delta_{m_3-m_1,m}\, \delta_{m_2-m_4,m}, \qquad (45'a)$$

$$B'_{\kappa_1\kappa_2\kappa_3\kappa_4} = (-)^{m_3-m_1} \frac{6[l]}{4\pi} \sqrt{[l_3][l_4][j_3][j_4]}\, C(l_3 l l_1; 00)\, C(l_4 l l_2; 00)$$
$$\times \sum_{f_1 f_2} \sqrt{[f_1][f_2]}\, W(l l_3 j_1 \tfrac{1}{2}; l_1 f_1)\, W(l l_4 j_2 \tfrac{1}{2}; l_2 f_2)$$
$$\times W(1\tfrac{1}{2}\, f_1 l_3; \tfrac{1}{2} j_3)\, W(1\tfrac{1}{2}\, f_2 l_4; \tfrac{1}{2} j_4)\, C(j_3 1 f_1; m_3 m_1+m-m_3)$$
$$\times C(j_4 1 f_2; m_4 m_2-m-m_4)\, C(l f_1 j_1; -m m_1+m)\, C(l f_2 j_2; m m_2-m)$$
$$\times \delta_{m_1+m_2,m_3+m_4}, \qquad (45'b)$$

$$C_{\kappa_1\kappa_2\kappa_3\kappa_4} = (-)^{m_1+m_2+m+1} \frac{\sqrt{[l_1][l_2][l_3][l_4][j_1][j_2][j_3][j_4]}}{4\pi[l]} C(l_1 l_4 l; 00)$$
$$\times C(l_2 l_3 l; 00)\, C(j_1 j_4 l; -m_1 m_4)\, C(j_2 j_3 l; -m_2 m_3)$$
$$\times W(j_1 l_1 j_4 l_4; \tfrac{1}{2} l)\, W(j_2 l_2 j_3 l_3; \tfrac{1}{2} l)$$
$$\times \delta_{m_4-m_1,m}\, \delta_{m_2-m_3,m}, \qquad (A3-1a)$$

$$C'_{\kappa_1\kappa_2\kappa_3\kappa_4} = (-)^{m_4-m_1}\frac{6[l]}{4\pi}\sqrt{[l_3][l_4][j_3][j_4]}\,C(l_4 l l_1;00)\,C(l_3 l l_2;00)$$

$$\times\sum_{f_1 f_2}\sqrt{[f_1][f_2]}\;W(l l_4 j_1 1/2;l_1 f_1)\,W(l l_3 j_2 1/2;l_2 f_2)$$

$$\times W(1/2\; f_1 l_4;1/2\; j_4)\,W(1/2\; f_2 l_3;1/2\; j_3)\,C(j_4 1 f_1;m_4\; m_1+m-m_4)$$

$$\times C(j_3 1 f_2;m_3\; m_2-m-m_3)\,C(l f_1 j_1;-m\; m_1+m)\,C(l f_2 j_2;m\; m_2-m)$$

$$\times\delta_{m_1+m_2,\,m_3+m_4}\,. \qquad (A3-1b)$$

A. Calculation of $B_i\bar{C}_j$

$B_i\bar{C}_j$ is expressed in the term of product of $B_{\kappa_1\kappa_2\kappa_3\kappa_4}$ and $C'_{\kappa_1\kappa_2\kappa_3\kappa_4}$ as

$$B_i\bar{C}_j = (4\pi)^2\sum_{m_1 m_2 m_3 m_4 m\bar{m}}\sqrt{[l_1][\bar{l}_1]}\,C(l_1 1/2\; j_1;0\,m_1)\,C(\bar{l}_1 1/2\;\bar{j}_1;0\,m_1)$$

$$\times B_{\kappa_1\kappa_2\kappa_3\kappa_4}\,C_{\bar{\kappa}_1\kappa_2\bar{\kappa}_3\bar{\kappa}_4}$$

$$= \frac{[l_1][\bar{l}_1]}{[l][\bar{l}]}[j_2][j_3][j_4][l_2]\sqrt{[j_1][\bar{j}_1][l_3][l_4][\bar{l}_3][\bar{l}_4]}\;C(l_1 l_3 l;00)$$

$$\times C(l_2 l_4 l;00)\,C(\bar{l}_1\bar{l}_4\bar{l};00)\,C(l_2\bar{l}_3\bar{l};00)$$

$$\times W(j_1 j_3 l_1 l_3;l 1/2)\,W(j_2 j_4 l_2 l_4;l 1/2)\,W(\bar{j}_1 j_4\bar{l}_1\bar{l}_4;\bar{l}\,1/2)$$

$$\times W(j_2 j_3 l_2\bar{l}_3;\bar{l}\,1/2)\sum_{m_1 m_2 m_3 m_4 m\bar{m}}(-)^{m+\bar{m}}\,C(l_1 1/2\; j_1;0\,m_1)$$

$$\times C(\bar{l}_1 1/2\;\bar{j}_1;0\,m_1)\,C(j_1 j_3 l;-m_1\,m_3)\,C(j_2 j_4 l;-m_2\,m_4)$$

$$\times C(\bar{j}_1 j_4\bar{l};-m_1\,m_4)\,C(j_2 j_3\bar{l};-m_2\,m_3)\,\delta_{m_3-m_1,m}\,\delta_{m_4-m_1,\bar{m}}\,\delta_{m_1+m_2,m_3+m_4}, \qquad (A3-2)$$

The sums over projection quantum numbers can be carried out using the relations of Racah and C coefficients, and the symmetric properties of C coefficients.

From Eq. (A2-2), we can write

$$C(j_1 j_3 \ell; -m_1 m_3)\, C(j_2 j_4 \ell; -m_2 m_4)$$
$$= (-)^{j_4+m_4} \left(\frac{[\ell]}{[j_2]}\right)^{1/2} \sum_L ([\ell][L])^{1/2} W(j_1 j_3 j_2 j_4; \ell L)$$
$$\times C(j_3 j_4 L; m_3 m_4)\, C(j_1 L j_2; -m_1, m_3+m_4) \quad (A3-3)$$

Using Eq. (A3-3), the term depending on magnetic quantum numbers is

$$\sum_{m_1 m_2 m_3 m_4 m \bar{m}} (-)^{m_3+m_4-2m_1} C(l, 1/2\, j_1; 0 m_1) C(\bar{l}, 1/2\, \bar{j}_1; 0 m_1)$$
$$\times C(j_1 j_3 \ell; -m_1 m_3)\, C(j_2 j_4 \ell; -m_2 m_4)\, C(\bar{j}_1 j_4 \bar{\ell}; -m_1 m_4)$$
$$\times C(j_2 j_3 \bar{\ell}; -m_2 m_3)$$
$$= \sum_{m_1 m_2 m_3 m_4 m \bar{m}} (-)^{m_3+2m_4-2m_1+j_4} \left(\frac{[\ell]}{[j_2]}\right)^{1/2} C(l, 1/2\, j_1; 0 m_1) C(\bar{l}, 1/2\, \bar{j}_1; 0 m_1)$$
$$\times \sum_L ([\ell][L])^{1/2} W(j_1 j_3 j_2 j_4; \ell L)\, C(j_3 j_4 L; m_3 m_4)$$
$$\times C(j_1 L j_2; -m_1, m_3+m_4)\, C(\bar{j}_1 j_4 \bar{\ell}; -m_1 m_4)$$
$$\times C(j_2 j_3 \bar{\ell}; -m_2 m_3)$$
$$= \left(\frac{[\ell]}{[j_2]}\right)^{1/2} \sum_L ([\ell][L])^{1/2} W(j_1 j_3 j_2 j_4; \ell L) \sum_{m_1} C(l, 1/2\, j_1; 0 m_1)$$
$$\times C(\bar{l}, 1/2\, \bar{j}_1; 0 m_1) \sum_{m_2 m_3 m_4} (-)^{j_4+m_3} C(j_3 j_4 L; m_3 m_4)\, C(j_1 L j_2; -m_1, m_3+m_4)$$
$$\times C(\bar{j}_1 j_4 \bar{\ell}; -m_1 m_4)\, C(j_2 j_3 \bar{\ell}; -m_2 m_3)$$

$$= \left(\frac{[l][\bar{l}]}{[j_1][\bar{j}_1]}\right)^{1/2} \sum_L (-)^{L-j_1-\bar{j}_1} ([l][L])^{1/2} W(j_1 j_3 j_2 j_4; lL)$$

$$\times \sum_{m_1 m_2} C(l_1 1/2\, j_1; 0\, m_1)\, C(\bar{l}_1 1/2\, \bar{j}_1; 0\, m_1) \sum_{m_3 m_4} C(j_3 j_4 L; m_3 m_4)$$

$$\times C(L j_2 j_1; m_3+m_4 - m_2)\, C(j_4 \bar{l} \bar{j}_1; -m_4\, m_4 - m_1)\, C(j_3 j_2 \bar{l}; m_3 - m_2)$$

$$= \frac{[l][\bar{l}]}{[j_1]} \sum_L (-)^{l-L} [L] W(j_1 j_3 j_2 j_4; lL) W(j_4 j_3 j_1 j_2; L\bar{l})$$

$$\times \sum_{m_1} C(l_1 1/2\, j_1; 0\, m_1)\, C(\bar{l}_1 1/2\, j_1; 0\, m_1)\, \delta_{j_1 \bar{j}_1}$$

$$= \frac{[l][\bar{l}]}{[j_1]} \sum_L (-)^{l-L} [L] W(j_3 j_4 j_1 j_2; Ll) W(j_4 j_3 j_1 j_2; L\bar{l}) \frac{[j_1]}{[l_1]} \delta_{\kappa_1 \bar{\kappa}_1}$$

$$= \frac{[l][\bar{l}]}{[l_1]} (-)^{1+j_3+j_4} \sum_L (-)^{j_3+j_4-L} [L] W(j_3 j_4 j_1 j_2; Ll)$$

$$\times W(j_4 j_3 j_1 j_2; L\bar{l}). \qquad (A3-4)$$

Applying Racah's sum rule* we obtain

$$\sum_e (-)^{a+b-e} [e] W(abcd; ef) W(bacd; eg) = W(afgb; cd).$$

Eq. (A3-4) becomes

$$\sum_{m_1 m_2 m_3 m_4 m \bar{m}} (-)^{m_3+m_4-l} C(l_1 1/2\, j_1; 0\, m_1)\, C(\bar{l}_1 1/2\, \bar{j}_1; 0 m_1)\, C(j_1 j_3 l; -m_1\, m_3)$$

$$\times C(j_2 j_4 l; -m_2\, m_4)\, C(\bar{j}_1 j_4 \bar{l}; -m_1\, m_4)\, C(j_2 j_3 \bar{l}; -m_2\, m_3)$$

$$= (-)^{1+j_3+j_4} \frac{[l][\bar{l}]}{[l_1]} W(j_3 l \bar{l} j_4; j_1 j_2)$$

---

* There is a mistake in Eq. (6.14) in Rose's text book.[57]

W(agfb;cd) should be replaced by *W(afgb;cd)*.

$$= (-)^{j_1+j_2+j_3+j_4+l+\bar{l}+1} \frac{[l][\bar{l}]}{[l_1]} W(j_1 j_3 j_4 j_2; l \bar{l}) . \quad (A3-5)$$

Inserting this expression into Eq. (A3-2), $B_i \bar{C}_j$ has the form

$$B_i \bar{C}_j = (-)^{j_1+j_2+j_3+j_4+l+\bar{l}+1} [j_1][j_2][j_3][j_4][l_1][l_2] \sqrt{[l_3][l_4][\bar{l}_3][\bar{l}_4]}$$

$$\times C(l_1 l_3 l; 00) C(l_2 l_4 l; 00) C(l_1 \bar{l}_4 \bar{l}; 00) C(l_2 \bar{l}_3 \bar{l}; 00)$$

$$\times W(j_1 j_3 l_1 l_3; l\, 1/2) W(j_2 j_4 l_2 l_4; l\, 1/2) W(j_1 j_4 l_1 \bar{l}_4; \bar{l}\, 1/2)$$

$$\times W(j_2 j_3 l_2 \bar{l}_3; \bar{l}\, 1/2) W(j_1 j_3 j_4 j_2; l \bar{l}) . \quad (57)$$

B. Calculations of $B_i \bar{C}'_j$

From Eqs. (45'a) and (A3-1b) $B_i \bar{C}'_j$ is

$$B_i \bar{C}'_j = (4\pi)^2 \sum_{m_1 m_2 m_3 m_4 m \bar{m}} \sqrt{[l_1][\bar{l}_1]}\, C(l_1 1/2\, j_1; 0\, m_1) C(\bar{l}_1 1/2\, \bar{j}_1; 0\, m_1)$$

$$\times B_{\kappa_1 \kappa_2 \kappa_3 \kappa_4} C'_{\bar{\kappa}_1 \kappa_2 \bar{\kappa}_3 \bar{\kappa}_4}$$

$$= \frac{6[\bar{l}]}{[l]} [l_1][j_3][j_4] \sqrt{[j_1][j_2][\bar{l}_1][l_2][l_3][l_4][\bar{l}_3][\bar{l}_4]}\, C(l_1 l_3 l; 00)$$

$$\times C(l_2 l_4 l; 00) C(\bar{l}_4 \bar{l} \bar{l}_1; 00) C(\bar{l}_3 \bar{l} l_2; 00) W(j_1 j_3 l_1 l_3; l\, 1/2)$$

$$\times W(j_2 j_4 l_2 l_4; l\, 1/2) \sum_{f_1 f_2} \sqrt{[f_1][f_2]}\, W(\bar{l} \bar{l}_4 \bar{j}_1 1/2; \bar{l}_1 f_1) W(\bar{l} \bar{l}_3 j_2 1/2; l_2 f_2)$$

$$\times W(1/2\, f_1 \bar{l}_4; 1/2\, j_4) W(1/2\, f_2 \bar{l}_3; 1/2\, j_3) \sum_{m_1 m_2 m_3 m_4 m \bar{m}} (-)^{m_2+m_4+m+1}$$

$$\times C(l_1 1/2\, j_1; 0\, m_1) C(\bar{l}_1 1/2\, \bar{j}_1; 0\, m_1) C(j_1 j_3 l; -m_1 m_3) C(j_2 j_4 l; -m_2 m_4)$$

$$\times C(j_4\,1\,f_1;\, m_4\; m_1+\bar{m}-m_4)\, C(j_3\,1\,f_2;\, m_3\; m_2-\bar{m}-m_3)\, C(\bar{l}\,f_1\,\bar{j}_1;\, -\bar{m}\; m_1+\bar{m})$$

$$\times C(\bar{l}\,f_2\,j_2;\, \bar{m}\; m_2-\bar{m})\, \delta_{m_3-m_1,m}\, \delta_{m_2-m_4,m}\,. \qquad (A3-6)$$

In the similar manner to Eqs. (A2-8) and (A2-9), the products of two C coefficients can be written by

$$C(j_4\,1\,f_1;\, m_4\; m_1+\bar{m}-m_4)\, C(\bar{l}\,f_1\,\bar{j}_1;\, -\bar{m}\; m_1+\bar{m})$$

$$= (-)^{\bar{l}+\bar{m}-m_4-f_1}\left(\frac{[\bar{j}_1][f_1]}{[1]}\right)^{1/2}\sum_{L}[L]^{1/2}\,W(\bar{l}\,\bar{j}_1\,1\,j_4;\,f_1 L)$$

$$\times C(\bar{j}_1\,j_4\,L;\, -m_1\, m_4)\, C(\bar{l}\,L\,1;\, -\bar{m}\; -m_1+m_4)\,, \qquad (A3-7a)$$

and

$$C(j_3\,1\,f_2;\, m_3\; m_2-\bar{m}-m_3)\, C(\bar{l}\,f_2\,j_2;\, \bar{m}\; m_2-\bar{m})$$

$$= (-)^{\bar{l}-\bar{m}-m_3-f_2}\left(\frac{[j_2][f_2]}{[1]}\right)^{1/2}\sum_{L'}[L']^{1/2}\,W(\bar{l}\,j_2\,1\,j_3;\,f_2 L')$$

$$\times C(j_2\,j_3\,L';\, -m_2\, m_3)\, C(\bar{l}\,L'\,1;\, \bar{m}\; -m_2+m_3)\,. \qquad (A3-7b)$$

From the symmetric properties of C coefficients, the sum over $\bar{m}$ yields just the orthonormality relation for C coefficients

$$\sum_{\bar{m}} C(\bar{l}\,L\,1;\, -\bar{m}\; -m_1+m_4)\, C(\bar{l}\,L'\,1;\, \bar{m}\; -m_2+m_3)\, \delta_{m_1+m_2,\,m_3+m_4}$$

$$= \left(\frac{[1]^2}{[L][L']}\right)^{1/2}(-)^{1+\bar{l}-L'}\sum_{\bar{m}} C(1\,\bar{l}\,L;\, m_4-m_1+\bar{m}\; -\bar{m})$$

$$\times C(1\,\bar{l}\,L';\, m_2-m_3+\bar{m}\; -\bar{m})\, \delta_{m_4-m_1,\,m_2-m_3}$$

$$= (-)^{1+\bar{l}-L}\frac{[1]}{[L]}\,\delta_{L,L'}. \qquad (A3-8)$$

By the use of Eqs. (A3-7a), (A3-7b), and (A3-8), the summations over magnetic quantum numbers can be expressed as

$$\sum_{m_1 m_2 m_3 m_4 m \bar{m}} (-)^{m_2+m_4+m+1} C(l_1 \tfrac{1}{2} j_1; 0 m_1) C(\bar{l}_1 \tfrac{1}{2} \bar{j}_1; 0 m_1)$$
$$\times C(j_1 j_3 l; -m_1 m_3) C(j_2 j_4 l; -m_2 m_4) C(j_4 1 f_1; m_4 m_1+\bar{m}-m_4)$$
$$\times C(j_3 1 f_2; m_3 m_2-\bar{m}-m_3) C(\bar{l} f_1 \bar{j}_1; -\bar{m} m_1+\bar{m}) C(\bar{l} f_2 j_2; \bar{m} m_2-\bar{m})$$
$$\times \delta_{m_3-m_1, m} \delta_{m_2-m_4, m}$$
$$= \sum_{m_1 m_2 m_3 m_4 L} (-)^{m_2-m_1-f_1-f_2+\bar{l}-L} \sqrt{[j_1][j_2][f_1][f_2]}\, W(\bar{l} \bar{j}_1 1 j_4; f_1 L)$$
$$\times W(\bar{l} j_2 1 j_3; f_2 L) C(l_1 \tfrac{1}{2} j_1; 0 m_1) C(\bar{l}_1 \tfrac{1}{2} \bar{j}_1; 0 m_1)$$
$$\times C(j_1 j_3 l; -m_1 m_3) C(j_2 j_4 l; -m_2 m_4) C(\bar{j}_1 j_4 L; -m_1 m_4)$$
$$\times C(j_2 j_3 L; -m_2 m_3). \qquad (A3-9)$$

The relation between magnetic quantum numbers,

$$m_1 + m_2 = m_3 + m_4,$$

can allow us to write

$$(-)^{m_2-m_1} = (-)^{m_1+m_2-1} = (-)^{m_3+m_4-1}. \qquad (A3-10)$$

Using this expression and Eq. (A3-5), Eq. (A3-9) is

$$\sum_{m_1 m_2 m_3 m_4 m \bar{m} L} (-)^{m_2+m_4+m-1-f_1-f_2+\bar{l}-L} \sqrt{[j_1][j_2][f_1][f_2]}\, W(\bar{l} \bar{j}_1 1 j_4; f_1 L)$$
$$\times W(\bar{l} j_2 1 j_3; f_2 L) C(l_1 \tfrac{1}{2} j_1; 0 m_1) C(\bar{l}_1 \tfrac{1}{2} \bar{j}_1; 0 m_1) C(j_1 j_3 l; -m_1 m_3)$$

$$\times C(j_2 j_4 l; -m_2 m_4) C(\bar{j}_1 j_4 L; -m_1 m_4) C(j_2 j_3 L; -m_2 m_3)$$

$$= \sum_L (-)^{\bar{l}-L-f_1-f_2} \sqrt{[\bar{j}_1][j_2][f_1][f_2]}\, W(\bar{l}\,\bar{j}_1\, 1\, j_4; f_1 L)$$

$$\times W(\bar{l}\, j_2\, 1\, j_3; f_2 L) \sum_{m_1 m_2 m_3 m_4} (-)^{m_3+m_4-1} C(l_1 \tfrac{1}{2} j_1; 0 m_1) C(\bar{l}_1 \tfrac{1}{2} \bar{j}_1; 0 m_1)$$

$$\times C(j_1 j_3 l; -m_1 m_3) C(j_2 j_4 l; -m_2 m_4) C(\bar{j}_1 j_4 L; -m_1 m_4)$$

$$\times C(j_2 j_3 L; -m_2 m_3)$$

$$= \sum_L (-)^{\bar{l}-L-f_1-f_2} \sqrt{[\bar{j}_1][j_2][f_1][f_2]}\, W(\bar{l}\, j_1\, 1\, j_4; f_1 L)$$

$$\times W(\bar{l}\, j_2\, 1\, j_3; f_2 L)\, (-)^{j_1+j_2+j_3+j_4+l+L+1} \frac{[l][L]}{[l_1]}$$

$$\times W(j_1 j_3 j_4 j_2; l L)\, \delta_{\kappa_1 \bar{\kappa}_1}$$

$$= (-)^{j_1+j_2+j_3+j_4+l+\bar{l}-f_1-f_2+1} \frac{[l]}{[l_1]} \sqrt{[j_1][j_2][f_1][f_2]} \sum_L [L]$$

$$\times W(\bar{l}\, j_1\, 1\, j_4; f_1 L)\, W(\bar{l}\, j_2\, 1\, j_3; f_2 L)\, W(j_1 j_3 j_4 j_2; l L)\, \delta_{\kappa_1 \bar{\kappa}_1}. \qquad (A3\text{-}11)$$

Inserting Eq. (A3-11) into Eq. (A3-6), $B_i \bar{C}'_j$ has the form

$$B_i \bar{C}'_j = (-)^{j_1+j_2+j_3+j_4+l+\bar{l}+1}\, 6\, [j_1][j_2][j_3][j_4][\bar{l}] \sqrt{[l_1][l_2][l_3][l_4][\bar{l}_3][\bar{l}_4]}$$

$$\times C(l_1 l_3 l; 00) C(l_2 l_4 l; 00) C(\bar{l}_4 \bar{l} l_1; 00) C(\bar{l}_3 \bar{l} l_2; 00)$$

$$\times W(j_1 j_3 l_1 l_3; l \tfrac{1}{2})\, W(j_2 j_4 l_2 l_4; l \tfrac{1}{2}) \sum_{f_1 f_2} (-)^{f_1+f_2} [f_1][f_2]$$

$$\times W(\bar{l}\,l_4\,j_1\,\tfrac{1}{2};\,l_1 f_1)\,W(\bar{l}\,\bar{l}_3\,j_2\,\tfrac{1}{2};\,l_2 f_2)\,W(1\,\tfrac{1}{2}\,f_1\,\bar{l}_4;\,\tfrac{1}{2}\,j_4)$$

$$\times W(1\,\tfrac{1}{2}\,f_2\,\bar{l}_3;\,\tfrac{1}{2}\,j_3)\sum_L [L]\,W(\bar{l}\,j_1\,1\,j_4;\,f_1 L)$$

$$\times W(\bar{l}\,j_2\,1\,j_3;\,f_2 L)\,W(j_1 j_3 j_4 j_2;\,l L)\,. \qquad (A3\text{-}12)$$

The summations over f_1 and f_2 are performed in the similar way to Eqs. (A2-13a) and (A2-13b). The resultant expression for $\mathcal{B}_i\bar{\mathcal{C}}'_j$ is

$$\mathcal{B}_i\bar{\mathcal{C}}'_j = (-)^{j_1+j_2+l+\bar{l}+1}\,6[j_1][j_2][j_3][j_4][\bar{l}]\sqrt{[l_1][l_2][l_3][l_4][\bar{l}_3][\bar{l}_4]}$$

$$\times C(l_1 l_3 l;00)\,C(l_2 l_4 l;00)\,C(\bar{l}_4\bar{l}\,l_1;00)\,C(\bar{l}_3\,\bar{l}\,l_2;00)$$

$$\times W(j_1 j_3 l_1 l_3;\,l\tfrac{1}{2})\,W(j_2 j_4 l_2 l_4;\,l\tfrac{1}{2})$$

$$\times \sum_L [L]\,X\begin{pmatrix}\bar{l} & 1 & L\\ \bar{l}_4 & \tfrac{1}{2} & j_4\\ l_1 & \tfrac{1}{2} & j_1\end{pmatrix} X\begin{pmatrix}\bar{l} & 1 & L\\ \bar{l}_3 & \tfrac{1}{2} & j_3\\ l_2 & \tfrac{1}{2} & j_2\end{pmatrix} W(j_1 j_3 j_4 j_2;\,l L)\,. \qquad (58)$$

C. Calculation of $\mathcal{B}'_i\bar{\mathcal{C}}'_j$

Making use of Eqs. (45'b) and (A3-1b), $\mathcal{B}'_i\bar{\mathcal{C}}'_j$ can be written by

$$\mathcal{B}'_i\bar{\mathcal{C}}'_j = (4\pi)^2\sum_{m_1 m_2 m_3 m_4 m\bar{m}}\sqrt{[l_1][\bar{l}_1]}\,C(l_1\tfrac{1}{2}j_1;0m_1)\,C(\bar{l}_1\tfrac{1}{2}\bar{j}_1;0m_1)$$

$$\times \mathcal{B}'_{K_1K_2K_3K_4}\,\mathcal{C}'_{\bar{K}_1\bar{K}_2\bar{K}_3\bar{K}_4}$$

$$= 36[l][\bar{l}][j_3][j_4]\sqrt{[l_1][\bar{l}_1][l_3][l_4][\bar{l}_3][\bar{l}_4]}\; C(l_3 l l_1; 00)$$

$$\times C(l_4 l l_2; 00)\, C(\bar{l}_4 \bar{l} \bar{l}_1; 00)\, C(\bar{l}_3 \bar{l} l_2; 00)$$

$$\times \sum_{f_1 f_2 \bar{f}_1 \bar{f}_2} \sqrt{[f_1][f_2][\bar{f}_1][\bar{f}_2]}\; W(l l_3 j_1 \tfrac{1}{2}; l_1 f_1) W(l l_4 j_2 \tfrac{1}{2}; l_2 f_2)$$

$$\times W(l \tfrac{1}{2} f_1 l_3; \tfrac{1}{2} j_3) W(l \tfrac{1}{2} f_2 l_4; \tfrac{1}{2} j_4) W(\bar{l} \bar{l}_4 \bar{j}_1 \tfrac{1}{2}; \bar{l}_1 \bar{f}_1)$$

$$\times W(\bar{l} \bar{l}_3 \bar{j}_2 \tfrac{1}{2}; l_2 \bar{f}_2) W(\bar{l} \tfrac{1}{2} \bar{f}_1 \bar{l}_4; \tfrac{1}{2} j_4) W(\bar{l} \tfrac{1}{2} \bar{f}_2 \bar{l}_3; \tfrac{1}{2} j_3)$$

$$\times \sum_{m_1 m_2 m_3 m_4 m \bar{m}} (-)^{m_3 + m_4 - 2m_1} C(l_1 \tfrac{1}{2} j_1; 0\, m_1) C(\bar{l}_1 \tfrac{1}{2} \bar{j}_1; 0\, m_1)$$

$$\times C(j_3 1 f_1; m_3\, m_1 + m - m_3)\, C(j_4 1 f_2; m_4\, m_2 - m - m_4)\, C(l f_1 j_1; -m\, m_1 + m)$$

$$\times C(l f_2 j_2; m\, m_2 - m)\, C(j_4 1 \bar{f}_1; m_4\, m_1 + \bar{m} - m_4)\, C(j_3 1 \bar{f}_2; m_3\, m_2 - \bar{m} - m_3)$$

$$\times C(\bar{l} \bar{f}_1 \bar{j}_1; -\bar{m}\, m_1 + \bar{m})\, C(\bar{l} \bar{f}_2 \bar{j}_2; \bar{m}\, m_2 - \bar{m})\, \delta_{m_1 + m_2, m_3 + m_4}. \quad (A3\text{-}13)$$

Using Eqs. (A2-15a) and (A2-15b), the product of four C coefficients can be summed over m to give

$$\sum_m C(j_3 1 f_1; m_3\, m_1 + m - m_3)\, C(l f_1 j_1; -m\, m_1 + m)$$

$$\times C(j_4 1 f_2; m_4\, m_2 - m - m_4)\, C(l f_2 j_2; m\, m_2 - m)$$

$$= \sum_L (-)^{l + L - 1 - m_3 - m_4 - f_1 - f_2} \sqrt{[j_1][j_2][f_1][f_2]}\; W(l j_1 1 j_3; f_1 L)$$

$$\times W(l j_2 1 j_4; f_2 L)\, C(j_1 j_3 L; -m_1 m_3)\, C(j_2 j_4 L; -m_2 m_4). \quad (A3\text{-}14a)$$

Similarly, the summation over $\bar{m}$ can be done using Eqs. (A3-7a), (A3-7b), and (A3-8). We obtain

$$\sum_{\bar{m}} C(j_4\, 1\, \bar{f}_1;\, m_4\, m_1+\bar{m}-m_4)\, C(\bar{l}\, \bar{f}_1\, \bar{j}_1;\, -\bar{m}\, m_1+\bar{m})$$
$$\times C(j_3\, 1\, \bar{f}_2;\, m_3\, m_2-\bar{m}-m_3)\, C(\bar{l}\, \bar{f}_2\, \bar{j}_2;\, \bar{m}\, m_2-\bar{m})$$
$$= \sum_{L'} (-)^{\bar{l}+L'-1-m_3-m_4-\bar{f}_1-\bar{f}_2} \sqrt{[j_1][j_2][f_1][f_2]}\, W(\bar{l}\, \bar{j}_1\, 1\, j_4;\, \bar{f}_2\, L')$$
$$\times W(\bar{l}\, \bar{j}_2\, 1\, j_3;\, \bar{f}_2\, L')\, C(\bar{f}_1\, j_4\, L';\, -m_1\, m_4)\, C(j_2\, j_3\, L';\, -m_2\, m_3). \qquad (A3\text{-}14b)$$

Using these expressions, Eqs. (A3-14a) and (A3-14b), the term concerning magnetic quantum numbers in Eq. (A3-13) is given as

$$\sum_{m_1 m_2 m_3 m_4 m \bar{m}} (-)^{m_3+m_4-1}\, C(l_1\, 1/2\, j_1;\, 0\, m_1)\, C(\bar{l}_1\, 1/2\, \bar{j}_1;\, 0\, m_1)$$
$$\times C(j_3\, 1\, f_1;\, m_3\, m_1+m-m_3)\, C(j_4\, 1\, f_2;\, m_4\, m_2-m-m_4)\, C(l\, f_1\, j_1;\, -m\, m_1+m)$$
$$\times C(l\, f_2\, j_2;\, m\, m_2-m)\, C(j_4\, 1\, \bar{f}_1;\, m_4\, m_1+\bar{m}-m_4)\, C(j_3\, 1\, \bar{f}_2;\, m_3\, m_2-\bar{m}-m_3)$$
$$\times C(\bar{l}\, \bar{f}_1\, \bar{j}_1;\, -\bar{m}\, m_1+\bar{m})\, C(\bar{l}\, \bar{f}_2\, \bar{j}_2;\, \bar{m}\, m_2-\bar{m})\, \delta_{m_1+m_2,\, m_3+m_4}$$
$$= \sum_{L\, L'} (-)^{l+\bar{l}+L+L'+f_1+f_2+\bar{f}_1+\bar{f}_2}\, [j_2] \sqrt{[j_1][\bar{j}_1][f_1][f_2][\bar{f}_1][\bar{f}_2]}$$
$$\times W(l\, j_1\, 1\, j_3;\, f_1\, L)\, W(l\, j_2\, 1\, j_4;\, f_2\, L)\, W(\bar{l}\, \bar{j}_1\, 1\, j_4;\, \bar{f}_1\, L')$$
$$\times W(\bar{l}\, j_2\, 1\, j_3;\, \bar{f}_2\, L') \sum_{m_1 m_2 m_3 m_4} (-)^{m_3+m_4-1}\, C(l_1\, 1/2\, j_1;\, 0\, m_1)\, C(\bar{l}_1\, 1/2\, \bar{j}_1;\, 0\, m_1)$$
$$\times C(j_1\, j_3\, L;\, -m_1\, m_3)\, C(j_2\, j_4\, L;\, -m_2\, m_4)\, C(\bar{j}_1\, j_4\, L';\, -m_1\, m_4)$$
$$\times C(j_2\, j_3\, L';\, -m_2\, m_3)\, \delta_{m_1+m_2,\, m_3+m_4}, \qquad (A3\text{-}15)$$

The summations over m_1, m_2, m_3, and m_4 can be done in the similar manner to Eq. (A3-5) and give

$$\sum_{m_1 m_2 m_3 m_4} (-)^{m_3+m_4-1} C(l_1 \tfrac{1}{2} j_1'; 0\, m_1)\, C(\bar{l}_1 \tfrac{1}{2} \bar{j}_1; 0\, m_1)\, C(j_1' j_3 L; -m_1 m_3)$$
$$\times C(j_2' j_4 L; -m_2\, m_4)\, C(\bar{j}_1 j_4 L'; -m_1 m_4)\, C(j_2' j_3 L'; -m_2\, m_3)$$
$$= (-)^{j_1'+j_2'+j_3+j_4+L+L'+1} \frac{[L][L']}{[l_1]} W(j_1' j_3 j_4 j_2'; L L')\, \delta_{\kappa_1, \bar{\kappa}_1} . \qquad (A3\text{-}16)$$

Then Eq. (A3-15) is written as

$$\sum_{m_1 m_2 m_3 m_4 m \bar{m}} (-)^{m_3+m_4-1} C(l_1 \tfrac{1}{2} j_1'; 0 m_1) C(\bar{l}_1 \tfrac{1}{2} \bar{j}_1; 0\, m_1)$$
$$\times C(j_3' 1 f_1; m_3\, m_1+m-m_3) C(j_4' 1 f_2; m_4\, m_2-m-m_4) C(l f_1 j_1'; -m\, m_1+m)$$
$$\times C(l f_2 j_2'; m\, m_2-m)\, C(j_4' 1 \bar{f}_1; m_4\, m_1+\bar{m}-m_4)\, C(j_3' 1 \bar{f}_2; m_3\, m_2-\bar{m}-m_3)$$
$$\times C(\bar{l} \bar{f}_1 \bar{j}_1; -\bar{m}\, m_1+\bar{m})\, C(\bar{l} \bar{f}_2 j_2'; \bar{m}\, m_2-\bar{m})\, \delta_{m_1+m_2, m_3+m_4}$$
$$= (-)^{j_1'+j_2'+j_3'+j_4'+l+\bar{l}+1+f_1+f_2+\bar{f}_1+\bar{f}_2} \frac{[j_1'][j_2']}{[l_1]} \sqrt{[f_1][f_2][\bar{f}_1][\bar{f}_2]}$$
$$\times \sum_{L L'} [L][L'] W(l j_1' 1 j_3'; f_1 L)\, W(l j_2' 1 j_4'; f_2 L)\, W(\bar{l} j_1' 1 j_4'; \bar{f}_1 L)$$
$$\times W(l j_2' 1 j_3'; \bar{f}_2 L')\, W(j_1' j_3' j_4' j_2'; L L') . \qquad (A3\text{-}17)$$

Substituting Eq. (A3-17) into Eq. (A3-13), $B_i \bar{C}_j'$ becomes

$$B_i' \bar{C}_j' = (-)^{j_1'+j_2'+j_3'+j_4'+l+\bar{l}+1}\, 36\, [j_1'][j_2'][j_3'][j_4'][l][\bar{l}] \sqrt{[l_3][l_4][\bar{l}_3][\bar{l}_4]}$$
$$\times C(l_3 l l_1; 00)\, C(l_4 l l_2; 00)\, C(\bar{l}_4 \bar{l} l_1; 00)\, C(\bar{l}_3 \bar{l} l_2; 00)$$

$$\times \sum_{f_1 f_2 \bar{f}_1 \bar{f}_2} (-)^{f_1+f_2+\bar{f}_1+\bar{f}_2} [f_1][f_2][\bar{f}_1][\bar{f}_2]\, W(\ell \ell_3 j_1 \tfrac{1}{2}; \ell_1 f_1)$$

$$\times W(\ell \ell_4 j_2 \tfrac{1}{2}; \ell_2 f_2)\, W(1\tfrac{1}{2} f_1 \ell_3; \tfrac{1}{2} j_3)\, W(1\tfrac{1}{2} f_2 \ell_4; \tfrac{1}{2} j_4)$$

$$\times W(\bar{\ell} \bar{\ell}_4 j_1' \tfrac{1}{2}; \ell_1' \bar{f}_1)\, W(\bar{\ell} \bar{\ell}_3 j_2' \tfrac{1}{2}; \ell_2' \bar{f}_2)\, W(1\tfrac{1}{2} \bar{f}_1 \bar{\ell}_4; \tfrac{1}{2} j_4')$$

$$\times W(1\tfrac{1}{2} \bar{f}_2 \bar{\ell}_3; \tfrac{1}{2} j_3') \sum_{L L'} [L][L']\, W(\ell j_1' 1 j_3'; f_1 L)$$

$$\times W(\ell j_2 1 j_4'; f_2 L)\, W(\bar{\ell} j_1' 1 j_4'; \bar{f}_1 L')\, W(\bar{\ell} j_2 1 j_3'; \bar{f}_2 L')$$

$$\times W(j_1' j_3 j_4' j_2; L L') . \qquad (A3\text{-}18)$$

The summation over f_1 is carried out from Eq. (A2-13a) as follows:

$$\sum_{f_1} (-)^{f_1} [f_1]\, W(\ell \ell_3 j_1' \tfrac{1}{2}; \ell_1 f_1)\, W(1\tfrac{1}{2} f_1 \ell_3; \tfrac{1}{2} j_3)$$

$$\times W(\ell j_1' 1 j_3'; f_1 L)$$

$$= (-)^{j_3'} X \begin{pmatrix} \ell & 1 & L \\ \ell_3 & \tfrac{1}{2} & j_3' \\ \ell_1 & \tfrac{1}{2} & j_1' \end{pmatrix} . \qquad (A3\text{-}19)$$

In the similar way, the summations over f_2, $\bar{f}_1$, and $\bar{f}_2$ can be performed. Using these expressions, we obtain the result for $B_i \bar{C}_j'$ in the following form:

$$B_i' \bar{C}_j' = (-)^{j_1'+j_2'+j_3'+j_4'+\ell+\bar{\ell}+1} 36 [j_1'][j_2'][j_3'][j_4'][\ell][\bar{\ell}] \sqrt{[\ell_3][\ell_4][\bar{\ell}_3][\bar{\ell}_4]}$$

$$\times C(\ell_3 \ell \ell_1; 00)\, C(\ell_4 \ell \ell_2; 00)\, C(\bar{\ell}_4 \bar{\ell} \ell_1'; 00)\, C(\bar{\ell}_3 \bar{\ell} \ell_2'; 00)$$

$$\times \sum_{LL'} [L][L'] X \begin{pmatrix} \ell & 1 & L \\ \ell_3 & 1/2 & j_3 \\ \ell_1 & 1/2 & j_1 \end{pmatrix} X \begin{pmatrix} \ell & 1 & L \\ \ell_4 & 1/2 & j_4 \\ \ell_2 & 1/2 & j_2 \end{pmatrix} X \begin{pmatrix} \bar{\ell} & 1 & L' \\ \bar{\ell}_4 & 1/2 & j_4 \\ \ell_1 & 1/2 & j_1 \end{pmatrix}$$

$$\times X \begin{pmatrix} \bar{\ell} & 1 & L' \\ \bar{\ell}_3 & 1/2 & j_3 \\ \ell_2 & 1/2 & j_2 \end{pmatrix} W(j_1 j_3 j_4 j_2 ; L L') . \qquad (59)$$

APPENDIX IV

EFFECT OF TARGET THICKNESS

Electron emission from the target of finite thickness by radiationless annihilation is considered as a two-step process. A positron incident on the target annihilates with an atomic electron, then another electron ejected form the atom as a result of annihilation moves to the other side of the target with or without scattering, and escapes from it and enters a detector. When traversing even a thin target, positrons will make an enormous numbers of collisions that result in small energy losses and angular deflections and a relatively small number of catastrophic collisions in which they may lose a major fraction of their energy or may be turned through a large angle. Owing to the finite thickness of the target, attenuation effect and energy degradation of positrons and electrons in the target must be taken into account. Since an exact treatment of this effect presents extreme difficulties, the following simplifying assumptions are made: (1) A mono-energetic beam of positrons is incident upon a target at the center with incident angle α. (2) The target is so thin that positrons and ejected electrons suffer no collision which causes appreciable angular deflection.

We assume that geometry is axially symmetric and that positrons hit the target of infinite radius at the center with

energy E_0. At a distance x from the surface of the target, the number of positrons with the kinetic energy of E is expressed as a function of E and x; $N(E,x)$. Let the total cross section per atom for radiationless annihilation of positrons with kinetic energy E be $\sigma(E)$; then the rate for this annihilation process at which positrons annihilate with energy between E and $E + dx$, in a slab of width dx located at a distance x from the surface on which positrons impinge, can be given by

$$G(E,x)\,dE\,dx = n\,N(E,x)\,\sigma(E)\,dE\,dx\,, \qquad (A4\text{-}1)$$

where n is the number of atoms per unit volume of the target. The kinetic energy of the ejected electron by this process is given according to Eq. (8) by $E' = E + 2m_0c^2 - B_\alpha - B_\beta$, where m_0 is the rest mass of the electron, and B_α and B_β are binding energies of the shell electrons concerned.

If θ is the angle between the direction of momentum of the incident positron and that of the ejected electron as shown in Fig. 24, the electron traverses a distance $(T - x)/\cos(\theta - \alpha)$ beofre escaping the foil. By $K(E,E";x,\theta)$ we denote the probability that the electron ejected at x with initial energy E' escapes from the target and is detected by the detector with energy between $E"$ and $E' + dE"$. The number of electrons which escape from the target, enter the detector of radius b placed at the distance a behind the target and are detected with energy between $E"$ and $E" + dE"$, can be

expressed as

$$R(E'')dE'' = \sum_{\substack{\text{all} \\ \text{electron} \\ \text{pairs}}} \int_0^T \int_0^{E_0} \int_{\alpha-\gamma}^{\alpha+\beta} K(E, E''; x, \theta) G(E, x) P(\theta) \sin\theta \, d\theta \, dE \, dx \, dE'', \quad (A4\text{-}2)$$

where T is the thickness of the target, $P(\theta)$ is the angular distribution of the ejected electrons, and the summation is over all the pairs of shell electrons involved. From Fig. 24 β and γ are given, respectively, by

$$\tan\beta = \frac{b + x\tan\alpha}{a + T - x}, \quad (A4\text{-}3a)$$

$$\tan\gamma = \frac{b - x\tan\alpha}{a + T - x}. \quad (A4\text{-}3b)$$

Since in the present case both T and x are very small compared with a and b, we can write

$$\tan\beta \doteqdot \tan\gamma \doteqdot \frac{b}{a} \equiv \tan\delta. \quad (A4\text{-}4)$$

Using this relation and Eq. (A4-1), Eq. (A4-2) becomes

$$R(E'')dE'' = n \sum_{\substack{\text{all} \\ \text{electron} \\ \text{pairs}}} \int_0^T \int_0^{E_0} \int_{\alpha-\delta}^{\alpha+\delta} N(E, x) \sigma(E) K(E, E''; x, \theta) P(\theta) \sin\theta \, d\theta \, dE \, dx \, dE''. \quad (72)$$

If we assume finite thickness effect to be negligible, the rate for radiationless annihilation at a distance x is given by the following equation:

$$G_0(x)dx = n N_0 \sigma(E_0) \sec\alpha \, dx, \quad (A4\text{-}5)$$

where N_0 is the total number of positrons incident on the

target. Then the number of the ejected shell electrons detected in the detector with kinetic energy between E'' and $E'' + dE''$ can be expressed by

$$R_0(E'')\,dE'' = \sum_{\substack{\text{all}\\ \text{electron}\\ \text{pairs}}} \int_0^T \int_{\alpha-\delta}^{\alpha+\delta} G_0(x)\, K(E_0, E''; T, \theta)\, P(\theta) \sin\theta\, d\theta\, dx\, dE''. \quad (A4\text{-}6)$$

Using Eq. (A4-5), this equation can be written by

$$R_0(E'')\,dE'' = n N_0 T \sec\alpha \sum_{\substack{\text{all}\\ \text{electron}\\ \text{pairs}}} \sigma(E_0) \int_{\alpha-\delta}^{\alpha+\delta} K(E_0, E''; T, \theta)\, P(\theta) \sin\theta\, d\theta\, dE''. \quad (A4\text{-}7)$$

The correction factor for the effect of finite thickness of the target is given by the ratio of the number of ejected electrons detected in the energy region concerned when the effect of the target thickness is neglected, to that when the effect is taken into account. From Eqs. (72) and (75), this correction factor, C_e/C_p, can be expressed as

$$C_e/C_p = \frac{N_0 T \sec\alpha \sum_{\text{all electron pairs}} \sigma(E_0) \int_{E_{min}}^{E_{max}} \int_{\alpha-\delta}^{\alpha+\delta} K(E_0, E''; T, \theta)\, P(\theta) \sin\theta\, d\theta\, dE''}{\sum_{\substack{\text{all}\\ \text{electron}\\ \text{pairs}}} \int_{E_{min}}^{E_{max}} \int_0^T \int_0^{E_0} \int_{\alpha-\delta}^{\alpha+\delta} N(E, x)\, \sigma(E)\, K(E, E''; x, \theta)\, P(\theta) \sin\theta\, d\theta\, dE\, dx\, dE''}, \quad (\%)$$

where E_{max} and E_{min} are the minimum and maximum energy determined from the peak portion of the ejected electron spectrum.

REFERENCES

1. P. A. M. Dirac, Proc. Camb. Phil. Soc. 26 (1930) 361; Proc. Roy. Soc. (London) A133 (1931) 60.
2. J. R. Oppenheimer, Phys. Rev. 35 (1930) 939.
3. C. D. Anderson, Phys. Rev. 41 (1932) 405; *ibid.* 43 (1933) 491.
4. P. M. S. Blackett and G. P. S. Occhialini, Proc. Roy. Soc. (London) A139 (1933) 699; *ibid.* A144 (1934) 235.
5. J. Thibaud, C. R. 197 (1933) 1629; Phys. Rev. 45 (1934) 781.
6. A. H. Spees and C. T. Zahn, Phys. Rev. 58 (1940) 861.
7. L. A. Page, P. Stehle, and S. B. Gunst, Phys. Rev. 89 (1953) 1273.
8. F. Joliot, C. R. 197 (1933) 1622; *ibid.* 198 (1934) 81.
9. O. Klemperer, Proc. Camb. Phil. Soc. 30 (1934) 347.
10. A. I. Alichanian, A. I. Alichanow, and L. A. Arzimovich, Nature 137 (1936) 703; Doklady. Ak. Nauk. S.S.S.R. 1 (1936) 287.
11. R. Beringer and C. G. Montgomery, Phys. Rev. 61 (1942) 222.
12. J. W. M. DuMond, D. A. Lind, and B. B. Watson, Phys. Rev. 75 (1949) 1226; D. E. Muller, H. C. Hoyt, D. J. Klein, and J. W. M. DuMond, Phys. Rev. 88 (1952) 775.
13. A. Hedgran and D. A. Lind, Arkiv för Fys. 5 (1952) 177.
14. S. Mohorovičić, Astron. Nacht. 253 (1934) 94.
15. A. E. Raurk, Phys. Rev. 68 (1945) 278.

16. J. A. Wheeler, Ann. N. Y. Acad. Sci. 48 (1946) 219.

17. E. A. Hylleraas, Phys. Rev. 71 (1947) 491.

18. E. A. Hylleraas and A. Ore, Phys. Rev. 71 (1947) 493.

19. A. Ore, Phys. Rev. 71 (1947) 913.

20. S. de Benedetti, C. E. Cowan, W. R. Konneker, and H. Primakoff, Phys. Rev. 77 (1950) 205.

21. A. Ore and J. L. Powell, Phys. Rev. 75 (1949) 1696.

22. J. A. Rich, Phys. Rev. 81 (1951) 140.

23. H. A. Bethe, Proc. Roy. Soc. (London) A150 (1935) 129.

24. W. Bothe and Z. W. Ho, *Nachr. Akad. Wiss. Göttingen, Math.-Phys. Kl.* (1946) 49.

25. W. H. Barkas, R. W. Deutsch, F. C. Gilbert, and C. E. Violet, Phys. Rev. 88 (1952) 1435.

26. M. Deutsch, Phys. Rev. 72 (1947) 729.

27. S. A. Colgate and F. C. Gilbert, Phys. Rev. 89 (1953) 790.

28. H. W. Kendall and M. Deutsch, Phys. Rev. 101 (1956) 20.

29. J. B. Gerhart, B. C. Carlson, and R. Sherr, Phys. Rev. 94 (1954) 917.

30. J. Solomon, J. de Phys. 6 (1935) 114.

31. E. Fermi and G. E. Uhlenbeck, Phys. Rev. 44 (1935) 510.

32. H. R. Hulme and H. J. Bhabha, Proc. Roy. Soc. (London) A146 (1934) 723.

3. Y. Nishina, S. Tomonaga, and H. Tamaki, Sci. Pap. Inst. Phys. Chem. Res. Tokyo 24 Suppl. No. 18 (1934) 7; *ibid.* 27 (1935) 178.

34. J. C. Jaeger and H. R. Hulme, Proc. Camb. Phil. Soc. 32 (1936) 158.

35. K. W. McVoy, Phys. Rev. 108 (1957) 365.

36. H. Banerjee, Nuovo Cim. 11 (1958) 220.

37. H. Banerjee, Nuovo Cim. 10 (1958) 863.

38. W. R. Johnson, D. J. Buss, and C. O. Carroll, Phys. Rev. 135 (1964) A1232.

39. W. R. Johnson, Phys. Rev. 159 (1967) 61.

40. S. Meric, Rev. fac. sci. univ. Istanbul 15A (1950) 136; *ibid.* 15A (1950) 179.

41. D. J. Farmer and J. F. Streib, Phys. Rev. 96 (1954) 855.

42. J. Whalen, Ph.D. thesis, Washington University, St. Louis, Missouri, 1955 (unpublished).

43. L. Sodickson, W. Bowman, J. Stephenson, and R. Weinstein, Phys. Rev. 124 (1961) 1851.

44. H. Langhoff, H. Weigmann, and A. Flammersfeld, Nucl. Phys. 41 (1963) 575.

45. H. Weigmann, H. Hansen, and A. Flammersfeld, Nucl. Phys. 45 (1963) 555.

46. H. Mazaki, M. Nishi, and S. Shimizu, Phys. Rev. 171 (1968) 408.

47. R. D. Present and S. C. Chen, Phys. Rev. 85 (1952) 447.

48. F. Perrin, C. R. 197 (1933) 1302.

49. J. Brunings, Physica 1 (1934) 996.

50. H. S. W. Massey and E. H. S. Burhop, Proc. Roy. Soc. (London) A167 (1938) 53.

51. S. Simizu, T. Mukoyama, and Y. Nakayama, Phys. L. 17 (1965) 295.

52. See, e.g. W. Heitler, *The Quantum Theory of Radiation* (Oxford University Press, New York, 1954).

53. C. Møller, Z. Phys. 70 (1931) 786.

54. C. G. Darwin, Proc. Roy. Soc. (London) A118 (1928) 654.

55. N. F. Mott, Proc. Roy. Soc. (London) A135 (1932) 429.

56. See, e.g. W. Magnus, F. Oberhettinger, and R. P. Soni, *Formulas and Theorems for the Special Functions of Mathematical Physics* (Springer-Verlag, Berlin, 1966).

57. M. E. Rose, *Elementary Theory of Angular Momentum* (John Wiley & Sons, Inc., New York, 1957), p.152.

58. M. E. Rose, *Relativistic Electron Theory* (John Wiley & Sons, Inc., New York, 1961), p.179.

59. M. E. Rose, Phys. Rev. 51 (1937) 484.

60. A. A. Abramov, *Table of* $\ln \Gamma(z)$ *for Complex Argument*, translated from Russian by D. G. Fry and B. A. Hons (Pergamon Press, New York, 1960).

61. *Handbook of Mathematical Functions with Formulas, Graphs, and Mathematical Tables*, edited by M. Abramowitz and I. A. Stegun (U. S. Department of Commerce, Washington, D. C., 1964), Appl. Math. Series No. 55.

62. Kyoto University Digital Computer No. 2, commercial name is HITAC-5020.

63. *Nuclear Spectroscopy Tables*, edited by A. H. Wapstra, G. J. Nijgh, and R. van Lieshout (North-Holland Publishing Company, Amsterdam, 1959).

64. *Table of the Clebsch-Gordan Coefficients*, edited by T. Inoue (Tokyo Tosho Co., Tokyo, 1966).

65. *Table of the Racah Coefficients*, edited by T. Ishizu (Pan-Pacific Press, Tokyo, 1960).

66. A. F. Nikiforov, V. B. Uvarov, and Yu. L. Levitan, *Tablitsy Koeffitsientov Raka* (Computing Centre of the Akademy of Science of the U.S.S.R., Moskow, 1962); English translation, *Table of Racah Coefficients*, translated by R. Basu (Pergamon Press, New York, 1965).

67. K. Smith and J. W. Stevenson, Argonne Natl. Lab. Rept. ANL-5776 (1957) unpublished.

68. K. Smith, Argonne Natl. Lab. Rept. ANL-5860, Part I (1958); Part II (1958), unpublished.

69. C. M. Lederer, J. M. Hollander, and I. Perlman, *Table of Isotopes* (John Wiley & Sons, Inc., New York, 1967).

70. Y. Nakayama and H. Hirata, Nucl. Phys. 40 (1963) 396.

71. H. Slätis and K. Siegbahn, Arkiv för Fys. 1 (1949) 339.

72. E. M. Pell, J. Appl. Phys. 31 (1960) 291.

73. S. Nishiu, T. Nakakado, Y. Nakayama, and S. Shimizu, Bull. Inst. Chem. Res., Kyoto University, 42 (1964) 319.

74. H. M. Mann and J. L. Yntema, IEEE Trans. Nucl. Sci. NS-11 (1964) 201.

75. J. A. Coleman and J. W. Rodgers, IEEE Trans. Nucl. Sci. NS-11 (1964) 213.

76. A. T. Nelms, Natl. Bur. Std. (U.S.A.) Circ. No. 577 (1956).

77. R. H. Pratt, R. D. Levee, R. L. Pexton, and W. Aron, Phys. Rev. 134 (1964) A898.

78. G. Racah, Phys. Rev. 62 (1942) 438; *ibid.* 63 (1943) 367.

79. See Ref. 57, p.64.

Table I. Calculated cross sections for radiationless annihilation of positrons by the K-K pair of lead in 10^{-26} cm^2.

	Energy of incident positron (keV)		
	100	300	500
Brunings*	5.3	0.21	0.02
Massey & Burhop**			
Nonrelativistic approximation	6.7	0.4	0.05
Plane wave for incident positron	1.6	1.4	0.9
Distorted wave for positron	0.1	0.35	0.2
Present work	0.112	0.323	0.157

* Calculated from Ref. 49.

** Obtained from Ref. 50.

Table II. Cross sections for annihilation of 100-keV positrons by various pairs of electrons in the lead atom, calculated using the nonrelativistic approximation.*

Electrons concerned	Cross section (10^{-26} cm^2)
K - K	6.7
K - L_I	2.5
K - M_I	0.6
L_I - L_I	0.1
K - $L_{II,III}$	4.1
L_I - $L_{II,III}$	1.5
$L_{II,III}$ - $L_{II,III}$	Very small

* Calculated by Massey and Burhop (Ref. 50).

Table III. Parameters defining the K-, L-, and M-shell radial wave functions for the Coulomb field.*

Subshell	γ	W	λ	a_0	a_1	a_2	c_0	c_1	c_2	N
K	$(1-\zeta^2)^{1/2}$	γ	ζ	1	0	0	1	0	0	$\frac{(2\zeta)^{\gamma+1/2}}{[2\Gamma(2\gamma+1)]^{1/2}}$
L_1	$(1-\zeta^2)^{1/2}$	$\left(\frac{1+\gamma}{2}\right)^{1/2}$	$\frac{\zeta}{2W}$	$2(W+1)$	$-\frac{\zeta}{W}\frac{2W+1}{2\gamma+1}$	0	$2W$	a_1	0	$\frac{(2\zeta)^{\gamma+1/2}}{2(2W)^{\gamma+1}}\left[\frac{2\gamma+1}{\Gamma(2\gamma+1)(2W+1)}\right]^{1/2}$
L_2	$(1-\zeta^2)^{1/2}$	$(\frac{1+\gamma}{2})^{1/2}$	$\frac{\zeta}{2W}$	$2W$	$-\frac{\zeta}{W}\frac{2W-1}{2\gamma+1}$	0	$2(W-1)$	a_1	0	$\frac{(2\zeta)^{\gamma+1/2}}{2(2W)^{\gamma+1}}\left[\frac{2\gamma+1}{\Gamma(2\gamma+1)(2W-1)}\right]^{1/2}$
L_3	$(4-\zeta^2)^{1/2}$	$\frac{1}{2}\gamma$	$\frac{\zeta}{2}$	1	0	0	1	0	0	$\frac{\zeta^{\gamma+1/2}}{[2\Gamma(2\gamma+1)]^{1/2}}$
M_1	$(1-\zeta^2)^{1/2}$	$\frac{2+\gamma}{(5+4\gamma)^{1/2}}$	$\frac{\zeta W}{2+\gamma}$	$\frac{3\lambda+\zeta}{\lambda}$	$-\frac{4(2\lambda+\zeta)}{2\gamma+1}$	$\frac{4\lambda(\lambda+\zeta)}{(2\gamma+1)(2\gamma+2)}$	$\frac{\zeta-1}{\lambda}$	$-\frac{4\zeta}{2\gamma+1}$	a_2	$(2\zeta)^{\gamma+3/2}\left[\frac{(2\gamma+1)(2\gamma+2)}{\Gamma(2\gamma+1)\zeta(\zeta+\lambda)32}\right]^{1/2}$

* Symbols used in this table are defined in Ref. 58.

Table IV. Calculated values of cross sections for the radiationless annihilation of 300-keV positrons for K-K, K-L, K-M, and L-L pairs of shell electrons in lead, and comparison with an experimental total cross section.

Shell electron pair	Kinetic energy of ejected shell electrons* (keV)	σ_{cal} (10^{-26} cm^2)	σ_{exp} (10^{-26} cm^2)
K - K	1146.0	0.322	
K - L_I	1218.1	0.117	
K - L_{II}	1218.8	0.085	
K - L_{III}	1221.0	0.080	
K - M_I	1230.1	0.028	0.727
L_I - L_I	1290.2	0.016	$0.8_{-0.3}^{+0.4}$
L_I - L_{II}	1290.9	0.037	
L_I - L_{III}	1293.1	0.042	

* Calculated by Eq. (8) using binding energies of K-, L_I-, L_{II} -, L_{III} -, and M_I-shell electrons in lead being 88.0, 15.9, 15.2, 13.0, and 3.9 keV, respectively (Ref. 63).

CAPTIONS OF FIGURES

Fig. 1. Diagrams for two-quantum annihilation of a free pair.

Fig. 2. Diagrams for three-quantum pair annihilation.

Fig. 3. Diagram for single-quantum annihilation.

Fig. 4. Diagram for radiationless annihilation of a positron and the figure illustrating the energy relation between an incident positron and two shell electrons involved.

Fig. 5. Normalized radial wave functions multiplied by r for K shell in lead. The abscissa gives r in units of $\hbar/m_0 c$.

Fig. 6. Same as Fig. 5 but for L_I shell.

Fig. 7. Same as Fig. 5 but for L_{II} shell.

Fig. 8. Same as Fig. 5 but for L_{III} shell.

Fig. 9. Same as Fig. 5 but for M_I shell.

Fig. 10. Calculated cross section for radiationless annihilation of positrons by the K-K pair of shell electrons in a lead atom as a function of kinetic energy of incident positron. Circles are the values calculated by Massey and Burhop (Ref. 50).

Fig. 11. Experimental arrangement of a thin lead target and lithium-drifted silicon junction detector in the beta-ray spectrometer. Positron trajectories are shown by O_1 (distance from the axis) and O_2 (vertical projection). (T) lead target, (D) silicon detector, (I) insulator, (P) polepiece, (L) lead shield, (S) spiral baffle, and (C) annular slit.

Fig. 12. Partial decay scheme of ^{22}Na.

Fig. 13. Observed positron spectrum of ^{22}Na.

Fig. 14. Relationship of pulse height vs incident electron energy. The solid curve shows that obtained without lead foil. The dotted curve shows that obtained with the 35.0-mg/cm^2 lead foil before the silicon detector. The dashed curve shows that with the 75.3-mg/cm^2 lead foil before the detector.

Fig. 15. Response shape of the solid state detector for monoenergetic electrons of energy of 1146 keV. The solid curve shows that obtained with the solid detector at the focus point of the beta-ray spectrometer. The dotted curve shows that obtained with the 75.3-mg/cm^2 lead foil before the detector.

Fig. 16. Energy resolution of the solid state detector for monoenergetic electrons produced by the beta-ray spectrometer.

Fig. 17. Peak-to-total ratio of the solid state detector for monoenergetic electrons.

Fig. 18. Solid circles show the electron spectrum in the low energy region observed by the silicon detector. Open circles show the background contributions from the strayed gamma rays and natural background.

Fig. 19. Observed peak of the shell electrons ejected from a thin lead foil by radiationless annihilation of 300-keV positrons. A K-shell electron ejected by this process with another K-shell electron in a lead atom is expected to have a kinetic energy of 1146 keV.

Fig. 20. Relative angular distribution of single-quantum annihilation for 300-keV positrons on lead. This curve is obtained from the theoretical results calculated by Johnson (Ref. 39).

Fig. 21. Relative angular distribution of K-shell photoelectrons for 1234-keV photons on lead. This curve is obtained from the theoretical results calculated by Pratt *et al* (Ref. 76).

Fig. 22. Relative angular distribution of the electrons ejected from radiationless annihilation for 300-keV positrons by K-K pair in lead. This curve is obtained using Figs. 19 and 20.

Fig. 23. Flow diagram of geometrical efficiency.

Fig. 24. Schematic diagram illustrating terms used for evaluation of the effect of the target thickness.

Fig. 25. The expected spectrum of the ejected shell electrons, which should be observed with the present experimental system. The solid curve shows that obtained by taking account of the effect of the target thickness. The dashed curve shows that obtained when this effect is not taken into account. A dotted curve is the presumed slope of the dashed peak representing the total absorption peak of the ejected shell electrons when such an effect can be neglected.

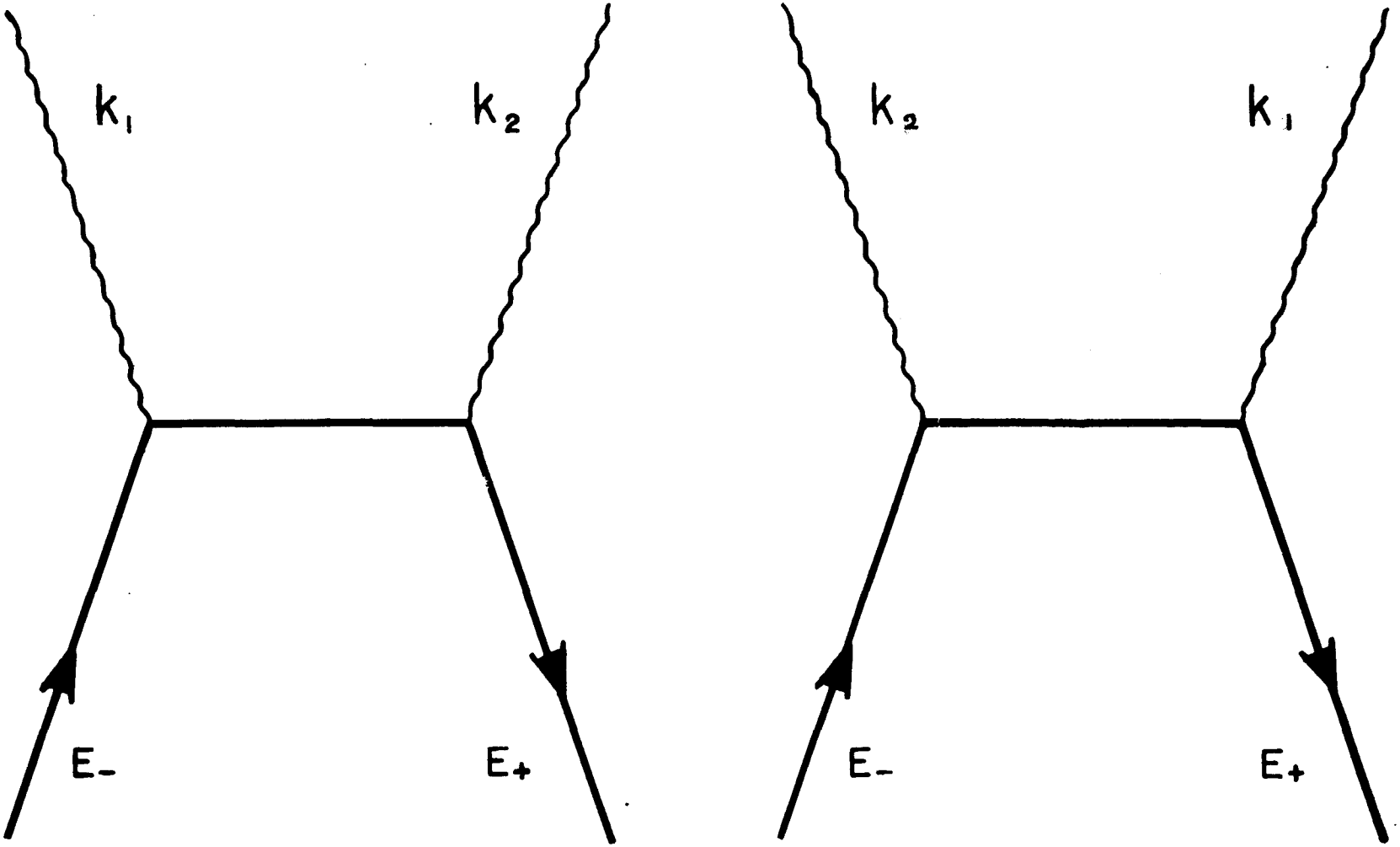

Fig. 1. Two-photon annihilation of a free pair

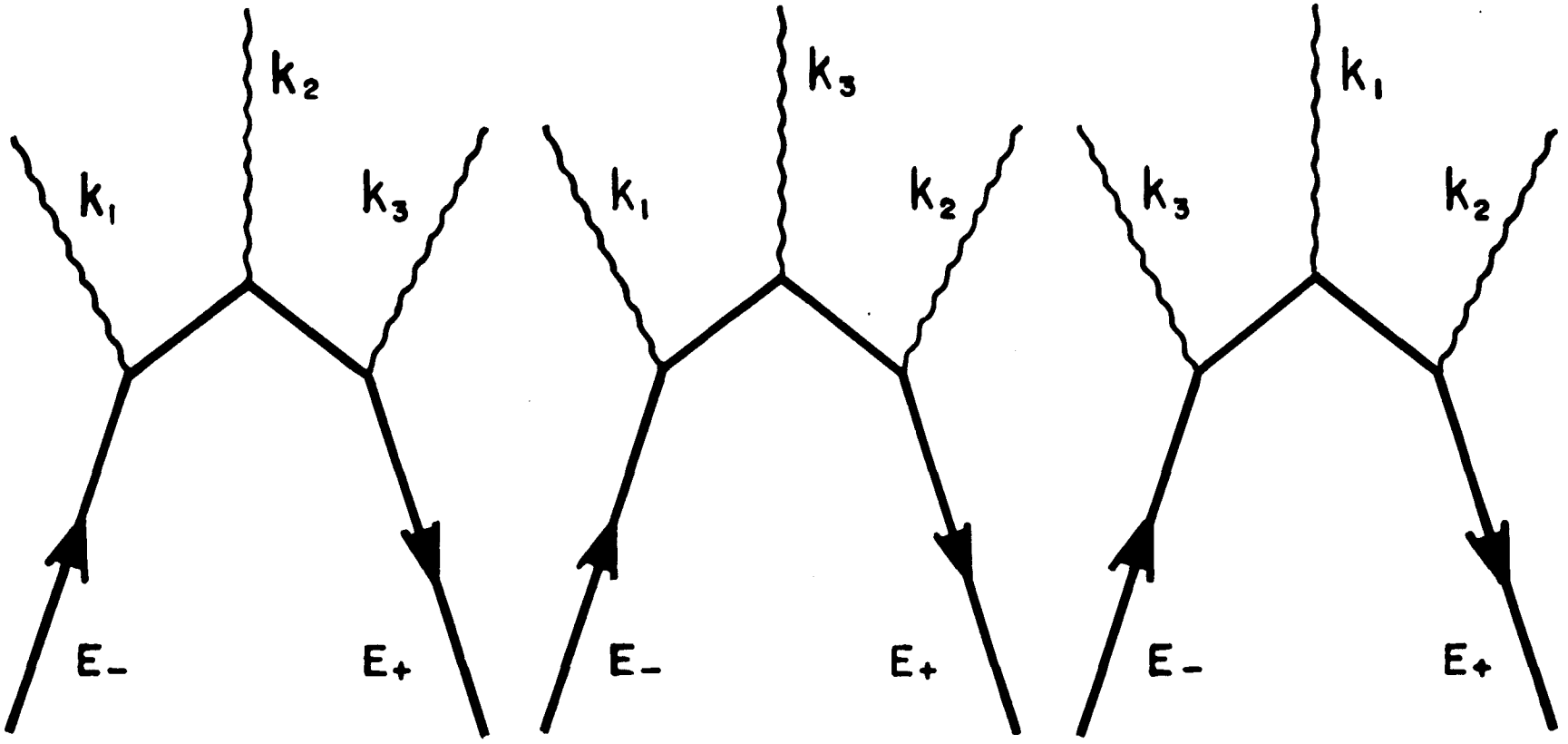

Fig. 2. Diagrams for three-quantum pair annihilation

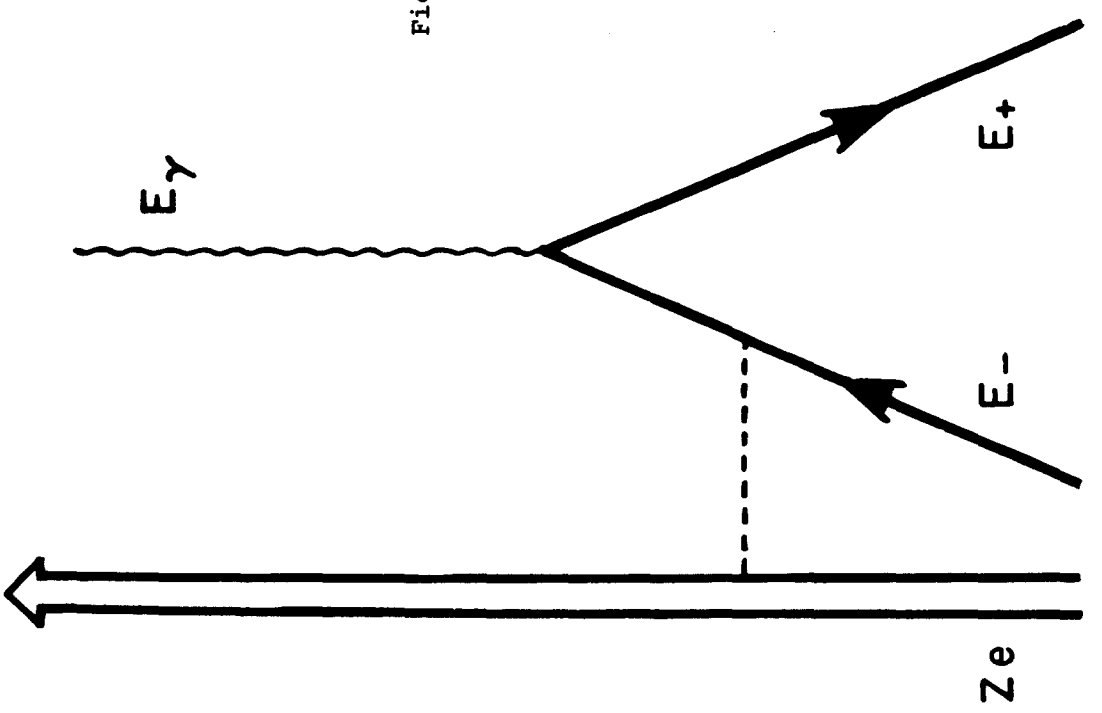

Fig. 3. Diagram for single-quantum annihilation

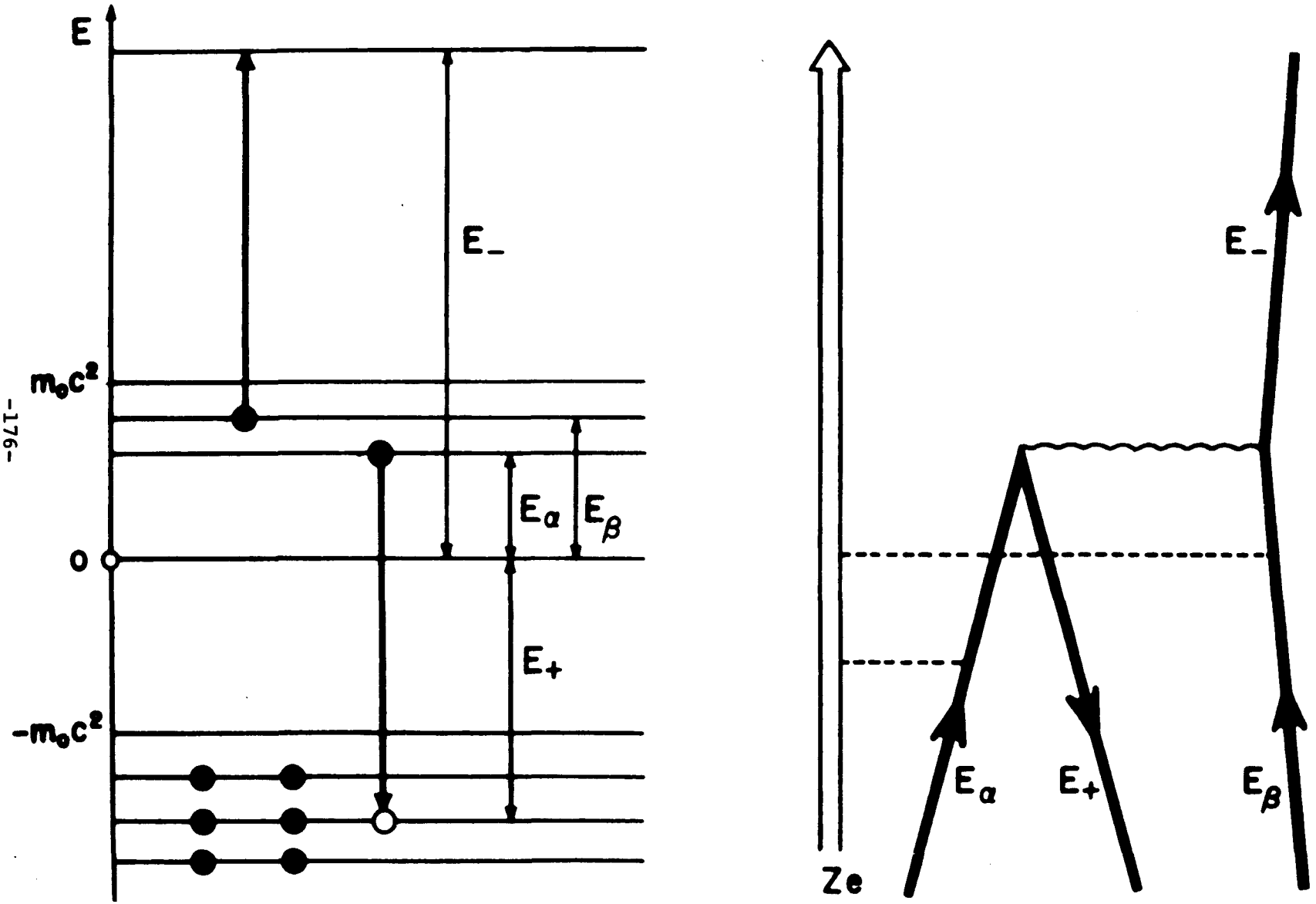

Fig. 4. Energy relation and diagram for radiationless annihilation

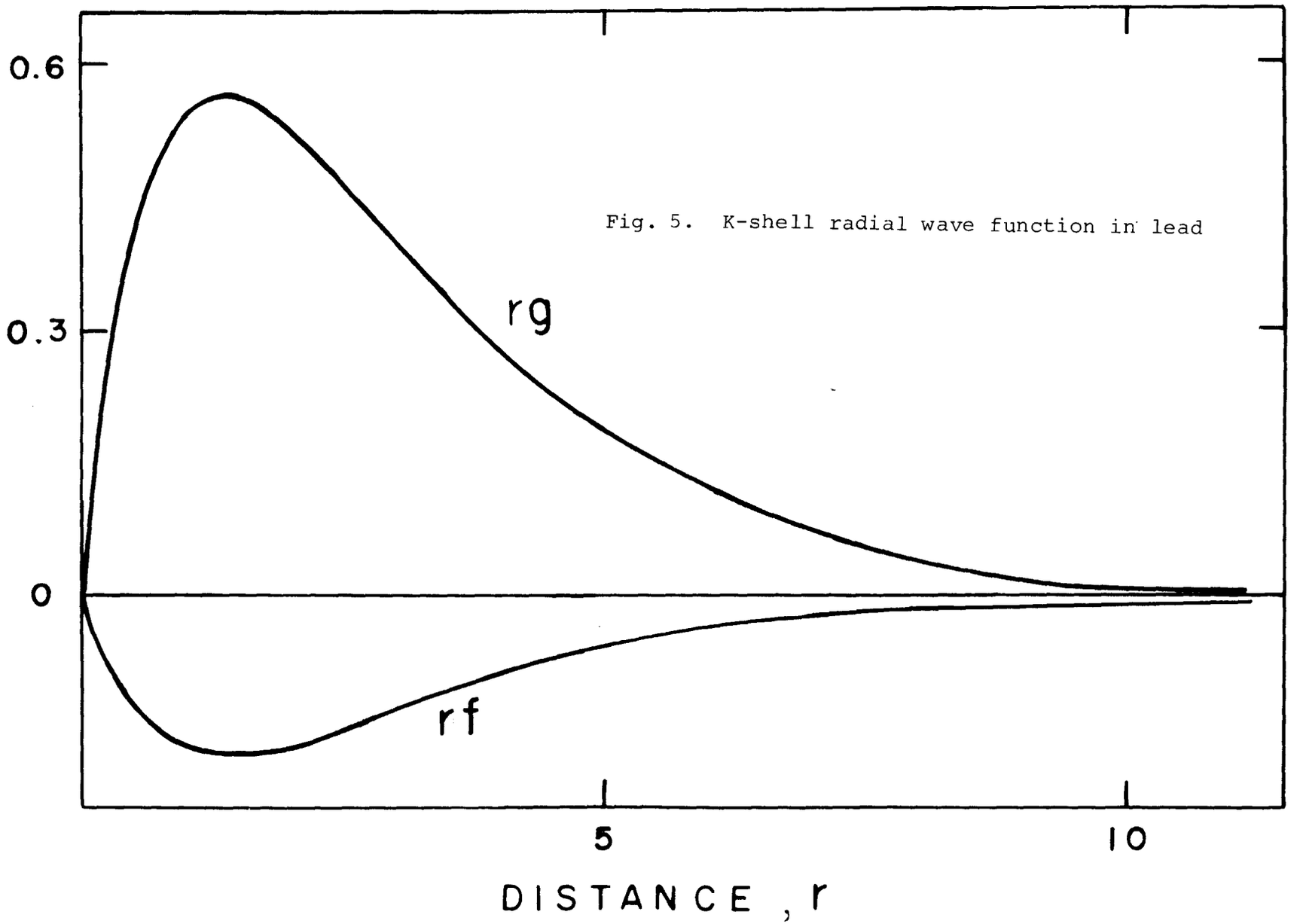

Fig. 5. K-shell radial wave function in lead

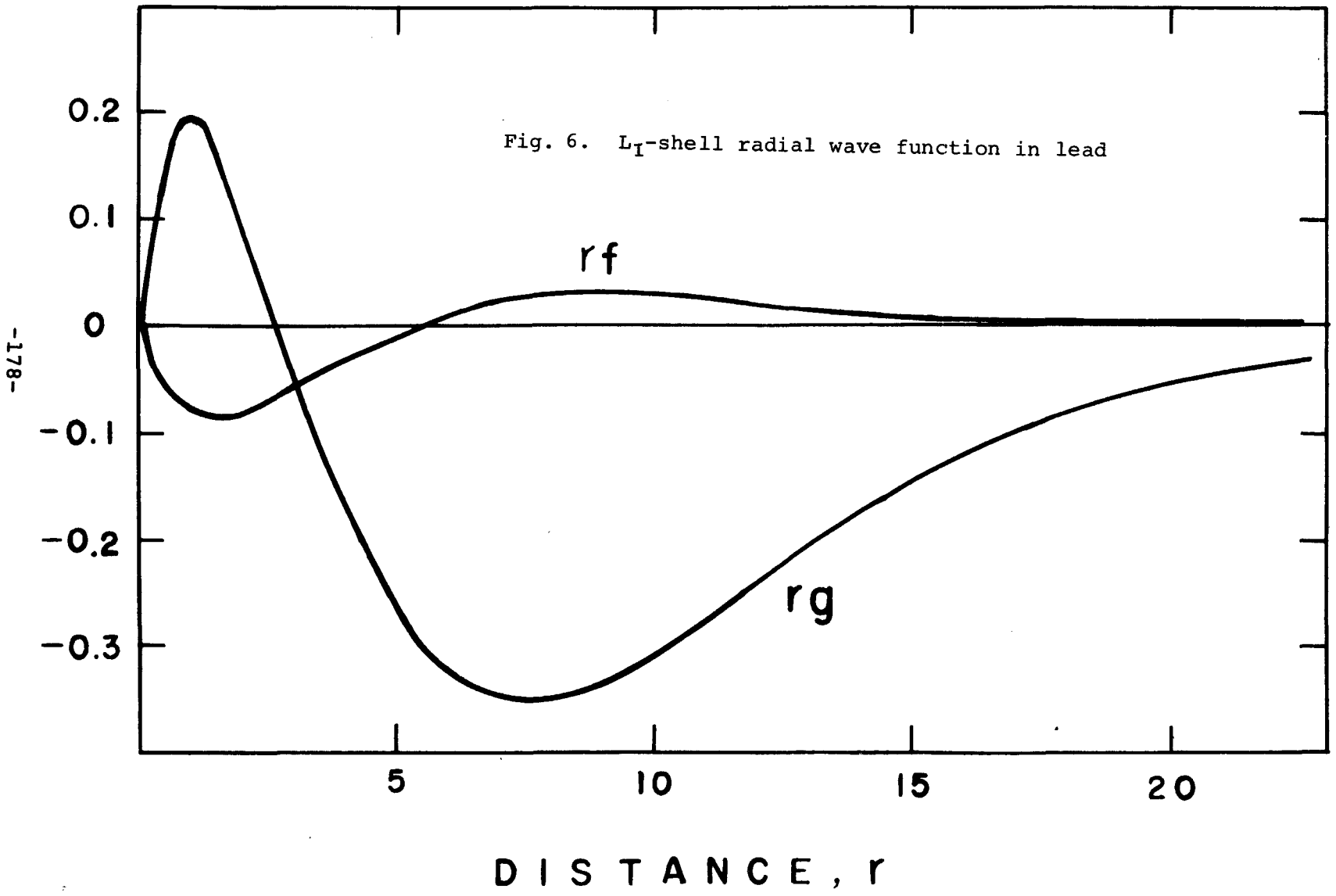

Fig. 6. L_I-shell radial wave function in lead

Fig. 7. L_{III}-shell radial wave function in lead

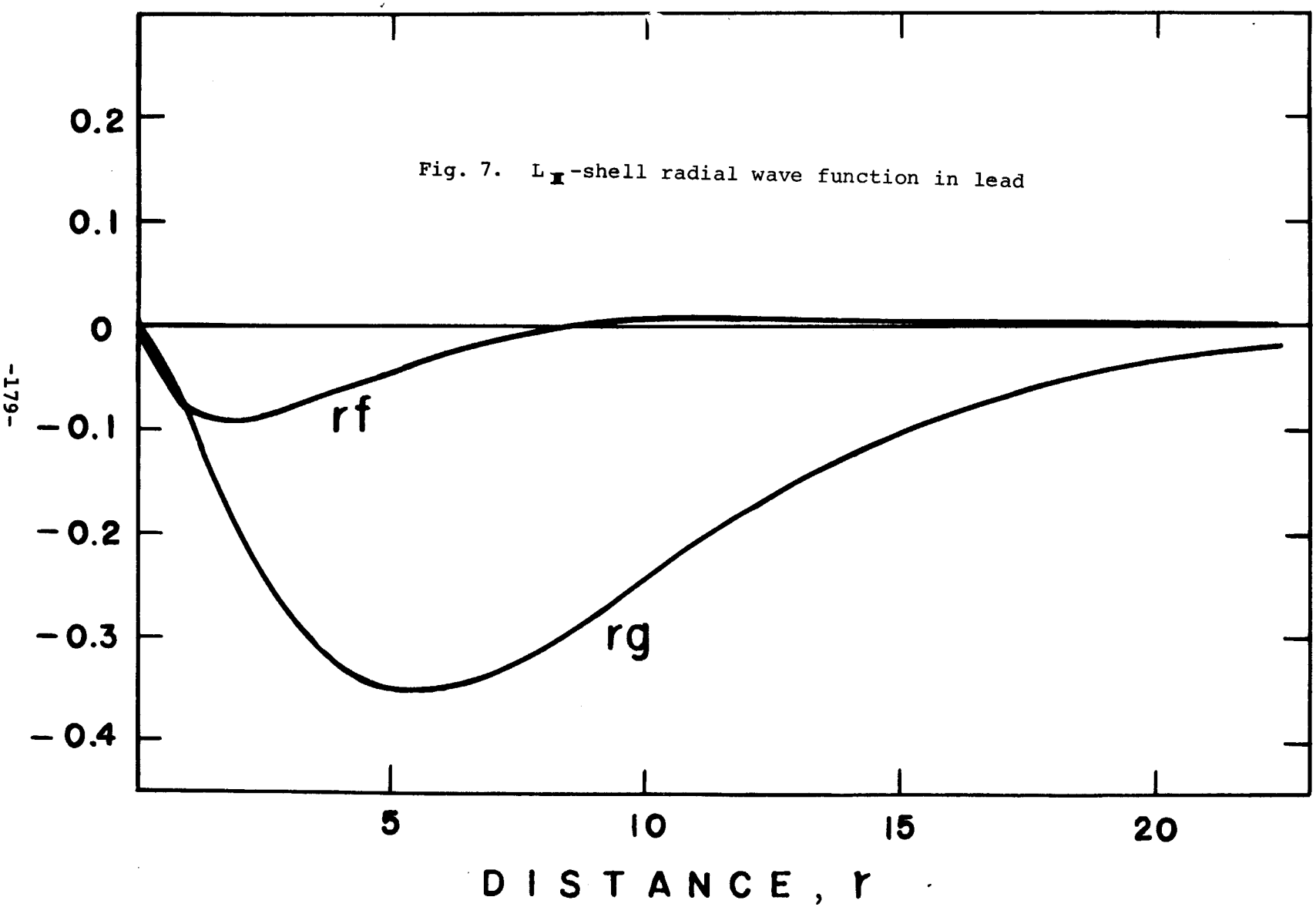

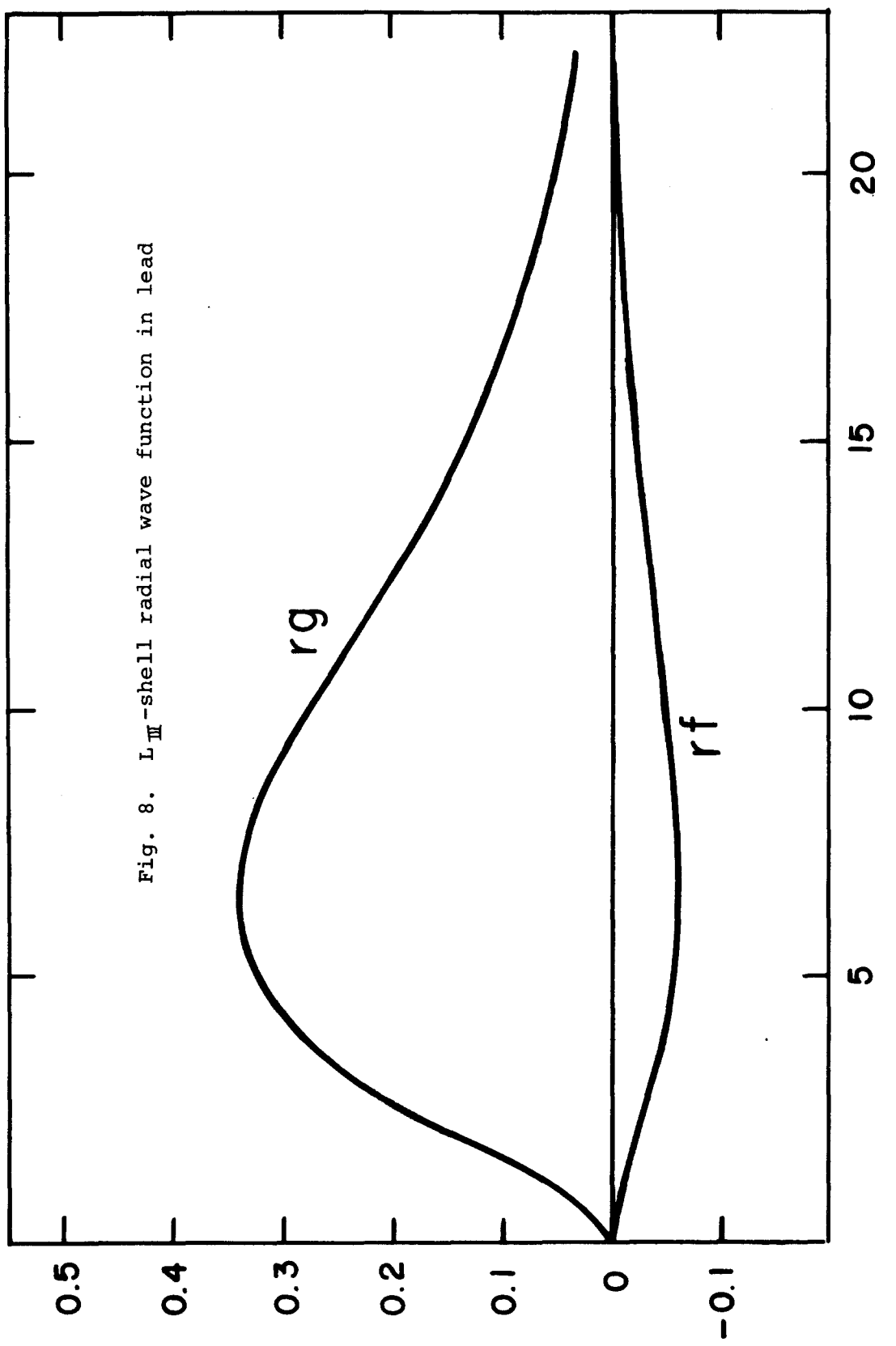

Fig. 8. L_{III}-shell radial wave function in lead

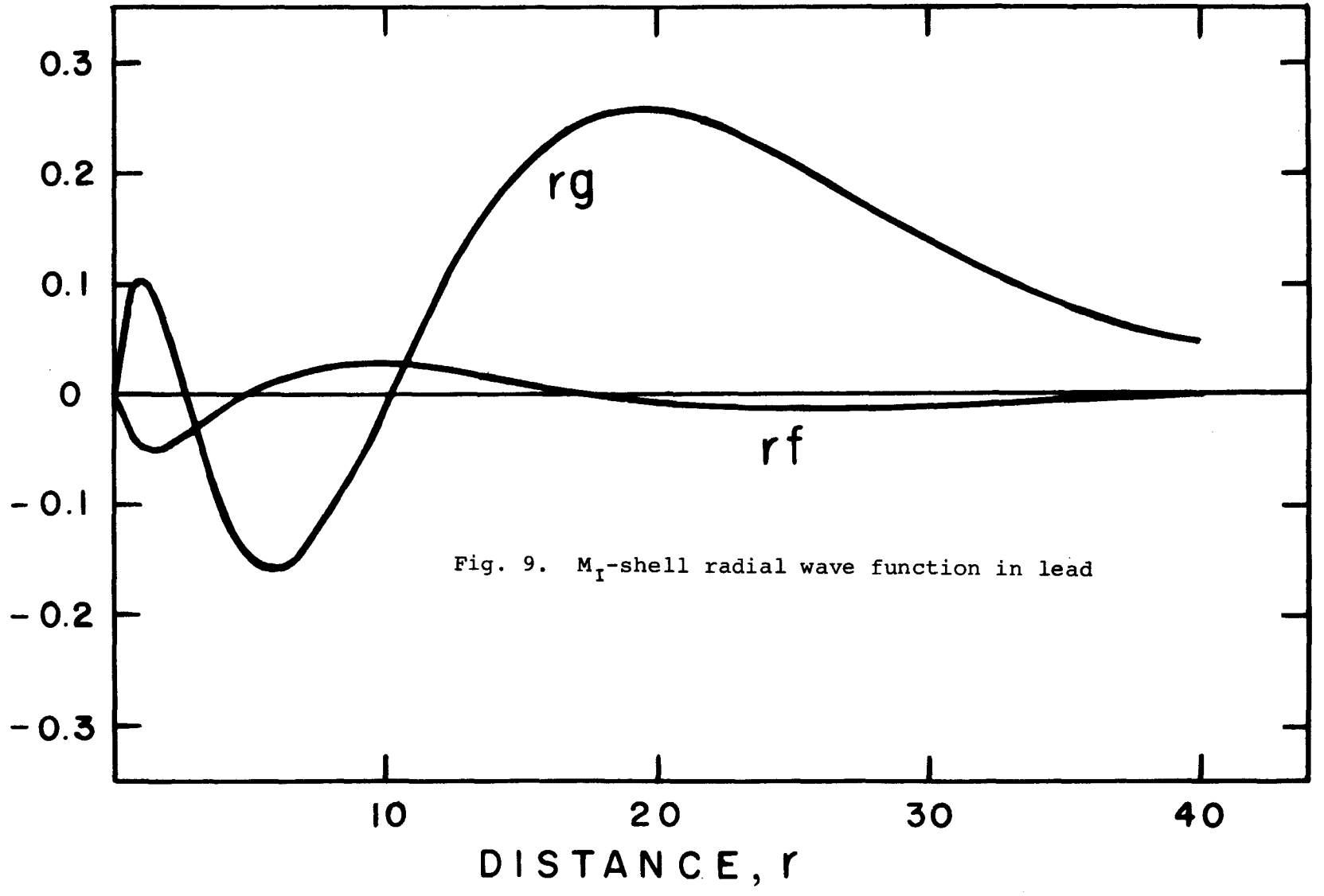

Fig. 9. M_I-shell radial wave function in lead

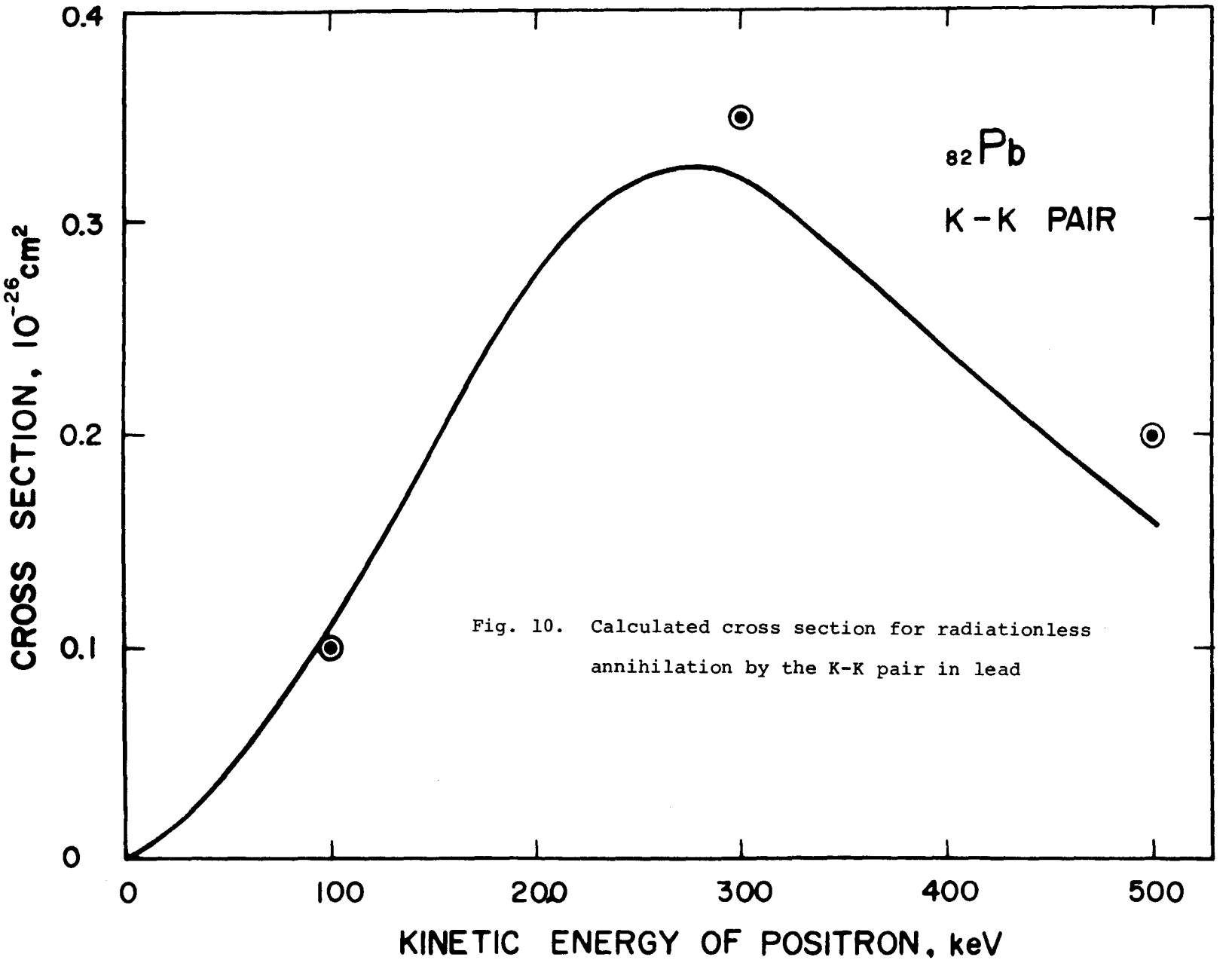

Fig. 10. Calculated cross section for radiationless annihilation by the K-K pair in lead

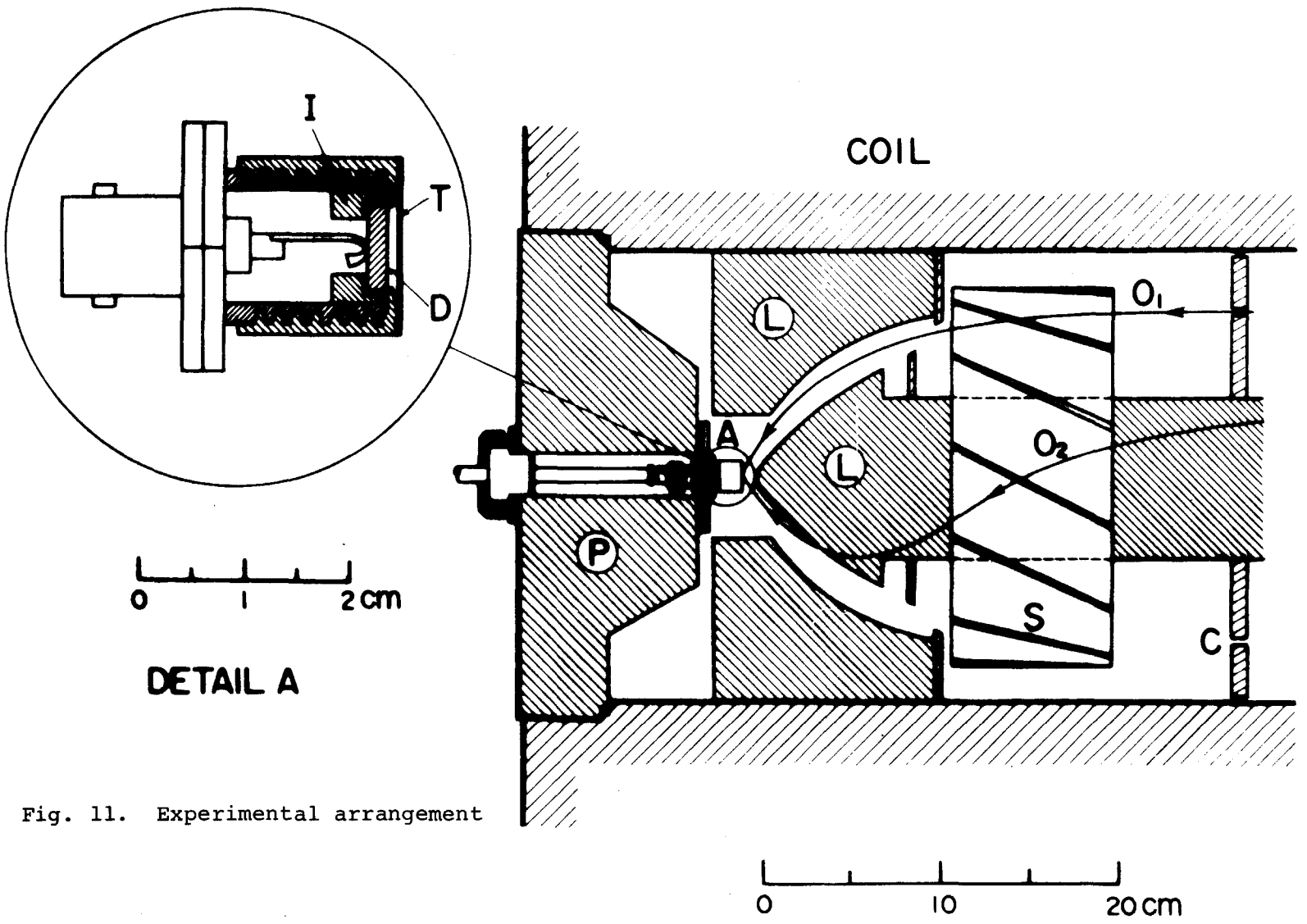

Fig. 11. Experimental arrangement

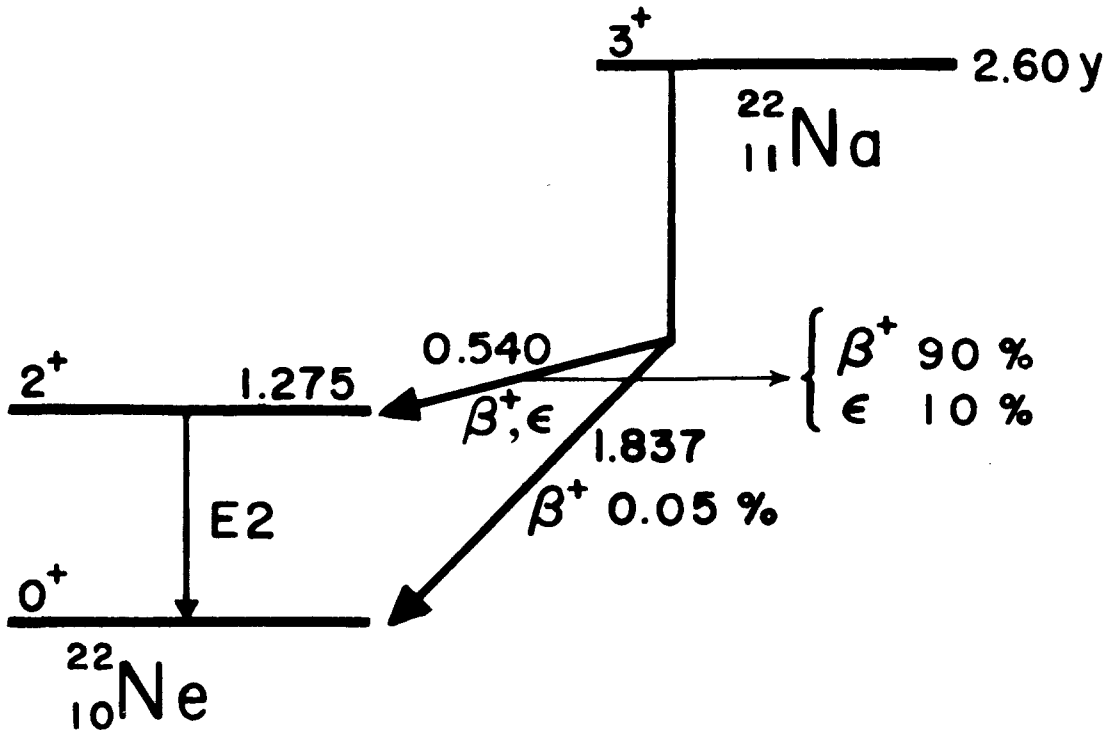

Fig. 12. Partial decay scheme of ^{22}Na

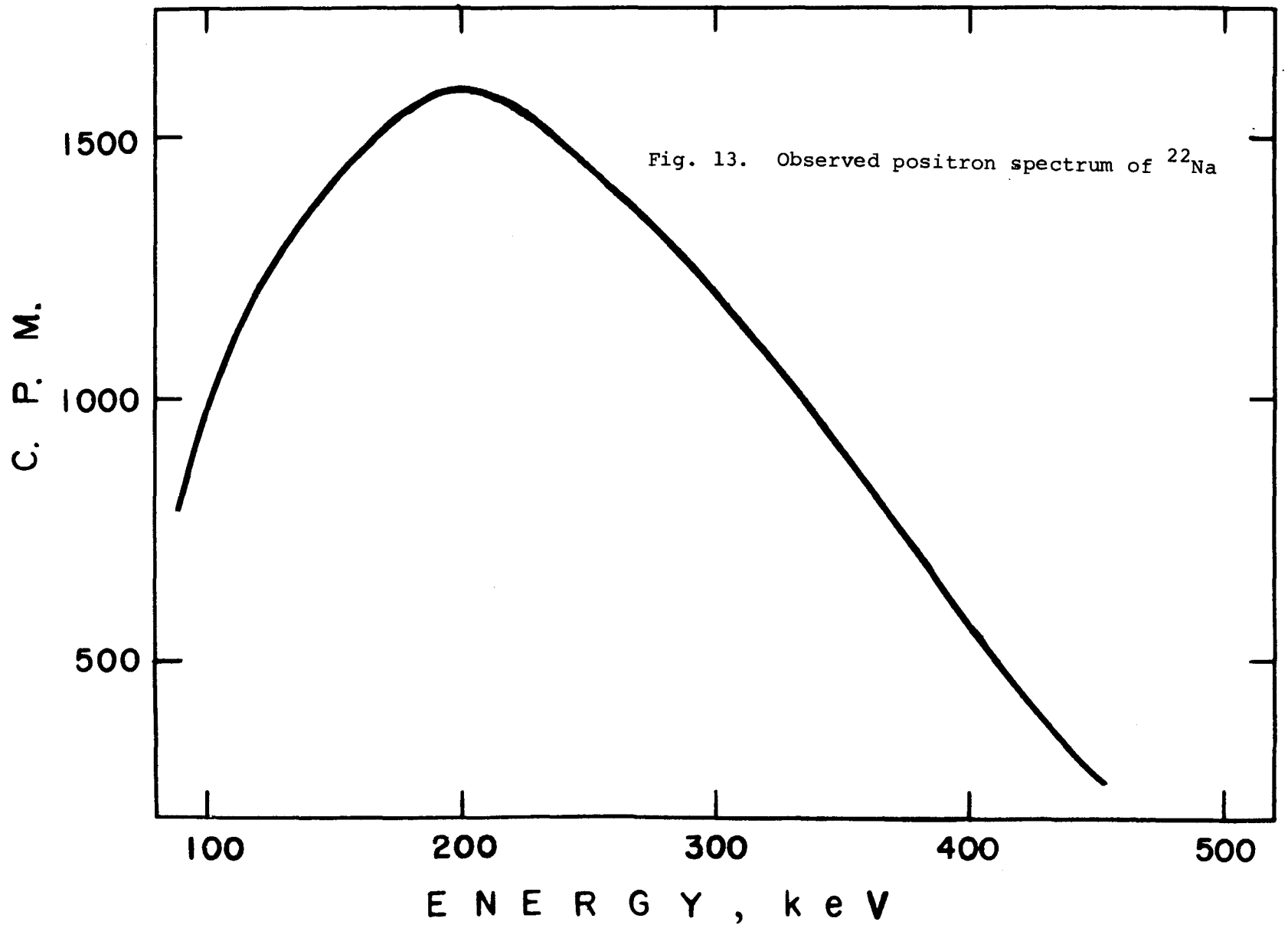

Fig. 13. Observed positron spectrum of ^{22}Na

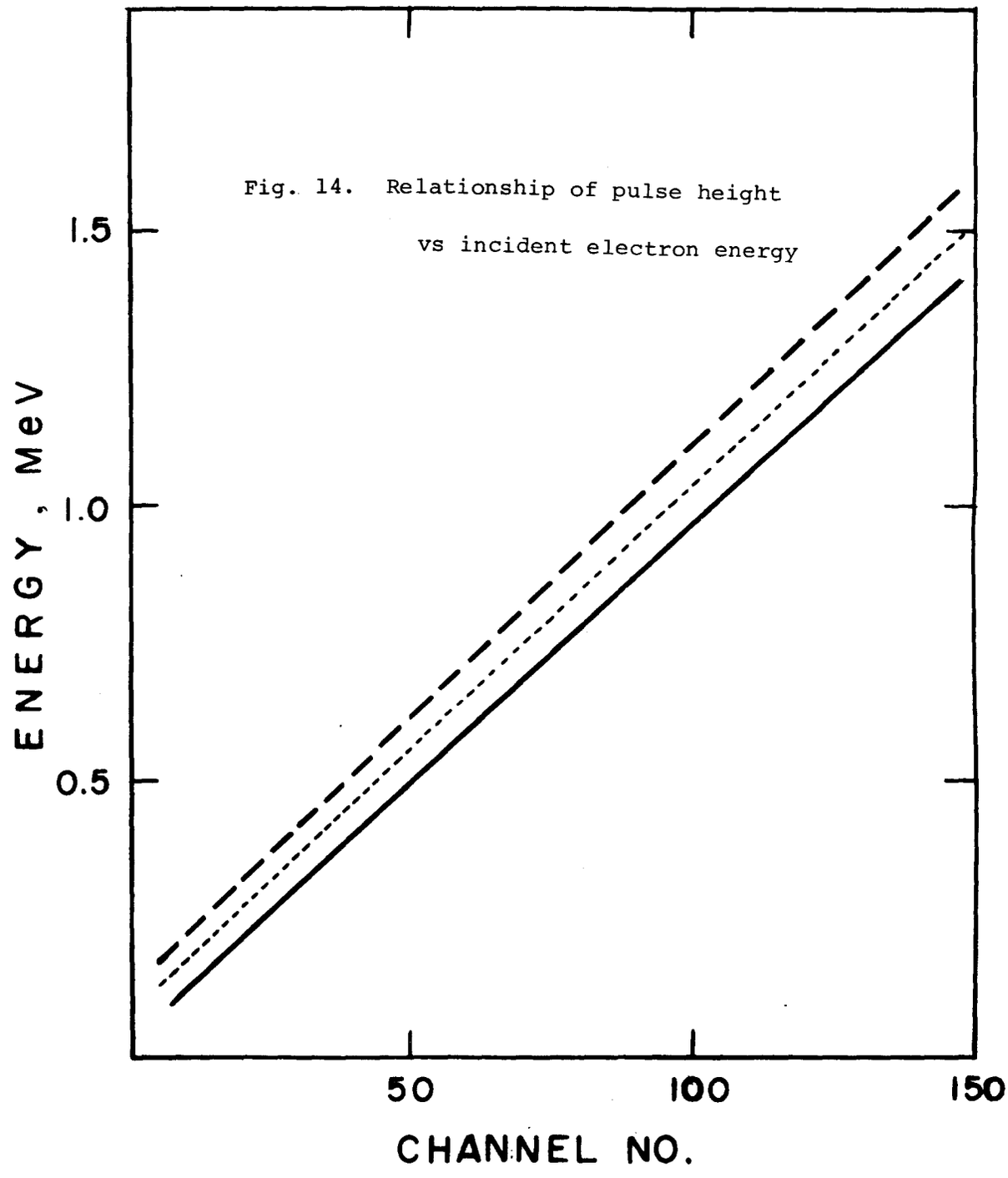

Fig. 14. Relationship of pulse height vs incident electron energy

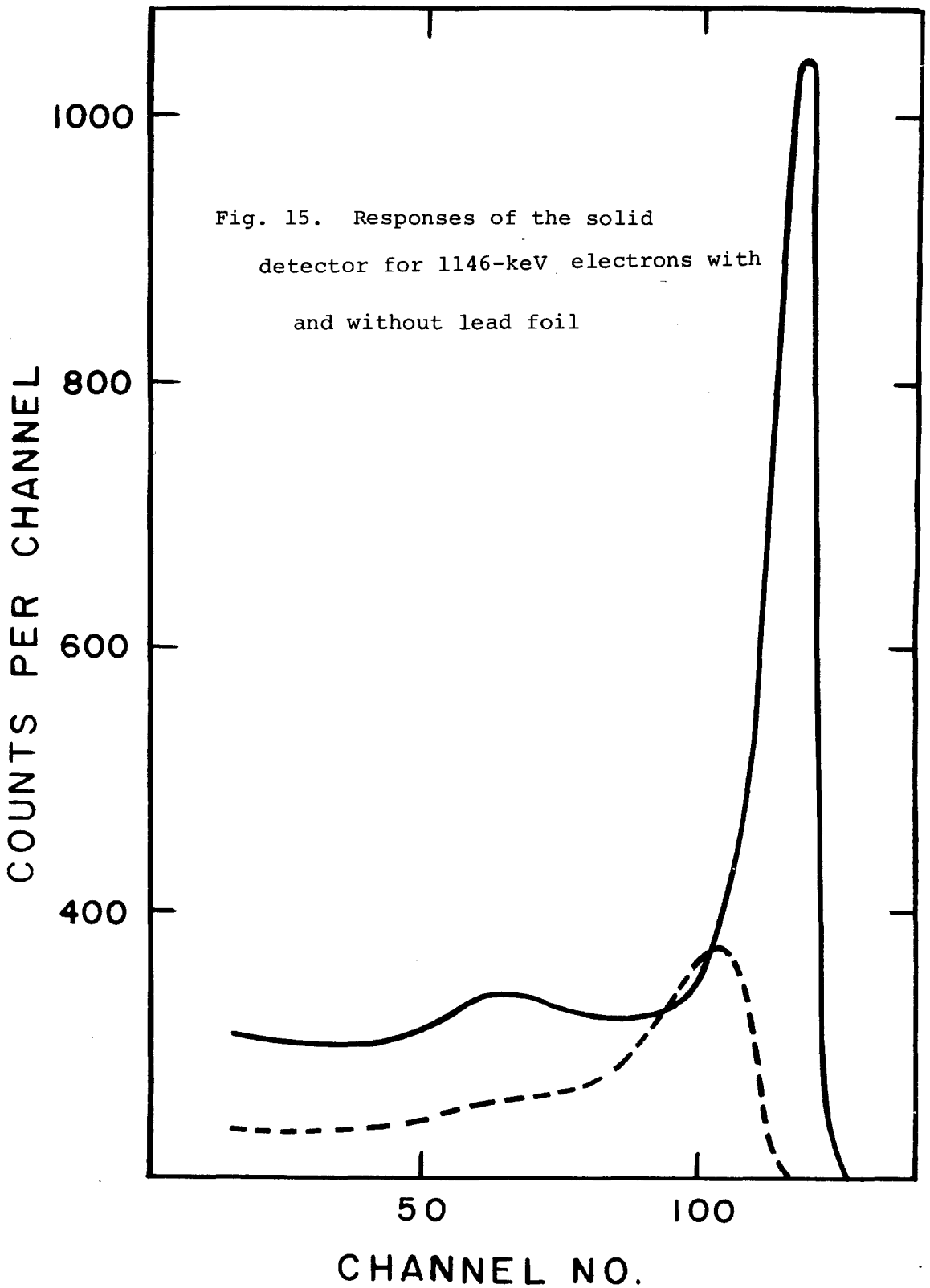

Fig. 15. Responses of the solid detector for 1146-keV electrons with and without lead foil

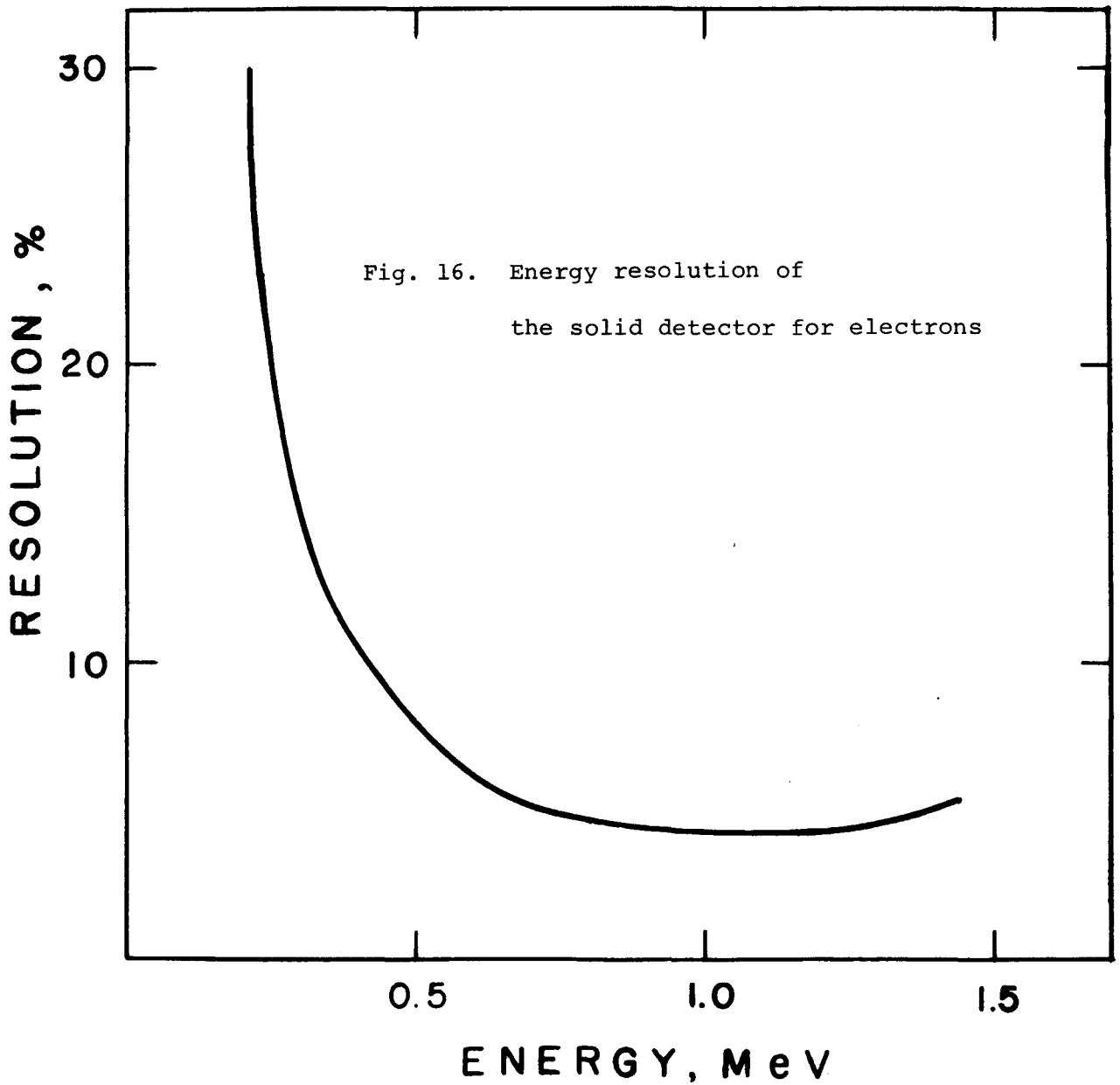

Fig. 16. Energy resolution of the solid detector for electrons

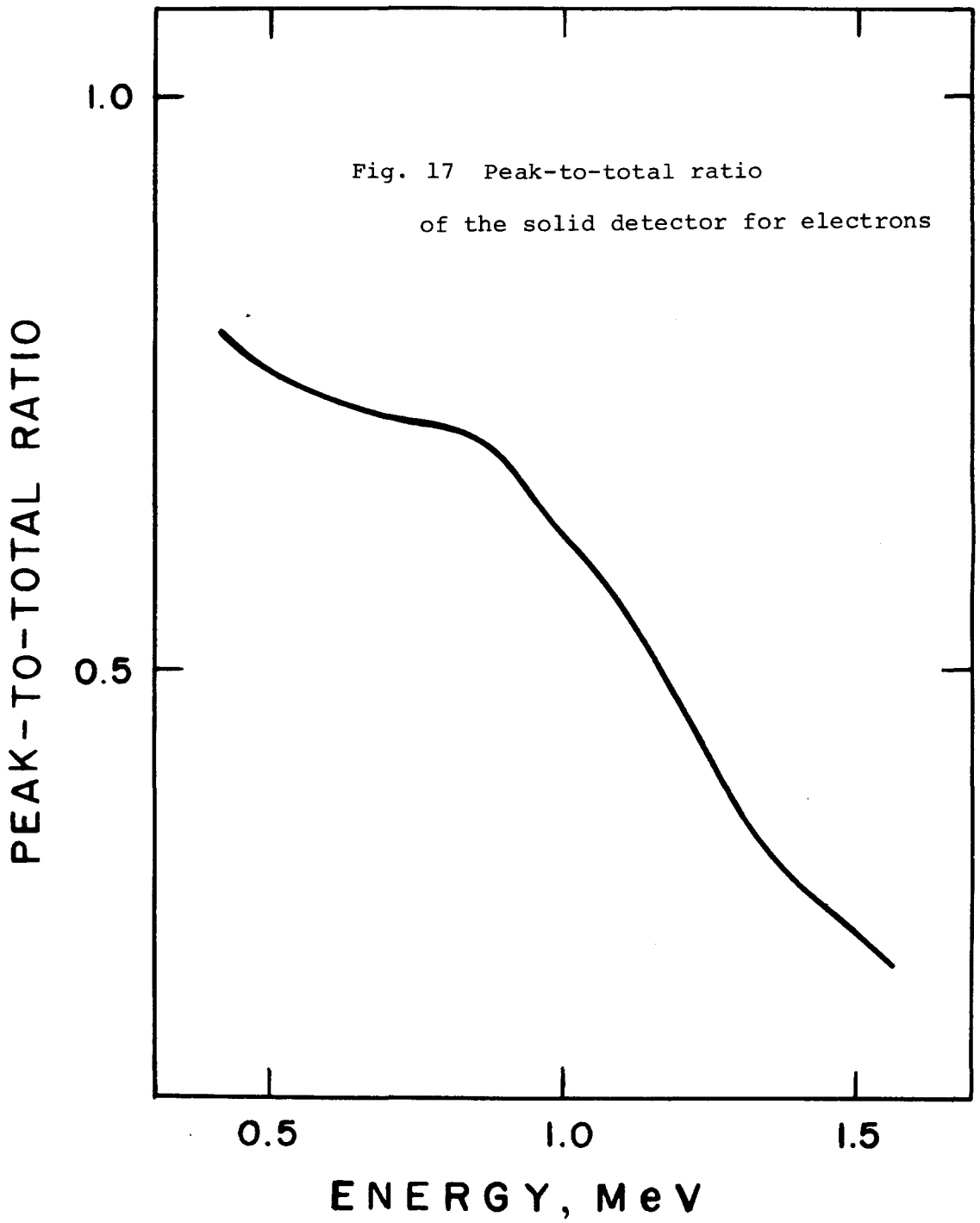

Fig. 17 Peak-to-total ratio of the solid detector for electrons

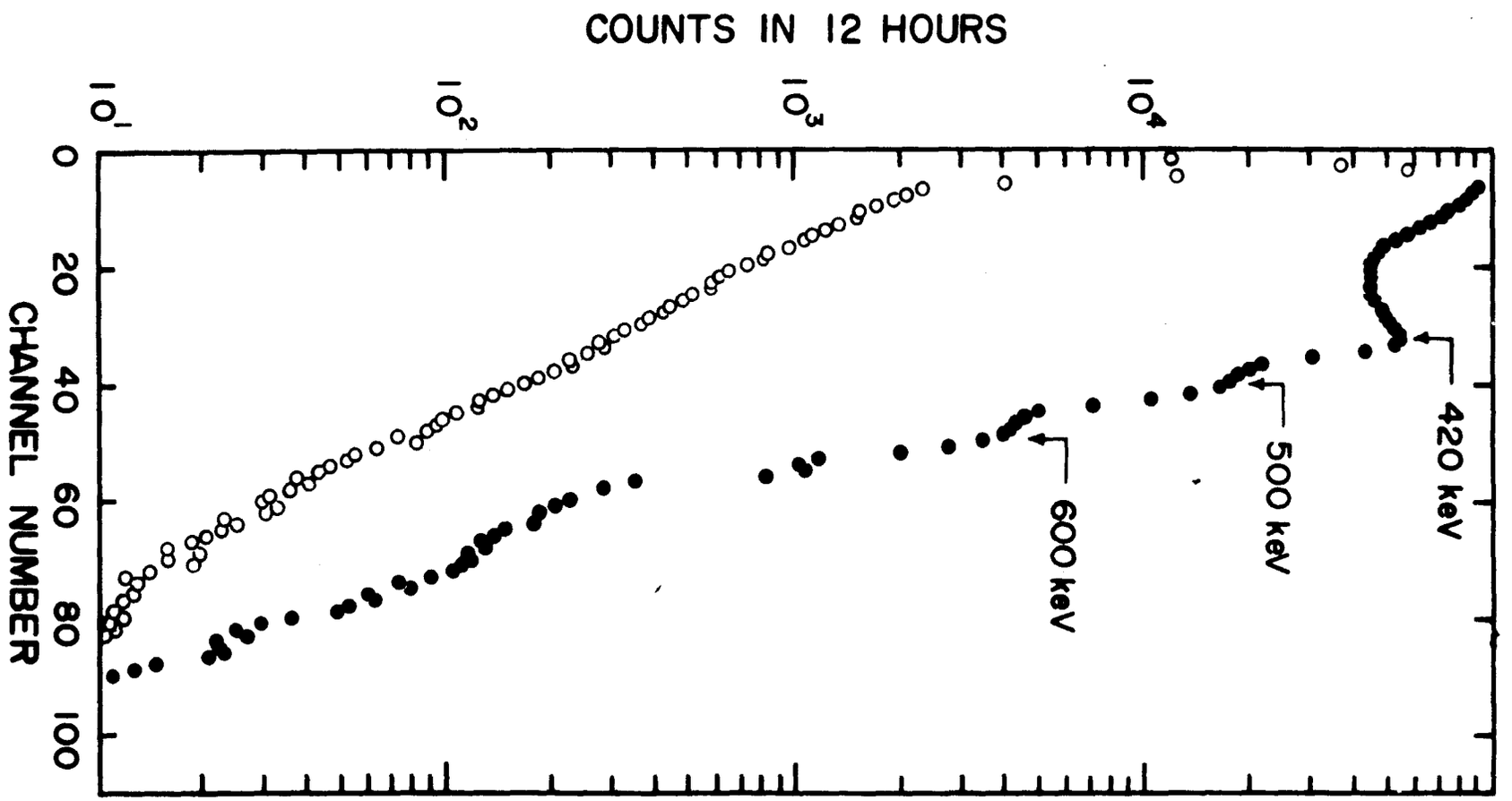

Fig. 18. Observed electron spectrum in low energy region

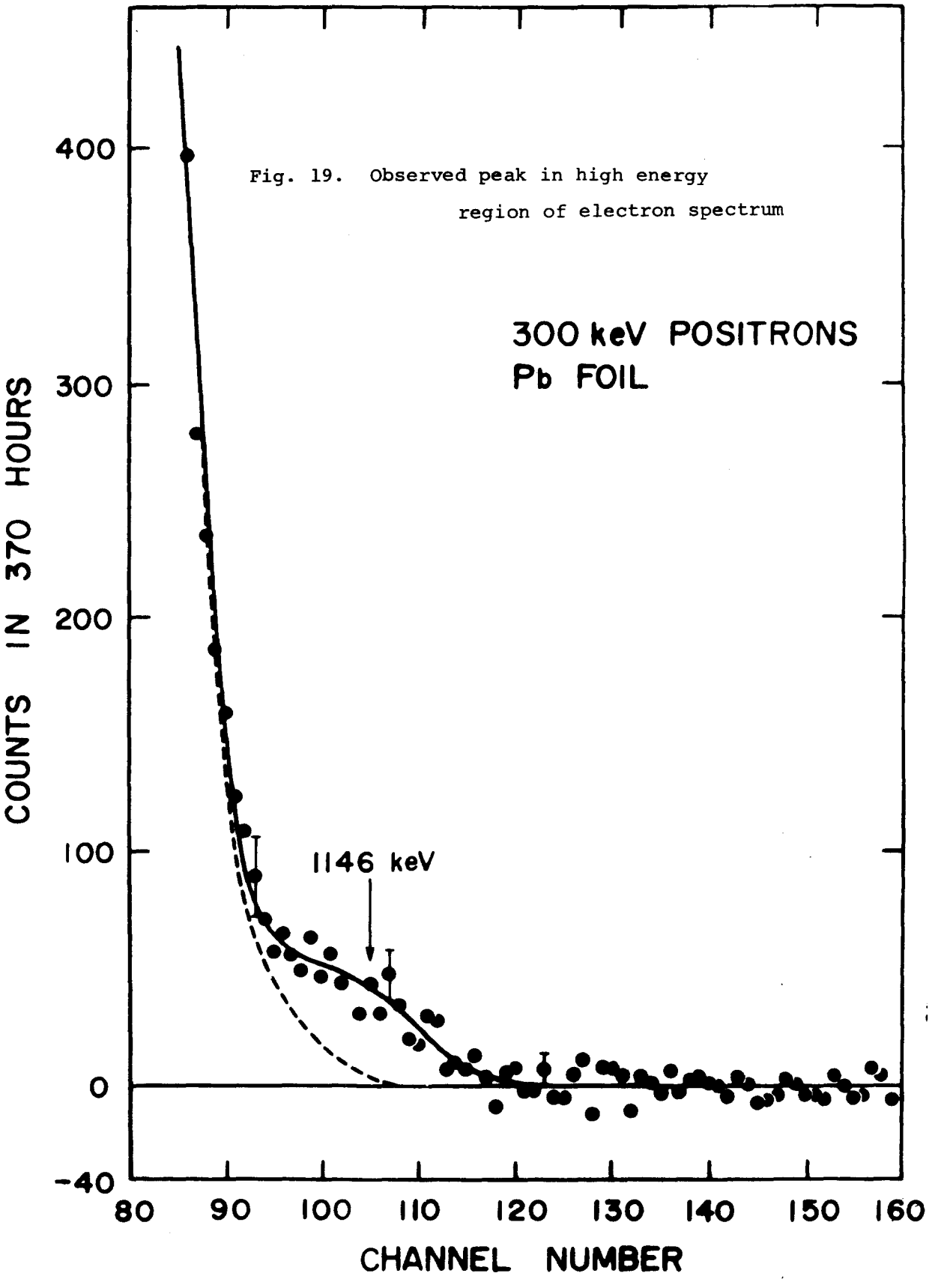

Fig. 19. Observed peak in high energy region of electron spectrum

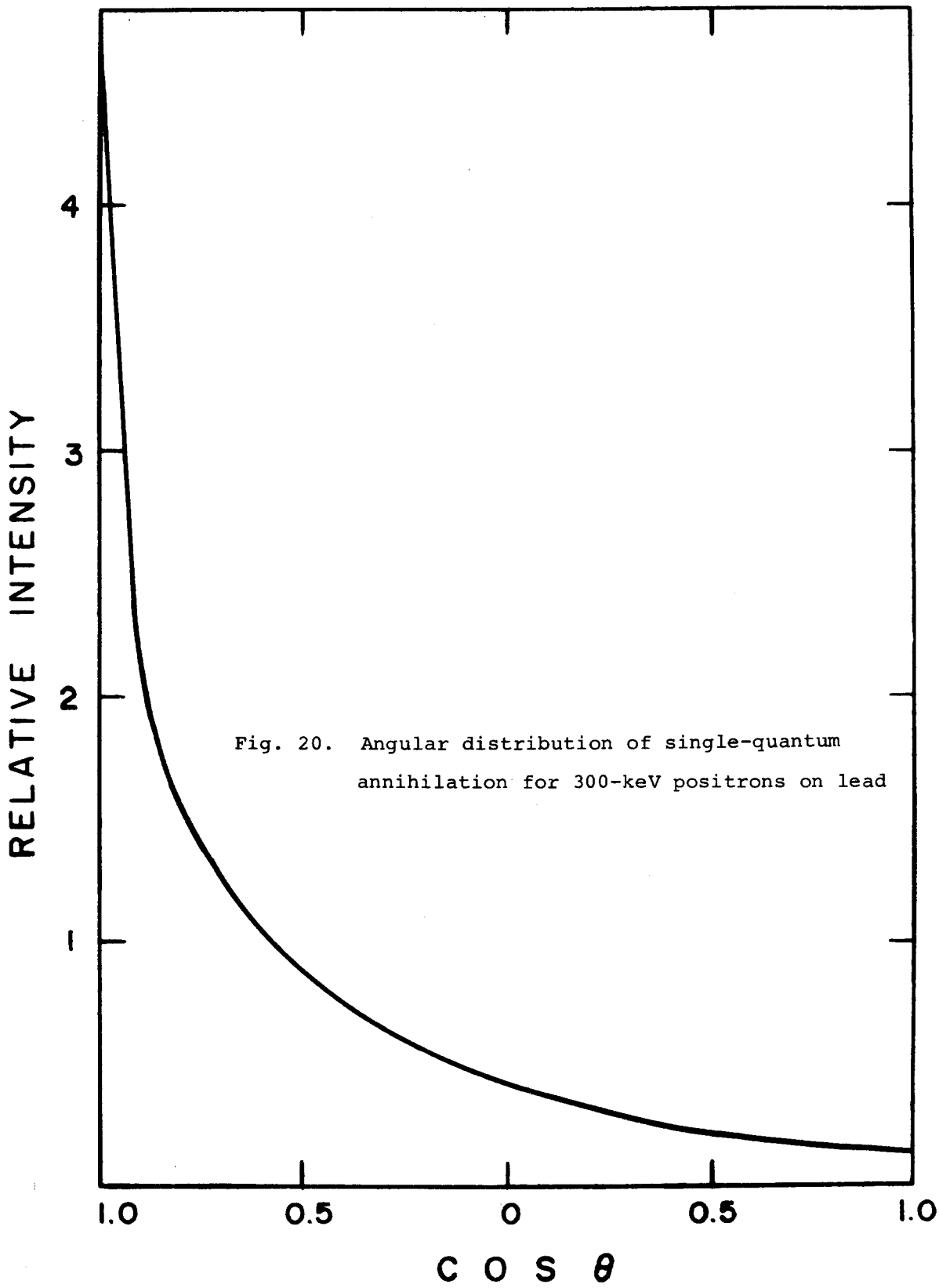

Fig. 20. Angular distribution of single-quantum annihilation for 300-keV positrons on lead

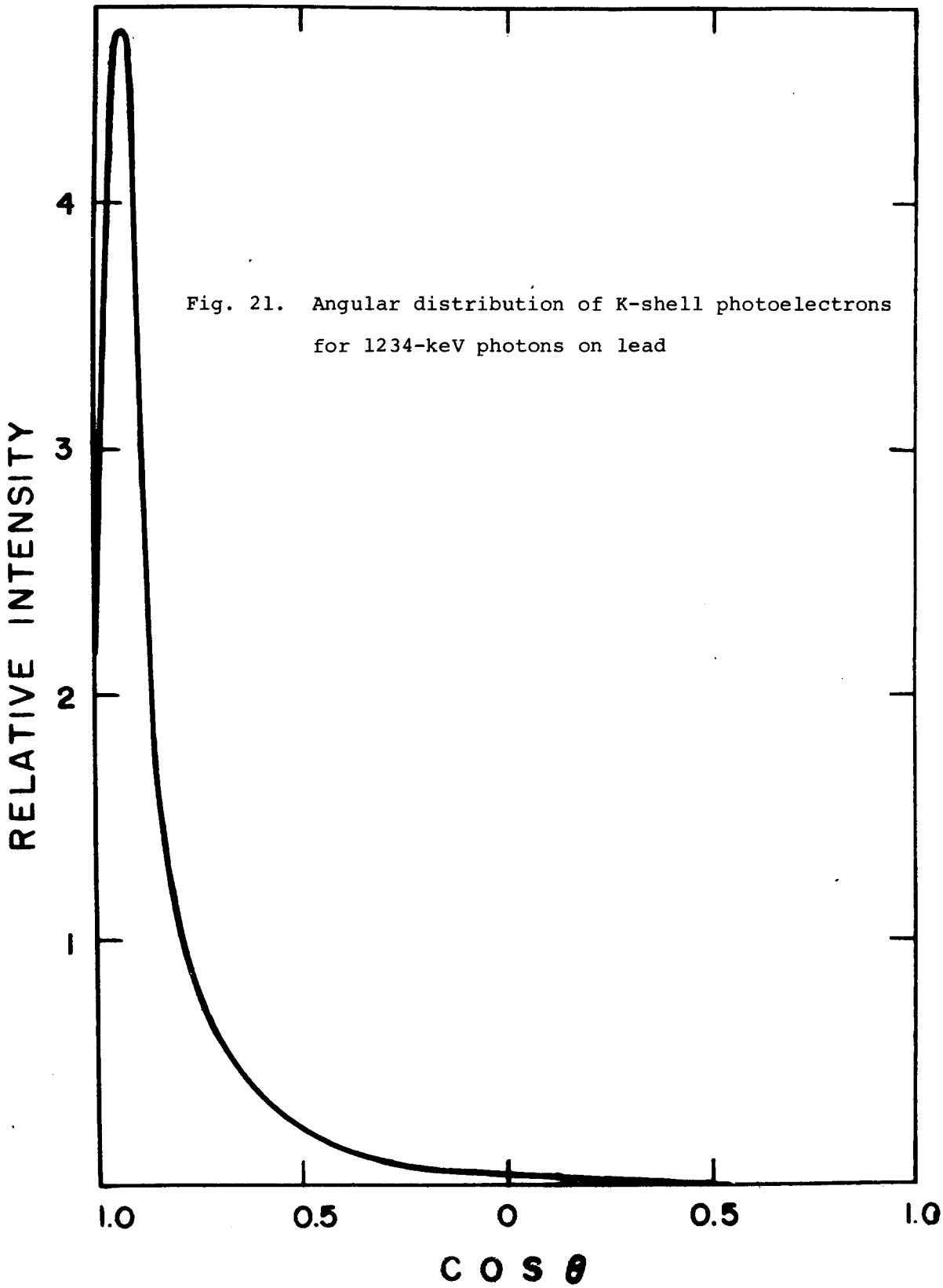

Fig. 21. Angular distribution of K-shell photoelectrons for 1234-keV photons on lead

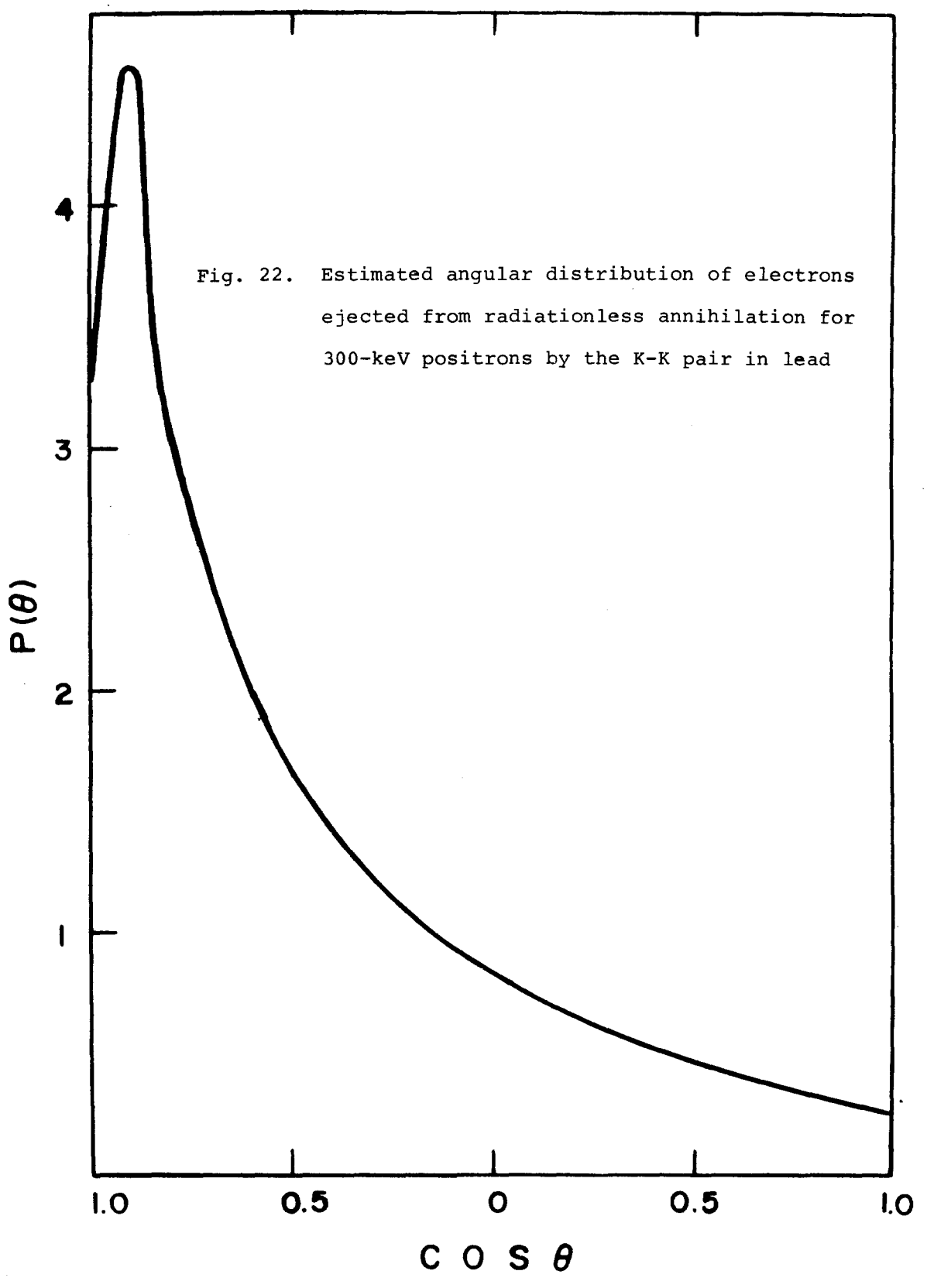

Fig. 22. Estimated angular distribution of electrons ejected from radiationless annihilation for 300-keV positrons by the K-K pair in lead

Fig. 23 Flow diagram for geometrical efficiency

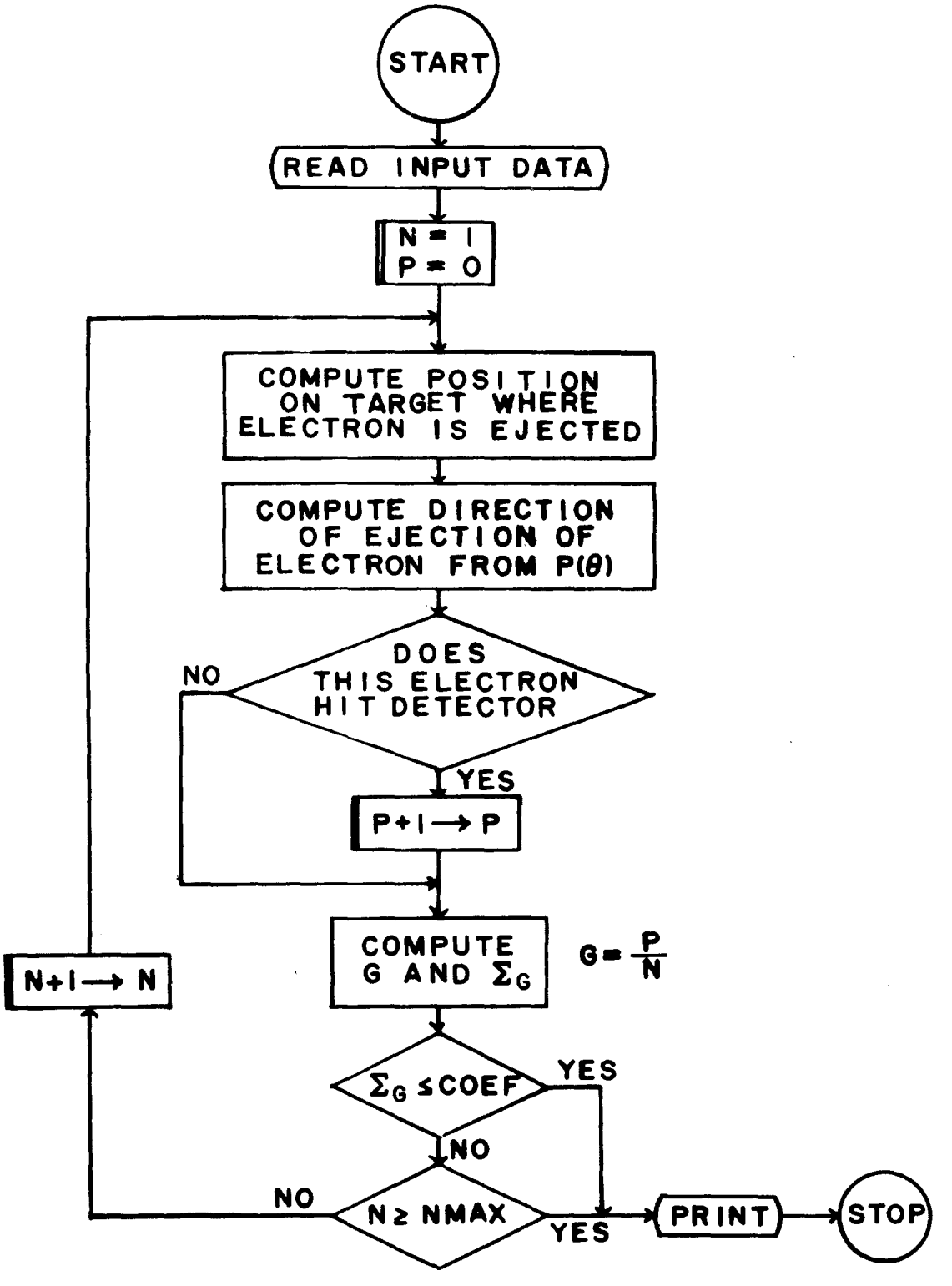

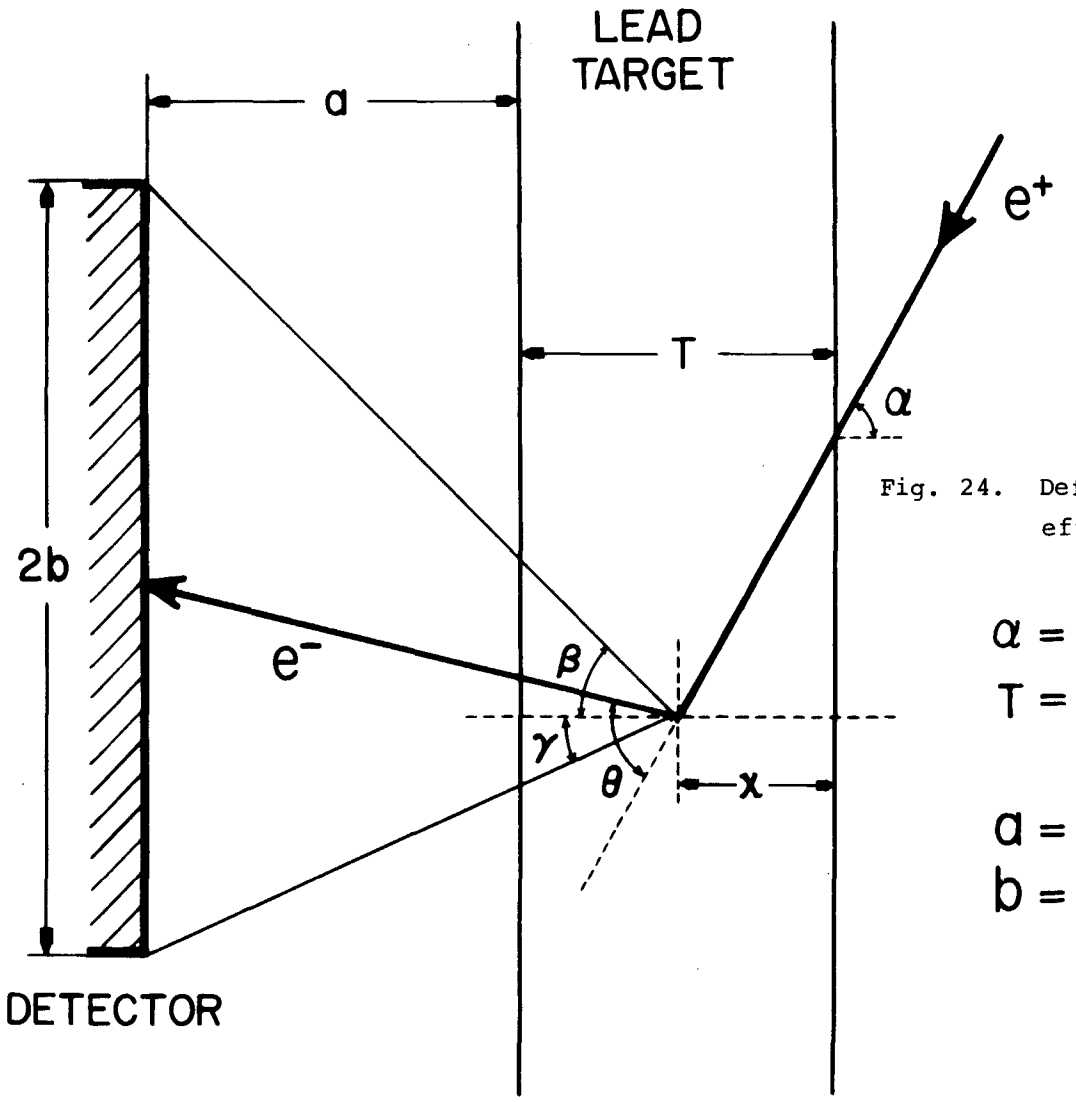

Fig. 24. Definition of terms for the effect of finite target thickness

$\alpha = 60^\circ$

$T = 75.3\ mg/cm^2$

$(6.64 \times 10^{-2}\ mm)$

$a = 1.0\ mm$

$b = 4.0\ mm$

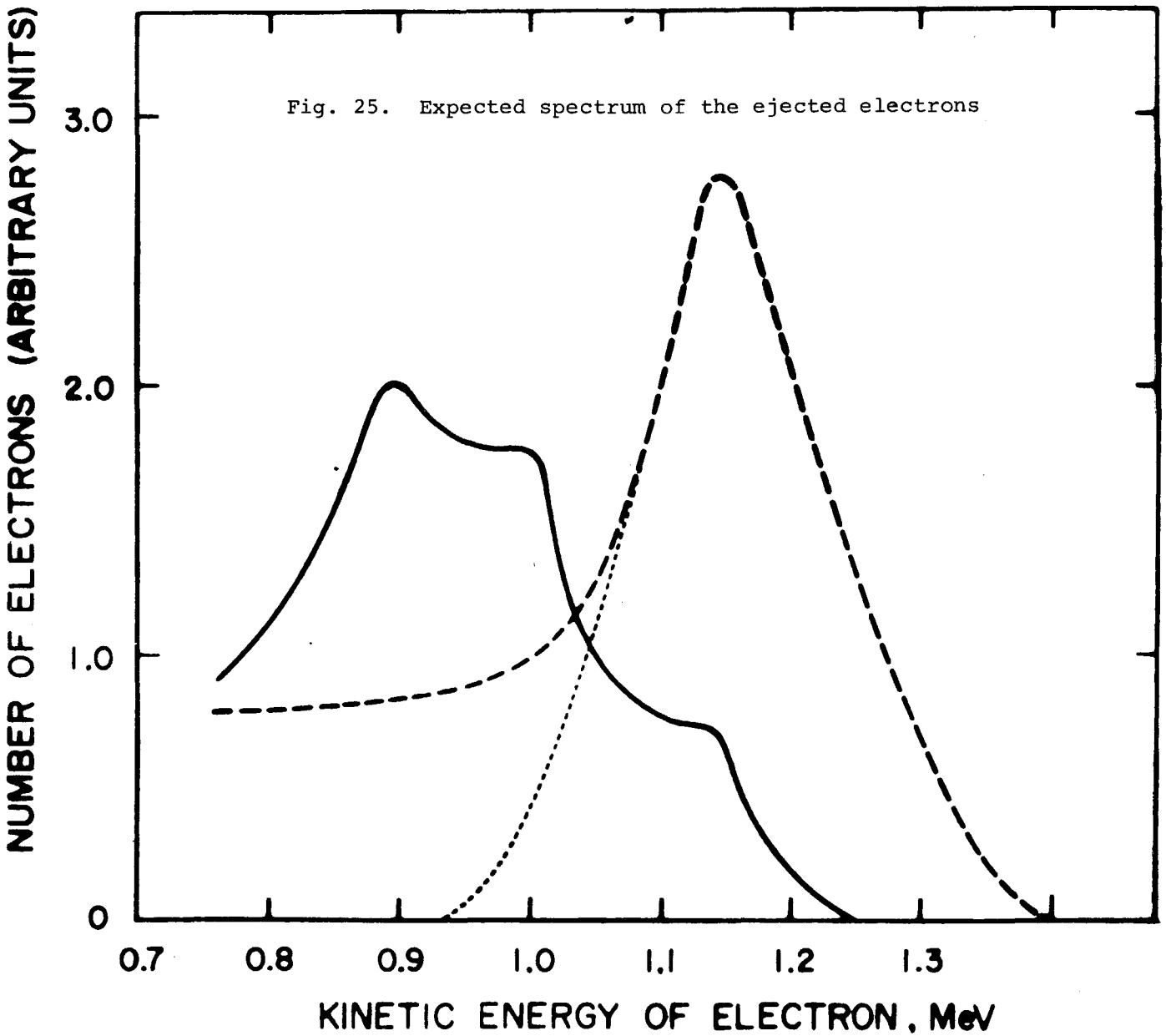

Fig. 25. Expected spectrum of the ejected electrons